NEW MEXICO BUREAU OF GEOLOGY AND MINERAL RESOURCES

Open-File Report 635 2026

Investigation of Hydrostratigraphic Units of the Santa Fe Group Aquifer in the Northwestern Albuquerque Basin, New Mexico

Daniel J. Koning, Luke Martin, Matthew J. Zimmerer, Ethan Mamer, Amanda L.M. Doherty, Laila Sturgis, and Nelia W. Dunbar



OPEN-FILE REPORT

Open-File Report 635—Investigation of Hydrostratigraphic Units of the Santa Fe Group Aquifer in the Northwestern Albuquerque Basin, New Mexico

Daniel J. Koning, Luke Martin, Matthew J. Zimmerer, Ethan Mamer, Amanda L.M. Doherty, Laila Sturgis, and Nelia W. Dunbar

Copyright © 2026

New Mexico Bureau of Geology and Mineral Resources
A research and service division of New Mexico Institute of Mining and Technology

Dr. Michael Jackson, *President, New Mexico Tech*

Dr. J. Michael Timmons, *Director and State Geologist, New Mexico Bureau of Geology*

Board of Regents

Ex Officio

Michelle Lujan Grisham, *Governor of New Mexico*

Stephanie Rodriguez, *Cabinet Secretary of Higher Education*

Appointed

Dr. David Lepre, Sr., *President, 2021–2026, Placitas*

Jerry A. Armijo, *Vice President, 2003–2026, Socorro*

Dr. Yolanda Jones King, *Secretary/Treasurer, 2019–2030, Moriarty*

Dr. Srinivas Mukkamala, *Regent, 2023–2028, Albuquerque*

Cody Johnston, *Student Regent, 2025–2026, Socorro*

Graphics/Mapping/Data Support: Michael FitsEmons, Amanda Doherty, Ethan Mamer, and Alyssa Baca

Copyediting: Frank Sholedice

Layout: Lauri Logan

Publications Program Manager: Barbara J. Horowitz

Cover Photograph: Photo of ledgy terrain characterizing the Ceja del Rio Puerco west of Rio Rancho. Photo shows the upper Santa Fe Group (light gray sediment in low area in center foreground) overlain by ledge-forming, post-Santa Fe Group sands and silty-clayey sands. The upper Santa Fe Group lies in fault juxtaposition with the middle Santa Fe Group (orange strata in left-center of photo). These strata project eastward into the subsurface and form aquifers under Rio Rancho. *Photo by Daniel Koning*

Project Funding: This project was funded by the City of Rio Rancho. Earlier funding by the STATEMAP component of the U.S. Geological Survey's (USGS) National Cooperative Geologic Mapping Program, provided by the USGS under the Grant/Cooperative Agreement and including funds from Award Numbers G13AC00186 and G16AC00287, was also essential for carrying out this research.

Suggested Citation: Koning, D.J., Martin, L., Zimmerer, M.J., Mamer, E., Doherty, A.L.M., Sturgis, L., and Dunbar, N.W., 2026, Investigation of hydrostratigraphic units of the Santa Fe Group aquifer in the northwestern Albuquerque Basin, New Mexico: New Mexico Bureau of Geology and Mineral Resources Open-File Report 635, 87 p., 17 plates. **https://doi.org/10.58799/OFR-635**

ACKNOWLEDGMENTS

This project was funded by the City of Rio Rancho and made possible by the information they provided us regarding their well field. Earlier funding by the STATEMAP component of the U.S. Geological Survey's National Cooperative Geologic Mapping Program was also essential for understanding the stratigraphic framework of the aquifer under the northwestern Albuquerque Basin. This funding was provided by the U.S. Geological Survey under the Grant/Cooperative Agreement and includes funds from Award Numbers G13AC00186 and G16AC00287. We thank Zia Pueblo for permission to access their land for the outcrop aquifer-analog component of this study (Appendix 9) and for allowing us to publish the results from that effort. The New Mexico Bureau of Geology and Mineral Resources' Electron Microprobe Laboratory and Nelia Dunbar assisted in the production of data tables and interpretations for Appendix 8. We appreciate the review that Geoff Rawling provided of an earlier draft of the report. Michael FitsEmons edited the map figures and plates.

CONTENTS

Executive Summary vi

Introduction 1
- Purpose 1
- Study Area 1
- Previous Work 1
- Organization of Report 4

Geologic Setting of the Study Area 5
- Geologic Structure 5
- Santa Fe Group Lithostratigraphy and Hydrostratigraphic Units 5
  - Zia Hydrostratigraphic Unit (Zia Formation, lower–middle Cerro Conejo Formation) 8
  - Lower Rio Rancho Hydrostratigraphic Unit (upper Cerro Conejo Formation, Benavidez unit) 10
  - Middle Rio Rancho Hydrostratigraphic Unit (Navajo Draw and Loma Barbon Members of Arroyo Ojito Formation, Benavidez unit) 12
  - Upper Rio Rancho Hydrostratigraphic Unit (Picuda Peak Member of Arroyo Ojito Formation, Ceja Formation) 12

Potentiometric Surface 14

3D Mapping of Hydrostratigraphic Units Within the Santa Fe Group Aquifer 19
- Delineation of Hydrostratigraphic Units 19
- Subsurface Mapping Methods 23
  - Mapping HSU Tops (includes both saturated and unsaturated zones) 23
  - Mapping Saturated HSU Tops 24
  - Creating Isopach Maps 24
- Subsurface Mapping Results 24
  - Extent and Geometry of HSUs 24
  - Hydrogeologic Implications 34

Assessing Permeability Differences Between and Within HSUs 36
- Outcrop Mapping 36
  - Methods 36
  - Results 36
- Determining Sand Versus Clayey Sediment for HSUs Using Well Data 38
  - Methods 38
  - Results 38
- Determining Sand Versus Clayey Sediment for HSUs Using Vshale Analyses and Density-Porosity Analyses 43
- Direct Permeability Analysis 49
  - Methods 49
  - Results 52

Preliminary Evaluation of Water Quality and Age 58
- Total Dissolved Solids Data 58
- Preliminary Radiocarbon Age Analyses 58

Discussion 62
- Comparison with Previous Hydrochemical Work 62
- Interpretations Relevant to Groundwater Management 63
- Stratigraphic and Tectonic Findings 66

Conclusions 68

References 69

Figures

1. Location of the study area within the larger Albuquerque Basin 2
2. Map of the study area with a satellite imagery background 3
3. Three-dimensional image illustrating the geologic structure of the Albuquerque Basin 6
4. Geologic map of the study area 7
5. Photograph of well-exposed badlands north of La Ceja 8
6. Lithostratigraphic nomenclature of and its correlation to the hydrostratigraphic units used in previous studies and this study 9
7. Photographs of the Zia HSU and Lower Rio Rancho HSU 10
8. West–east, schematic depiction of lithostratigraphic and hydrostratigraphic unit relations 11
9. Photographs of the Middle Rio Rancho HSU and Upper Rio Rancho HSU 13
10. Contours showing depth to the potentiometric surface 17
11. Contours showing the elevation of the approximate potentiometric surface 18
12. Illustration of well data displayed using Kingdom software 22
13. Elevation of the top of the Middle Rio Rancho HSU 25
14. Elevation of the top of the Lower Rio Rancho HSU 26
15. Elevation of the top of the saturated Upper Rio Rancho HSU 27
16. Elevation of the top of the saturated Middle Rio Rancho HSU 28
17. Elevation of the top of the saturated Lower Rio Rancho HSU 29
18. Thickness of the saturated part of the Upper Rio Rancho HSU 30
19. Thickness of the saturated part of the Middle Rio Rancho HSU 31
20. Three-dimensional block diagram of the hydrogeologic subsurface model under the northwestern Albuquerque Basin 32
21. Three-dimensional depiction of the HSU surfaces under the northwestern Albuquerque Basin 33
22. Results of lithologic analyses for 22 wells in the study area 40
23. Pie graphs showing the proportion of clay, muddy sand, and sand per HSU in a given well 41
24. Plots of percent sand and clay per well 42
25. Box-and-whisker plot of storage zone thickness 44
26. Bubble plot of net-to-gross ratios of sand bodies in the saturated zone for the Middle and Lower Rio Rancho HSUs 46
27. Bubble plot of net-to-gross ratios of sand bodies in both the saturated and unsaturated zones for the Middle Rio Rancho HSU 47
28. Bubble plots illustrating arithmetic means of density-porosity data for sand intervals in wells penetrating the Middle and Upper Rio Rancho HSUs 48
29. Map showing spatial distribution of hydraulic conductivities calculated from pumping tests 51
30. Box-and-whisker plots of hydraulic conductivity and specific capacity data for the Upper, Middle, and Lower Rio Rancho HSUs 53
31. Hydraulic conductivity from the Kozeny-Carman model 55
32. Permeability from the Berg model 56
33. Comparison of various permeability methods versus hydraulic conductivity derived from pumping tests, as calculated per well 57
34. Map of TDS values obtained from well samples 60
35. Map of TDS values obtained from well samples, but with radiocarbon ages of groundwater and approximate groundwater flow 61
36. Gamma-ray, deep-induction, density-porosity, and Vshale wireline curves for the Santa Fe Pacific No. 1 well 67

Tables

1. Well data used to construct the potentiometric surface 15
2. Well information and HSU elevations for the northwestern Albuquerque Basin 20
3. Results of the HSU outcrop study on Zia Pueblo 37
4. Compilation of lithologic texture thicknesses per well 39
5. Sand body versus total sediment ratios (net-to-gross) in wells using Vshale values, and density-porosity compilations 45
6. Well hydraulic conductivity (K), TDS, and age data 50

Appendices

1. Consultant reports whose data were used in this study.
2. Tabulation of well data generated in this study or compiled from previous studies.
3. Description of cuttings data for select Rio Rancho wells.
4. Well logs used in this study, illustrated by graphics produced by Kingdom software.
5. Lithologic texture picks per well and thickness compilation.
6. ArcGIS geodatabase and related ArcPro project used for 3D model construction.
7. Subsurface mapping methods and details regarding the methodology of making the 3D hydrostratigraphic model.
8. Tephrochronologic data and related interpretation for the ash bed found at 2,070–2,080 ft depth in well RRU-18.
9. Results from the study of outcrop faces of the upper Zia HSU and Middle Rio Rancho HSU.

Appendix files are available for download at **https://geoinfo.nmt.edu/publications/openfile/details.cfml?Volume=635**

Plates

1. Elevation of the top of the Upper Rio Rancho HSU
2. Elevation of the top of the Middle Rio Rancho HSU
3. Elevation of the top of the Lower Rio Rancho HSU
4. Elevation of the top of the Zia HSU
5. Thickness of the Upper Rio Rancho HSU
6. Thickness of the Middle Rio Rancho HSU
7. Thickness of the Lower Rio Rancho HSU
8. Thickness of the Zia HSU
9. Elevation of the top of the saturated part of the Upper Rio Rancho HSU
10. Elevation of the top of the saturated part of the Middle Rio Rancho HSU
11. Elevation of the top of the saturated part of the Lower Rio Rancho HSU
12. Elevation of the top of the saturated part of the Zia HSU
13. Saturated thickness of the Upper Rio Rancho HSU
14. Saturated thickness of the Middle Rio Rancho HSU
15. Saturated thickness of the Lower Rio Rancho HSU
16. Saturated thickness of the Zia HSU
17. HSU units present at the potentiometric surface

Plate figures are available for download at
https://geoinfo.nmt.edu/publications/openfile/details.cfml?Volume=635

EXECUTIVE SUMMARY

The purposes of this study were to delineate and map subsurface hydrostratigraphic units (HSU) within the Santa Fe Group aquifer found in the northwestern part of the Albuquerque Basin, and to assess the permeability differences between and within those units. A hydrostratigraphic unit is a zone in an aquifer that has unique physical properties pertaining to groundwater, such as permeability, porosity, yield, or hydraulic conductivity. In our study, four HSUs, corresponding to stratigraphic layers typically hundreds to thousands of feet thick (>100 m thick), could be correlated across the study area using subsurface data in 41 wells (i.e., cuttings logs and wireline logs that included resistivity, neutron, and gamma-ray data). These HSUs (with their lithostratigraphic counterparts in parentheses, per Connell, 2008a) are the Upper Rio Rancho HSU (Ceja Formation plus the Picuda Peak Member of the Arroyo Ojito Formation), Middle Rio Rancho HSU (Loma Barbon and Navajo Draw Members of the Arroyo Ojito Formation and Benavidez unit of Koning et al., 2021), Lower Rio Rancho HSU (upper, sand-dominated part of the Cerro Conejo Formation), and Zia HSU (lower–middle Cerro Conejo Formation plus all of the Zia Formation, extending down to bedrock).

Three-dimensional mapping of the Santa Fe Group aquifer entailed constructing stacked raster surfaces corresponding to the bounding surfaces of the HSUs. Contours of each HSU surface were drawn manually in ArcMap GIS software. We began contouring a given HSU surface where it was exposed in escarpments near La Ceja and Ceja del Rio Puerco, and we extrapolated the contact into the subsurface (southward and eastward) using available map attitude data and HSU elevation picks in the 41 wells. Major faults were explicitly incorporated into the 3D mapping, and HSU contacts were offset by fault lines using displacements inferred from cross sections or from geologic mapping. This procedure was employed for the tops of the Zia HSU, Lower Rio Rancho HSU, and Middle Rio Rancho HSU; the top of the Upper Rio Rancho HSU corresponds to surface topography. We used a raster of the top of bedrock (constructed by Grauch and Connell, 2013, given to us by V.J.S. Grauch) for the base of the Zia HSU. The contours and elevations of the HSU contacts at the 41 wells were used as inputs in the Topo to Raster ArcGIS tool, whose output for each contact is a raster image with 50-m grid spacing.

To determine the extent and thickness of saturated zones within each HSU, the approximate potentiometric surface was mapped using groundwater level measurements from 58 wells across the study area, where water levels were measured from 1985 to 2021, with most data collected from 2008 to 2021. In order to cover the entire study area, seven water level measurements were included near the northern and western boundaries of the study area that date between 1956 and 1984. The groundwater elevation data from these wells were contoured in ArcMap and then converted to a raster image using the Topo to Raster ArcGIS tool.

The saturated tops and bases of each HSU needed to be determined in order to map saturated thicknesses in each HSU. To calculate the saturated thickness of a given HSU, the saturated base of the HSU was subtracted from its saturated top or, where the top was not saturated, the sloping potentiometric surface within the HSU.

We produced elevation-contour maps for the tops of the HSUs and the tops of the saturated zone within an HSU. In addition, we provide a 3D visualization of the Santa Fe Group by stacking the HSU

raster surfaces and incorporating the potentiometric surface in this visualization. These products and the detailed investigation of well logs support the following interpretations: (1) HSUs and saturated HSUs thicken eastward across the Zia and San Ysidro faults. (2) East of the Zia fault, both HSUs and saturated HSUs thicken southward and southeastward, becoming thickest in the southeast corner of the study area (near the intersection of Paseo del Norte and Coors). (3) Relatively thickened HSUs, most notably the Middle Rio Rancho HSU, extend northward in the Montoyas graben (new name proposed in this work; this structure approximately coincides with the upper reaches of Arroyo de los Montoyas and Arroyo de las Calabacillas) that is bounded on the west by the Zia fault and on the east by the Coronado-Alameda fault and Ziana horst. (4) The Upper and Middle Rio Rancho HSUs (and saturated HSUs) become thinner eastward across a geologic structure called the Ziana horst and pinch out northward on this structure. (5) To the east of the Tamaya fault, the Upper and Middle Rio Rancho HSUs thicken under the city of Bernalillo. (6) The Middle Rio Rancho HSU commonly displays a coarsening-upward trend. (7) The apparent lack of notable thinning of the Lower Rio Rancho HSU across the Ziana horst, coupled with 500–1,000 ft (150–300 m) of apparent vertical displacement of an 11.3–11.2 Ma ash zone by a fault bounding the east side of the horst, indicates notable tectonic activity associated with the horst after 11 Ma. In addition, thinning of the Upper and Middle Rio Rancho HSUs across the Ziana horst and thickening in the Montoyas graben indicate late Miocene, tectonically controlled stratal thickening.

Permeability assessments were conducted using three methods. The first entailed outcrop mapping of the two HSUs that have aboveground vertical faces: the upper Zia HSU (i.e., lower–middle Cerro Conejo Formation) and the Middle Rio Rancho HSU (Arroyo Ojito Formation). The outcrop mapping was conducted on base imagery consisting of stitched, high-resolution photographs taken by uncrewed aerial vehicles. Two outcrops of the upper Zia HSU and four outcrops of the Middle Rio Rancho HSU were analyzed. Contacts separating sand versus clayey sediment (clayey sand or clay-silt beds) were delineated in this imagery using ArcMap GIS software, and various ArcGIS tools were used to calculate the 2D proportion of the following permeability proxies: sand versus clayey sand in a given image, sand body thicknesses, and the amalgamation ratio (length of sand-on-sand contacts versus total contact lengths). These analyses suggest slightly more favorable permeability proxies in the upper Zia HSU compared to the Middle Rio Rancho HSU. We infer that the relatively restricted spatial extent of this method, particularly in terms of the proportion of the studied stratigraphic interval relative to the thickness of the entire unit, imparts higher uncertainty in this approach, especially vertical trends, compared to various permeability-related data in wells.

The second permeability assessment consisted of detailed differentiation of sand versus clayey sediment in 22 wells (interpreted from wireline logs with the aid of cuttings) for stratigraphic intervals in the saturated part of HSUs. The resulting data indicate that the highest non-clayey sediment (i.e., clean sand) ratios are in the Upper Rio Rancho HSU and Lower Rio Rancho HSU. Assuming that clay-poor sediment is a proxy for higher permeability, this analysis suggests higher permeability for the Upper and Lower Rio Rancho HSUs compared to the other two HSUs.

The third permeability assessment involved compiling hydraulic conductivity and specific capacity values from pumping tests for wells that were screened in more than 80% of either the Upper, Middle, or Lower Rio Rancho HSUs. Pumping test data were lacking for the Zia HSU. We plotted these values per HSU on a box-and-whisker plot to compare differences between HSUs. We also plotted the hydraulic conductivity (K) values on a map to visually compare any spatial trends within an HSU. These analyses indicate that the Upper Rio Rancho HSU generally exhibits higher K values than the Middle Rio Rancho HSU, although there is appreciable overlap in values. The median K value for the Upper Rio Rancho HSU is 9.25 ft/day, and the median K value for the Middle Rio Rancho HSU is 3.25 ft/day. Also, about 50% of the K values of the Upper Rio Rancho HSU are higher than the

maximum range of the Middle Rio Rancho HSU (excluding outliers). More overlap occurs when comparing specific capacities, and the associated median values are 10.5 gallons per minute (gpm)/ft (Upper) and 8.5 gpm/ft (Middle). The interpretation that the Upper Rio Rancho HSU is generally more permeable than the Middle Rio Rancho HSU is consistent with its higher sand proportions (at a given location) and higher density-porosity values in its sand bodies (the latter probably reflecting less compaction and less cementation). Based on a single pumping test (Rio Rancho Utility [RRU] Well 23), the Lower Rio Rancho HSU may also have relatively high hydraulic conductivity, consistent with the second permeability assessment results, but more pumping test data are needed to confirm that possibility. No lateral permeability trends were apparent in the Upper Rio Rancho HSU. In the Middle Rio Rancho HSU, pumping test data suggest higher hydraulic conductivity values in the southwestern part of the study area, west of the west end of Paseo del Norte. We speculate that these higher conductivity values may reflect coarse sand tongues associated with the Benavidez unit of Koning et al. (2021), a sandy Santa Fe Group lithostratigraphic unit derived from the erosion of a thick, gravelly sand layer that once capped the southeastern Colorado Plateau. North of approximately 35°20′0″ north latitude, there may possibly be a northward lateral trend in the Middle Rio Rancho HSU of increasing sand concentrations and higher permeabilities, but more data are needed to confirm this trend.

To better understand groundwater quality and recharge, we compiled radiocarbon ages and total dissolved solids (TDS) measurements for each well from previous studies (Plummer et al., 2004a, 2004b, 2004c). Wells with elevated TDS are spatially associated with the Ziana horst and possibly the Lower Rio Rancho HSU, suggesting the possibility that faults bounding the horst may be expelling salty groundwater from fractured, structurally elevated bedrock; similar expulsion may adversely affect the Lower Rio Rancho and Zia HSUs across the study area. Radiocarbon ages are oldest in the northwestern part of the study area (in the Middle Rio Rancho HSU) and youngest in the southeast corner of the study area near the Rio Grande (in the Upper Rio Rancho HSU). Given the westward slope of the potentiometric elevation surface in the southeast corner of the study area, these data suggest a component of recharge to the Upper Rio Rancho HSU from the Rio Grande. In contrast, a deep potentiometric surface and radiocarbon ages greater than 20,000 years in the northwestern study area, west of the Zia fault and near well RRU-9, suggest low rates of groundwater recharge via deep and long groundwater flow paths, likely in bedrock.

Collectively, our study's HSU mapping data provide guidance regarding groundwater management for the Santa Fe Group aquifer in the Rio Rancho area. Building on the hydrochemical zones of Plummer et al. (2004a, 2004c), we propose five hydrogeologic regimes based on groundwater chemistry, inferred groundwater flow direction, and faults that appear to impact groundwater flow. Even though the groundwater is of relatively good quality in the Middle Rio Rancho HSU in the western and northwestern parts of the study area (in the northern West-Central hydrogeologic regime of this report), it is of limited quantity and located several hundred feet below the ground surface; in addition, old radiocarbon ages and notable cones of depression suggest relatively low permeabilities (or fault barriers) in the Middle Rio Rancho HSU and limited recharge to that area. The higher TDS values found near the Ziana horst (Ziana hydrogeologic regime) are a deterrent for future well drilling there unless economic desalination or blending with fresher water can be achieved. The area east of the Ziana horst and in the southern part of the study area, east of approximately Universe Boulevard (Central zone of Plummer et al., 2004a, 2004c), coincides with the thickest saturated HSUs, including the high-permeability Upper Rio Rancho HSU, and exhibits relatively low TDS and young radiocarbon ages. These two areas are interpreted to be the most favorable for groundwater extraction. Our 3D hydrostratigraphic model and compiled hydraulic conductivities can be used in future studies pertaining to groundwater flow and management in the northwestern Albuquerque Basin.

INTRODUCTION

PURPOSE

The purpose of this study was to delineate hydrostratigraphic units (HSU) in the Santa Fe Group of the northwestern Albuquerque Basin and map these units in the subsurface. We also assessed permeability differences between HSUs and laterally within a given HSU using pumping test hydraulic conductivities and permeability proxies; these proxies include sediment texture (i.e., proportion of clay), sand body thickness, and sand body amalgamation ratios. The following were constructed as ancillary products: an approximate groundwater elevation (potentiometric surface) map and depth-to-groundwater map, a map of compiled total dissolved solids (TDS) values (for each well and HSU), and a map of compiled radiocarbon ages (for each well and HSU). The study was initiated and paid for by the City of Rio Rancho so the city may more effectively plan future well sites and manage groundwater resources.

STUDY AREA

The study area is located in the northwestern part of the Albuquerque Basin, approximately 30–45 mi (~50–70 km) northwest of downtown Albuquerque (Fig. 1). It is underlain by variable thicknesses of the Santa Fe Group, which consists of sand-dominated, clastic sediment intercalated with minor volcanic rocks. The Santa Fe Group aggraded in the Rio Grande rift while the rift was subsiding during the late Oligocene through the early Pleistocene (Spiegel and Baldwin, 1963; Chapin and Cather, 1994). The study area includes the City of Rio Rancho and extends several miles northward and westward from the municipality's northern and western boundaries, respectively (Fig. 2). The placement of the western and northern study area boundaries allows mapped outcrops of exposed HSUs to be incorporated into the 3D map of these units. Important wells used in our study and major faults are plotted on the study area map of Figure 2.

Much of the study area is underlain by a mesa-like feature called the Llano de Albuquerque (Fig. 1). The west and north sides of the "Llano" correspond to steep slopes and badlands called Ceja del Rio Puerco and La Ceja (Fig. 1). This badland topography grades westward and northward into the broad valley floors of the Rio Puerco and Jemez River, respectively. The Llano de Albuquerque slopes eastward toward the Rio Grande, which is along the eastern border of the study area.

PREVIOUS WORK

Investigation of the geologic history of the northwestern Albuquerque Basin began in the mid-1900s, but it accelerated in the 1990s and continues to this day. The earliest investigations of the Santa Fe Group recognized three main stratigraphic units: the upper buff, middle red, and lower gray members within the Santa Fe Formation (Bryan and McCann, 1937, 1938; Wright, 1946; Spiegel, 1961; Connell, 2008a). Note that the Santa Fe stratigraphic unit was originally a formation rank but was raised to group rank by Spiegel and Baldwin (1963); however, this change was not universally accepted until the 1980s. The lower gray unit was renamed the Zia Formation (Galusha, 1966) and subdivided into three members (in ascending order): Piedra Parada, Chamisa Mesa, and Cañada Pilares (Galusha, 1966; Gawne, 1981; Tedford, 1982; Tedford and Barghoorn, 1999). The stratigraphic nomenclature of Kelley (1977) proposed formalizing two members within the Santa Fe Formation: the Ceja Member (formerly the upper buff member) and Zia Member (downgrading the Zia Formation of Galusha [1966] to member status). Black and Hiss (1974) made inferences regarding stratigraphy and structure from a deep oil well in the study area, the Shell Oil Co. Santa Fe Pacific No. 1 test well, including the first documentation of the Ziana horst (which they referred to as the Ziana anticline).

Intensive geological and geophysical investigations began during the early 1990s and continued through 2000 to 2010, contemporaneous with the drilling of deep water wells in and near the city of Rio Rancho and in western Albuquerque (Appendix 1[1]; Allen et al., 1998; Connell et al., 1998). An important component of these investigations was 1:24,000-scale geologic mapping (Cather et al., 1997; Connell, 1997; Koning et al., 1998; Personius et al., 2000; Koning and Personius, 2002; Personius, 2002; Thompson et al., 2009) that was synthesized and compiled at lower scales by Connell (2008b) and Williams and Cole (2007). Graduate student investigations of the sedimentology and petrography of the Santa Fe Group in the northwestern Albuquerque Basin include Lozinsky (1988, 1994), Gillentine (1994), Brandes (2002), and Smyth (2004). Interpretations of Santa Fe Group strata encountered in a deep oil well in the study area (the Tamara No. 1-Y well) are presented in Connell et al. (2001). Relatively up-to-date treatments of the lithostratigraphy of Santa Fe Group strata in the study area are given in Connell et al. (1999, 2007) and Connell (2008a). Thorough treatments of the geologic history of the Albuquerque Basin, including age control, are provided in Connell (2004) and Connell et al. (2013). Geophysical interpretations of the basin's geologic structure include those containing seismic data (May and Russell, 1994; Russell and Snelson, 1994), aeromagnetic data (Grauch, 1999; Grauch et al., 2001), and gravity data (Grauch et al., 1999). An essential publication of Albuquerque Basin structure that integrates geophysical data and well interpretations is Grauch and Connell (2013).

1 Appendix files are available for download at https://geoinfo.nmt.edu/publications/openfile/details.cfml?Volume=635.

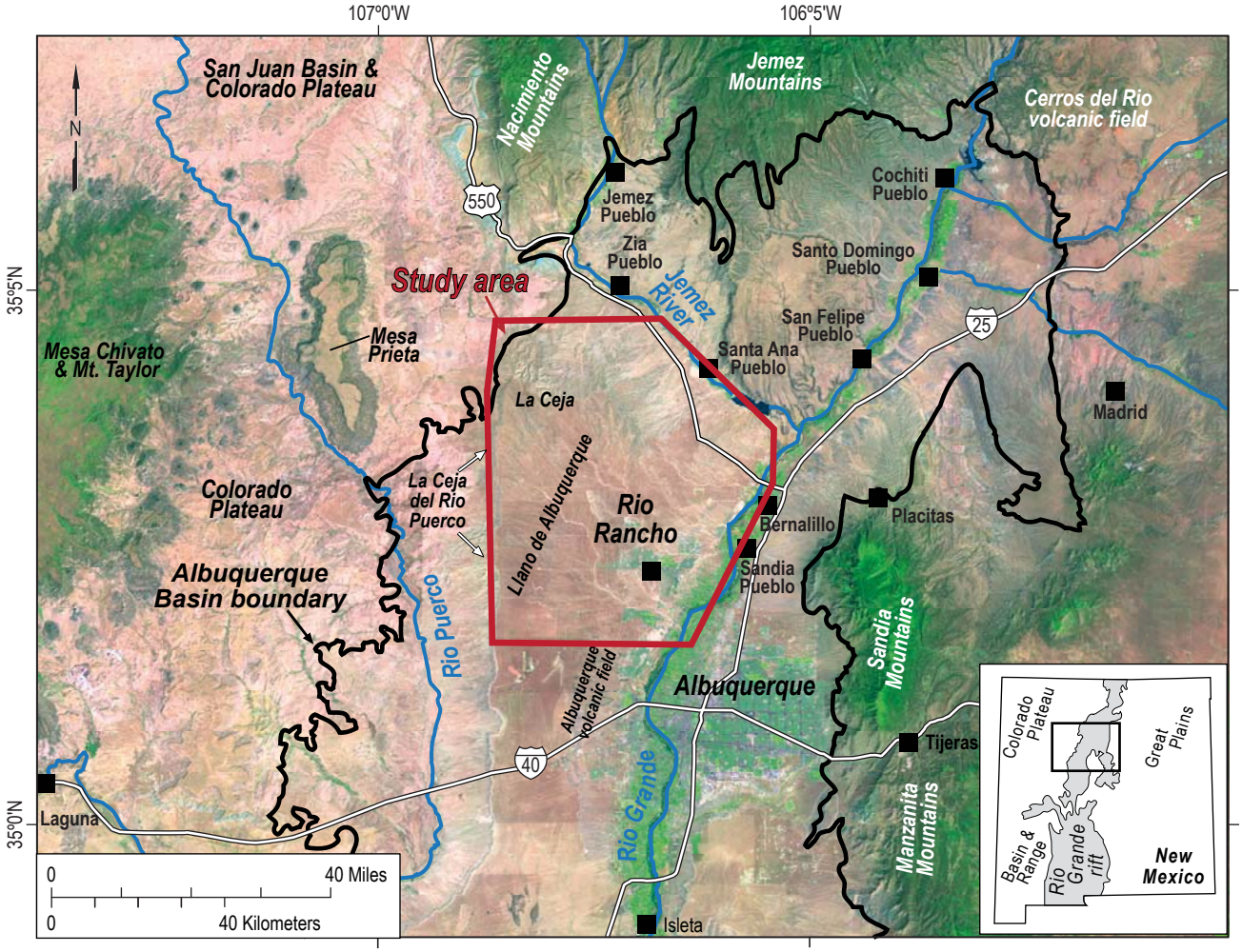

Figure 1. Location of the study area within the larger Albuquerque Basin. Interstates and highways are depicted as thick white lines and rivers as thick blue lines. The basin boundary is shown by the thick black line.

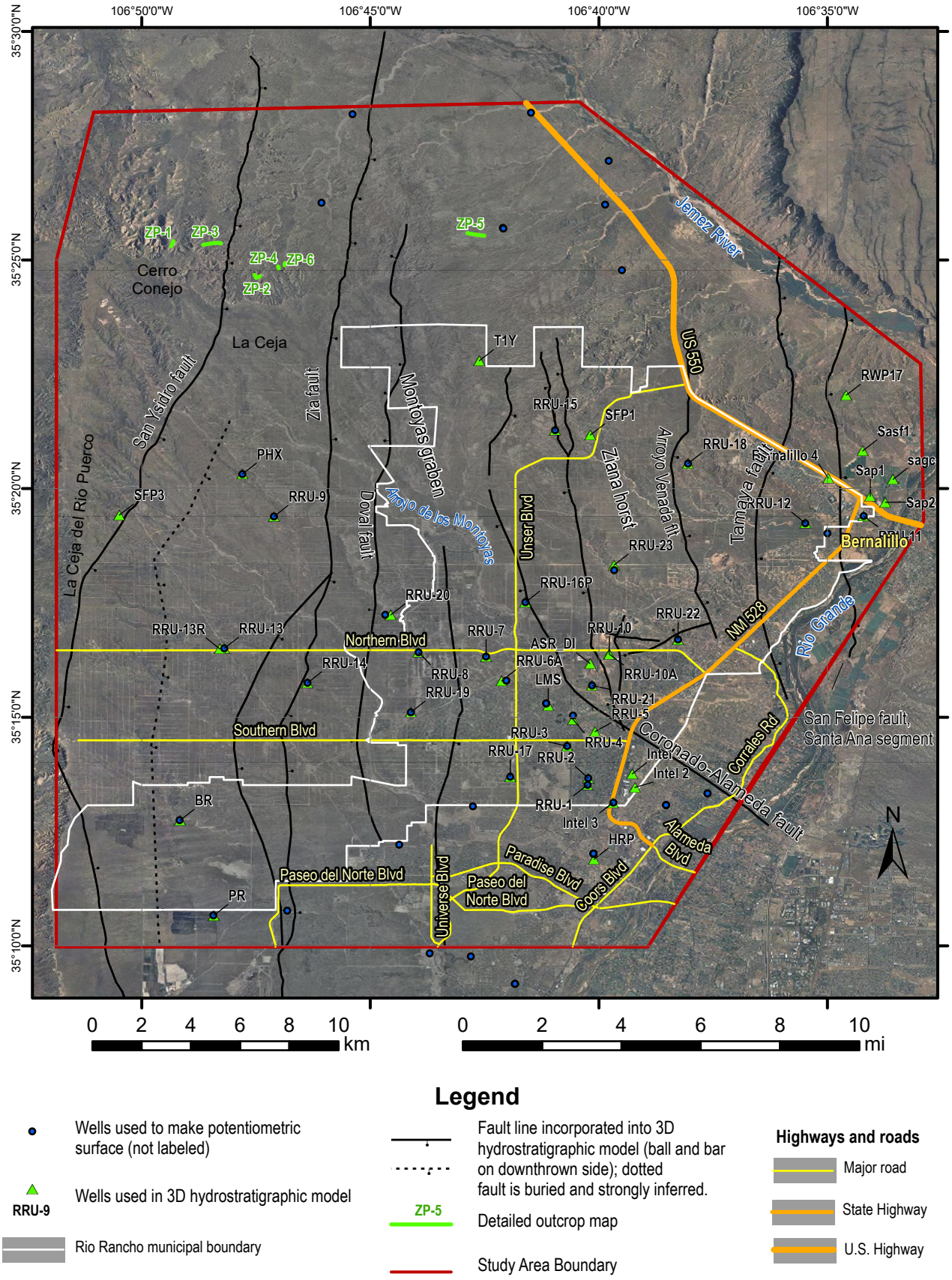

Legend

- Wells used to make potentiometric surface (not labeled)
- RRU-9 — Wells used in 3D hydrostratigraphic model
- Rio Rancho municipal boundary
- Fault line incorporated into 3D hydrostratigraphic model (ball and bar on downthrown side); dotted fault is buried and strongly inferred.
- ZP-5 — Detailed outcrop map
- Study Area Boundary

Highways and roads

- Major road
- State Highway
- U.S. Highway

Figure 2. Map of the study area with a satellite imagery background. Select highways and roads are shown, along with important wells and faults. See Figure 4 for fault names. Figures 10 and 11 label the wells used to make the potentiometric surface.

Mapping and paleoseismic data of Quaternary faults were compiled by Machette et al. (1998), and fault data from the Quaternary Faults and Folds Database were used in our study (**https://earthquakes.usgs.gov/hazards/qfaults**). Studies of fault zone architecture in the Santa Fe Group in or near the study area include Minor and Hudson (2006), Caine and Minor (2009), Rawling and Goodwin (2006), and Rawling et al. (2001). Recent geologic mapping efforts have focused on the Rio Puerco Valley and the well-exposed badlands between Ceja del Rio Puerco and the Rio Puerco (Cikoski et al., 2012; Koning and Jochems, 2014; Koning and Rawling, 2017). Subsurface mapping of lithostratigraphic units that approximated hydrostratigraphic units was conducted east and southeast of Rio Rancho (Koning et al., 2019), which informed our structural contouring efforts in the southeast corner of the study area.

Detailed groundwater investigations in the northwestern Albuquerque Basin generally began in conjunction with the accelerated growth of Rio Rancho during the early 1990s. Most of these investigations involved evaluating newly drilled wells or planning new wells for the city (Appendix 1) or for northwestern Albuquerque (Allen et al., 1998; Connell et al., 1998). Comprehensive investigations of the hydrogeologic framework of the Albuquerque Basin were initiated by Hawley and Haase (1992), Hawley et al. (1995), Hawley (1996), and Thorn et al. (1993). Groundwater temperature and hydrothermal studies were conducted by Reiter (2001, 2003).

The U.S. Geological Survey conducted many noteworthy hydrogeologic studies in the Albuquerque Basin during the 1990s and 2000s. These efforts included early groundwater flow modeling in the basin (Kernodle and Scott, 1986; Kernodle et al., 1987, 1995; Kernodle, 1998). The U.S. Geological Survey also spearheaded several geochemistry investigations: Sanford et al. (2004a, 2004b), Plummer et al. (2001, 2004a, 2004b, 2004c), Bexfield and Plummer (2003), and Bexfield et al. (1999). Plummer et al. (2004a, 2004b, 2004c) used a variety of geochemical data to map various groundwater hydrochemical zones for the upper 2,000 ft (600 m) of the Santa Fe Group aquifer system. Groundwater level maps include those of Bexfield and Anderholm (2000, 2002), which indicated a curious north-south groundwater low (trough) feature west of the Rio Grande. These studies were used to make updated groundwater flow models relevant to our study area (McAda and Barroll, 2002; Bexfield et al., 2004) and an assessment of groundwater resources (Bartolino and Cole, 2002). Minor and Hudson (2006) investigated how faults in the northwestern Albuquerque Basin affect groundwater flow.

A consultant report by Glorieta Geoscience, Inc. (Riesterer et al., 2004) is particularly relevant to our study (Appendix 1). Riesterer et al. (2004) used available data from 35 production wells and piezometers to determine if there were geologic controls on well production and water quality. If so, these could be used to identify the most promising areas for future groundwater production. This effort involved making a structural contour map of the upper, middle, and lower subdivisions of the Santa Fe Group (per Hawley and Kernodle, 2000). Riesterer et al. (2004) concluded that the most important factors influencing well production were well depth and total length of screen, regardless of geologic unit or proximity to faults. Arsenic did not vary in a predictable manner, and water quality did not seem to decline with depth (up to 2,500 ft [760 m]). Other consultant reports from which we derived data for our study (such as pumping test and chemical data) are listed in Appendix 1.

ORGANIZATION OF REPORT

This open-file report is organized as follows. First, we provide the geologic setting of the study area, including the geologic structure and stratigraphy of the Santa Fe Group. Because it is used in many of the later analyses, how we constructed the potentiometric surface is discussed. We then treat the three main topics in our study: (1) 3D mapping of the Santa Fe Group aquifer (including mapping the tops of the HSUs, mapping the tops of the saturated parts of the HSUs, and creating associated isopach maps), (2) assessing permeability differences between and within HSUs, and (3) a preliminary treatment of spatial differences in total dissolved solids (TDS), which may be considered as an approximate groundwater quality proxy, as well as the spatial distribution of radiocarbon ages. For each of the three main topics, we include a methods and results section.

GEOLOGIC SETTING OF THE STUDY AREA

GEOLOGIC STRUCTURE

The study encompasses much of the northwest corner of the Albuquerque Basin (Fig. 1), one of the largest and deepest basins of the Rio Grande rift (Grauch and Connell, 2013). The Albuquerque Basin can be subdivided into three subbasins (listed from north to south): the Santo Domingo, Calabacillas, and Belen subbasins (Fig. 3, reproduced from Grauch and Connell, 2013). The overall geometry of the Calabacillas subbasin is asymmetrical, deepening eastward toward major west-down faults near the foot of the Sandia Mountains (Grauch and Connell, 2013). Two large-displacement, east-down, north-striking normal faults are present in the western part of the study area: the San Ysidro and Zia faults (Fig. 4). A graben lies between the Zia fault and the Ziana horst block (the horst is discussed below), merging to the south-southeast with the deeper portion of the Calabacillas subbasin (Grauch and Connell, 2013). We informally refer to this graben as the "Montoyas graben" after the nearby geographic feature of Arroyo de los Montoyas (Figs. 3 and 4). The graben is structurally deepest between the Zia fault and the west-down Doval fault.

An important structural feature in the northwestern Albuquerque Basin, found in the northeastern part of the study area, is the south-plunging Ziana horst block, located east of the Montoyas graben (Figs. 3 and 4). Note that this feature was previously referred to as an anticline (Black and Hiss, 1974), but detailed mapping indicates that the term "horst" is more appropriate in the southern part of the structure (Personius et al., 2000). We use "horst" in this report since it is clearly bounded on both sides by oppositely dipping faults, even though to the north the structure is folded into an anticline geometry (Koning and Personius, 2002; Riesterer et al., 2008, cross section B–B´). The Ziana horst is bounded on the west by the west- to southwest-down Coronado-Alameda fault and on the east by a series of east-down, north-striking normal faults (listed from west to east): the Arroyo Venada, Tamaya, and San Felipe faults (Fig. 4). Southeast of the Ziana horst block, gravity data (Grauch and Connell, 2013) indicate a subdued structural high that extends southeastward to the northern part of the Sandia Mountains. The Ziana horst and this southeast-trending structural high separate the Calabacillas subbasin from the Santo Domingo subbasin to the north and northeast (Fig. 3).

The way layered rock is tilted (described by stratal strikes and dips) is critical for producing the 3D geologic model in this project; data on stratal geometries were obtained from previous geologic mapping (Fig. 4). Mapped strata dip 3–8° east on the footwall (west side) of the San Ysidro fault (Cather et al., 1997; Connell, 2008b). In the escarpment north of La Ceja, east of the Zia fault, strata have a strong southward component of dip (Koning et al., 1998; Koning and Personius, 2002; Connell, 2008b). Dips shallow (fan) upsection north of La Ceja between the San Ysidro and Zia faults, from 5–7° S to 0–2° S between the Cerro Conejo Formation and the top of the Arroyo Ojito Formation (Koning et al., 1998). On the western flank of the Ziana horst, strata mostly strike north-northwest and dip 5–10° west-southwest. East of the Ziana horst, strata dip to the south and have northwest, west, or southwest strikes (Connell, 2008b). The complete structural picture of the study area is obtained by structural contouring of contacts using these attitudes and well picks and will be discussed in one of the Results sections of this report.

SANTA FE GROUP LITHOSTRATIGRAPHY AND HYDROSTRATIGRAPHIC UNITS

Connell et al. (1999) synthesized investigations of the Santa Fe Group exposed north and west of Rio Rancho, particularly the geologic mapping of Cather et al. (1997) and Koning et al. (1998).

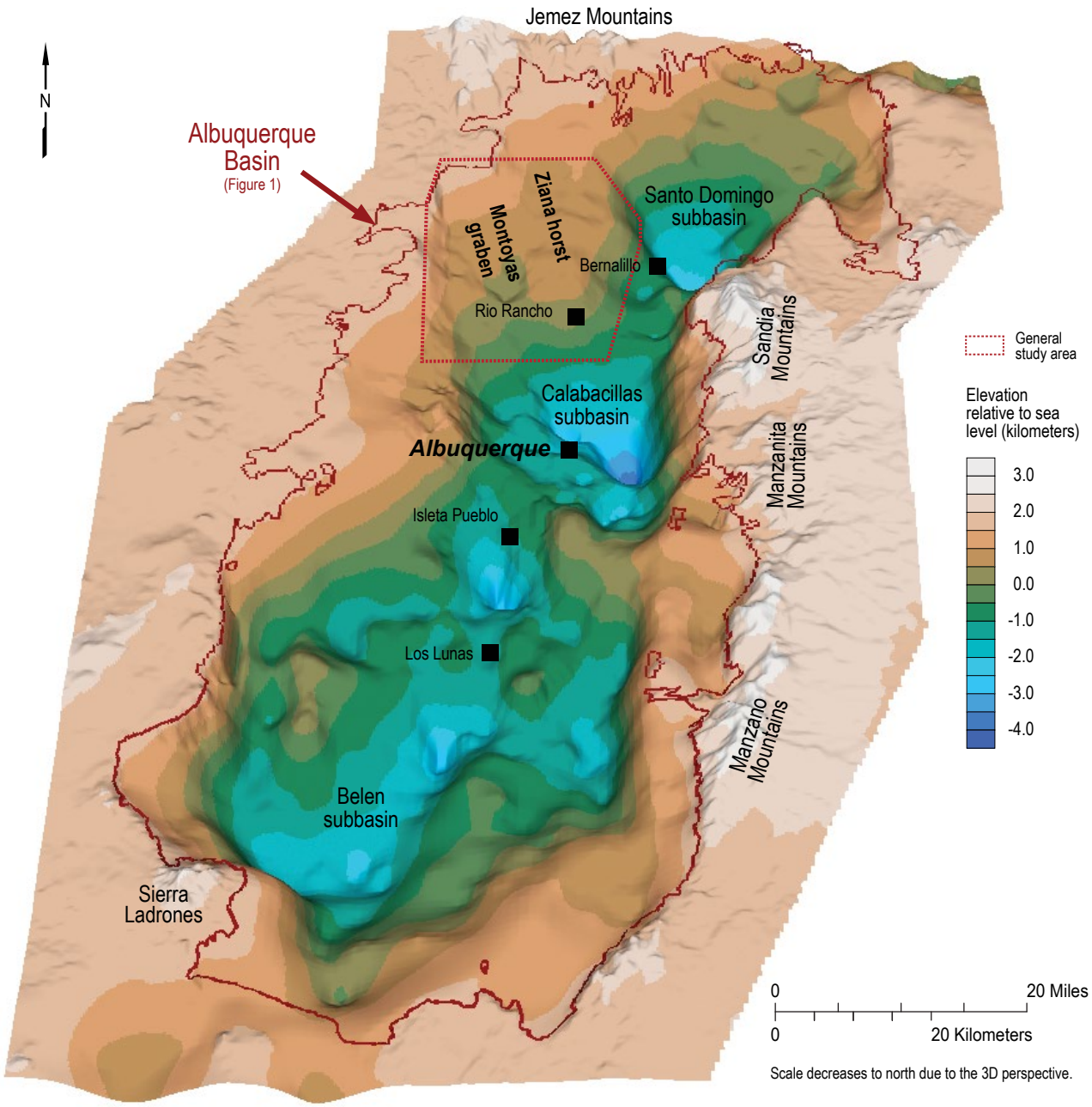

Figure 3. Three-dimensional image illustrating the geologic structure of the Albuquerque Basin. The image shows what the Albuquerque Basin would look like if the rift sediment (Santa Fe Group) were removed, effectively revealing the shape (geometry) of the top of the underlying bedrock. Note the variation in the depth to bedrock due to rift tectonic activity. The study area is on the northwest side of the Calabacillas subbasin, which deepens southeastward and eastward toward the Sandia Mountains. The image is very slightly modified from Grauch and Connell (2013).

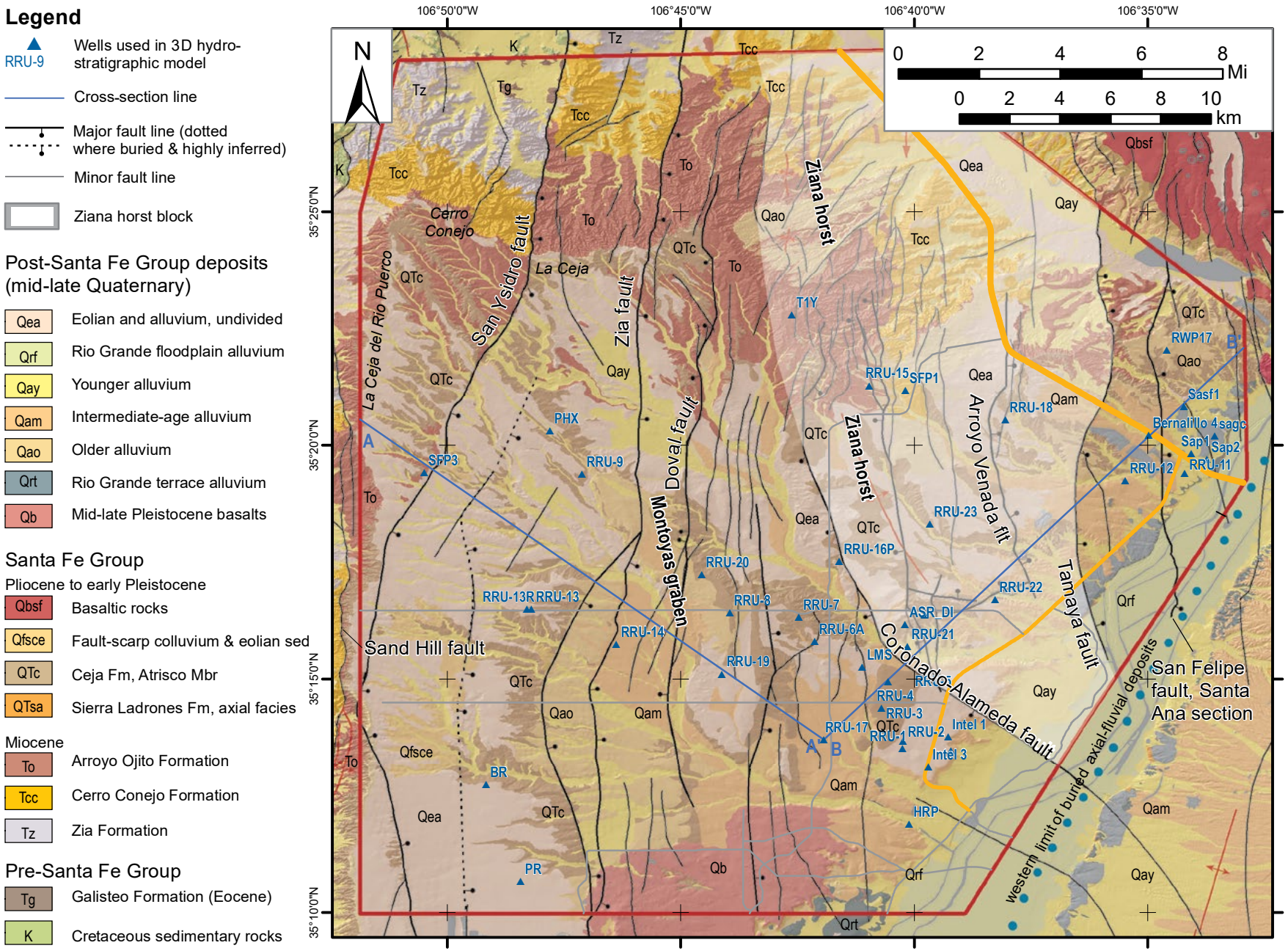

Figure 4. Geologic map of the study area, modified from Connell (2008a). Annotated blue lines are locations of cross sections A–A´ and B–B´ (Fig. 20). The Ziana horst block is shown by the white shade.

Revisions of the Santa Fe Group nomenclature across the Albuquerque Basin were published in Connell (2008a). A slightly different stratigraphy was proposed by Williams and Cole (2007). We follow the stratigraphic scheme of Connell (2008a) and summarize its lithostratigraphic units below, in addition to discussing how hydrostratigraphic units relate to the lithostratigraphic units. Note that the terms "formation" and "members" relate strictly to lithostratigraphy, where rock units are recognized by physical attributes such as composition, texture, and color. A hydrostratigraphic unit, in contrast, is a zone (a layer in this study) in an aquifer that has unique physical properties pertaining to groundwater, including permeability, porosity, yield, or hydraulic conductivity. The Santa Fe Group sequence hosting both types of stratigraphic units is particularly well exposed north of La Ceja (Fig. 5) and west of Ceja del Rio Puerco. Figure 6 relates Santa Fe Group lithostratigraphic units to the hydrostratigraphic units devised in this study.

Zia Hydrostratigraphic Unit (Zia Formation, lower–middle Cerro Conejo Formation)

The lowest formation in the Santa Fe Group is a 300- to 3,000-ft-thick (90–900 m), sand-dominated succession called the Zia Formation (Fig. 6). We include all of the Zia Formation, plus the lower–middle Cerro Conejo Formation, in the Zia HSU (Fig. 6). The lowest unit of the Zia Formation, the Piedra Parada Member (Galusha, 1966), is primarily a medium- to coarse-grained, light-gray sandstone that is commonly cross-stratified (Fig. 7A); it ranges in thickness from 50 to 260 ft (15–80 m) near La Ceja to 1,280 ft (390 m) in the Santa Fe Pacific No. 1 well on the Ziana horst. The overlying Chamisa Mesa Member (Galusha, 1966), 100–125 ft (30–35 m) thick west of the



Figure 5. Photograph of well-exposed badlands north of La Ceja. Cabezon Peak is on the skyline to the left. Two HSUs are separated by the San Ysidro fault: the Middle Rio Rancho and Zia HSUs. The Middle Rio Rancho HSU includes two lithostratigraphic units of the Arroyo Ojito Formation: the Loma Barbon and Navajo Draw Members, whose respective strata (Tob and Ton) are labeled in the photograph. In addition to differences in gravel composition, the Loma Barbon Member is slightly redder compared to the pale yellowish colors of the Navajo Draw Member (Connell et al., 1999). Two lithostratigraphic units of the upper Zia HSU are labeled as Tcc (lower–middle Cerro Conejo Formation) and Tzcm (Chamisa Mesa Member of Zia Formation). Correlation of lithostratigraphy to hydrostratigraphy is given in Figure 6. Many of our outcrop study sites are located in this area. In addition, lithostratigraphic contacts corresponding to HSU boundaries were projected southward from here into the subsurface. The land is owned by Zia Pueblo, and permission is required before entry. Photograph is used with permission from Zia Pueblo.

San Ysidro fault, is a light reddish-brown to buff-colored, very fine- to medium-grained sandstone and silty sandstone (Fig. 7B) typified by medium to very thick, tabular beds that locally contain rhizoliths. West of Ceja del Rio Puerco, the highest unit of the Zia Formation is the 100-ft-thick (30 m) Cañada Pilares Member (Gawne, 1981), which is characterized by reddish-brown clay that interfingers with very fine- to medium-grained sand tongues along its margins (Fig. 7B). These three members are interpreted to reflect a succession of the following paleoenvironments: eolian and high-energy alluvial, distal piedmont slope, and playa and playa margins (Gawne, 1981; Tedford and Barghoorn, 1999; Koning and Jochems, 2014; Koning and Rawling, 2017). Available age control indicates a range of 22–16 Ma (Tedford and Barghoorn, 1999). The upper contact of the Zia Formation is a major unconformity or a compressed stratigraphic section west of the Zia fault, but it is likely conformable on the southern hanging wall (east side) of the fault, particularly south of the latitude corresponding to the Ziana horst.

The lower–middle Cerro Conejo Formation is assigned to slightly reddish to orangish, tabular-bedded, mainly fine- to medium-grained sandstone and silty to muddy sandstone that locally form prominent ledges (Fig. 7C), particularly near the Ceja del Rio Puerco and north of Cerro Conejo (Fig. 4). The entire Cerro Conejo Formation is 1,037 ft (316 m) thick north of La Ceja (where its type section is located; Connell et al., 1999) and 650–800 ft (200–250 m) thick west of Ceja del Rio Puerco (Koning and Jochems, 2014; Koning and Rawling, 2017). The formation likely thickens south and east of these exposures, respectively. The lower–middle Cerro Conejo Formation is 15 to around 12 Ma where exposed above the aforementioned unconformity (Connell et al., 1999; Connell, 2004, 2008a), but the age of the formation's basal strata likely increases toward the southeast toward the depocenter of the Albuquerque Basin.

In well data, it is not possible to confidently pick the base of the Cerro Conejo Formation. However, the upper, sandy fluvial unit of the Cerro Conejo can be differentiated in well data. Thus, the lower–middle Cerro Conejo Formation is lumped with the Zia Formation in our mapping of HSUs, but the upper Cerro Conejo is assigned its own HSU (i.e., the Lower Rio Rancho HSU; Figs. 6 and 7D).

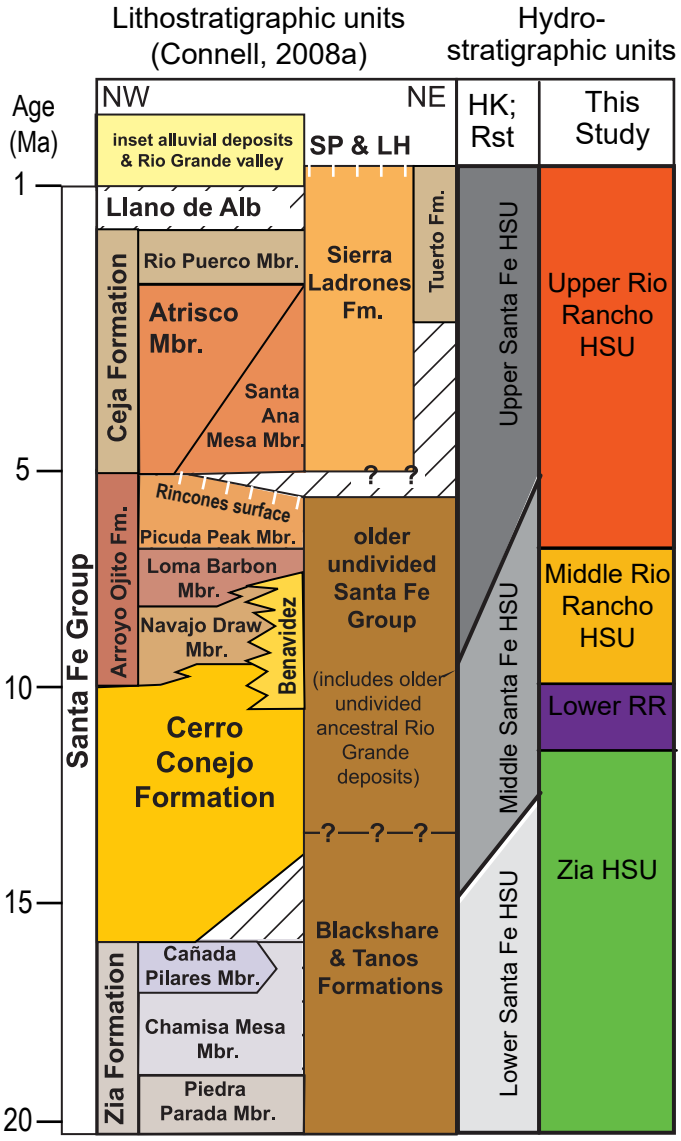

Notes:
Ma = age in millions of years
HK: Hawley and Kernodle (2000)
Rst: Riesterer et al. (2004)
SP & LH: Sunport and Las Huertas geomorphic surfaces

Figure 6. Lithostratigraphic nomenclature of and its correlation to the hydrostratigraphic units used in previous studies and this study. Figure modified from Connell (2008a) based on Koning and Jochems (2014), Koning and Rawling (2017), Koning et al. (2021), and unpublished age control.

Lower Rio Rancho Hydrostratigraphic Unit (upper Cerro Conejo Formation, Benavidez unit)

Of particular interest in our study is the upper Cerro Conejo Formation, corresponding to Unit 8 in the type section of Connell et al. (1999), which constitutes the Lower Rio Rancho HSU. The upper Cerro Conejo Formation is composed of cross-stratified to massive, fine- to coarse-grained sand with a notable paucity of mud beds (Fig. 7D). It extends across most of the study area but interfingers westward with a light-red to light-orange, thickly bedded, sandy piedmont facies called the Benavidez member of the Cerro Conejo Formation (Fig. 8; Koning et al., 2021); the inferred location of this interfingering boundary is close to the Zia fault, west of the well control in our study. Because of the pending revision of the rank of the Benavidez member (i.e., it might be raised to a formation-rank term), in the remainder of this report, we refer to the associated strata as the "Benavidez unit." The upper Cerro Conejo Formation is nicely exposed along U.S. Route 550, where it contains a white bed of 11.3 Ma Trapper Creek B tephra (Koning and Personius, 2002).

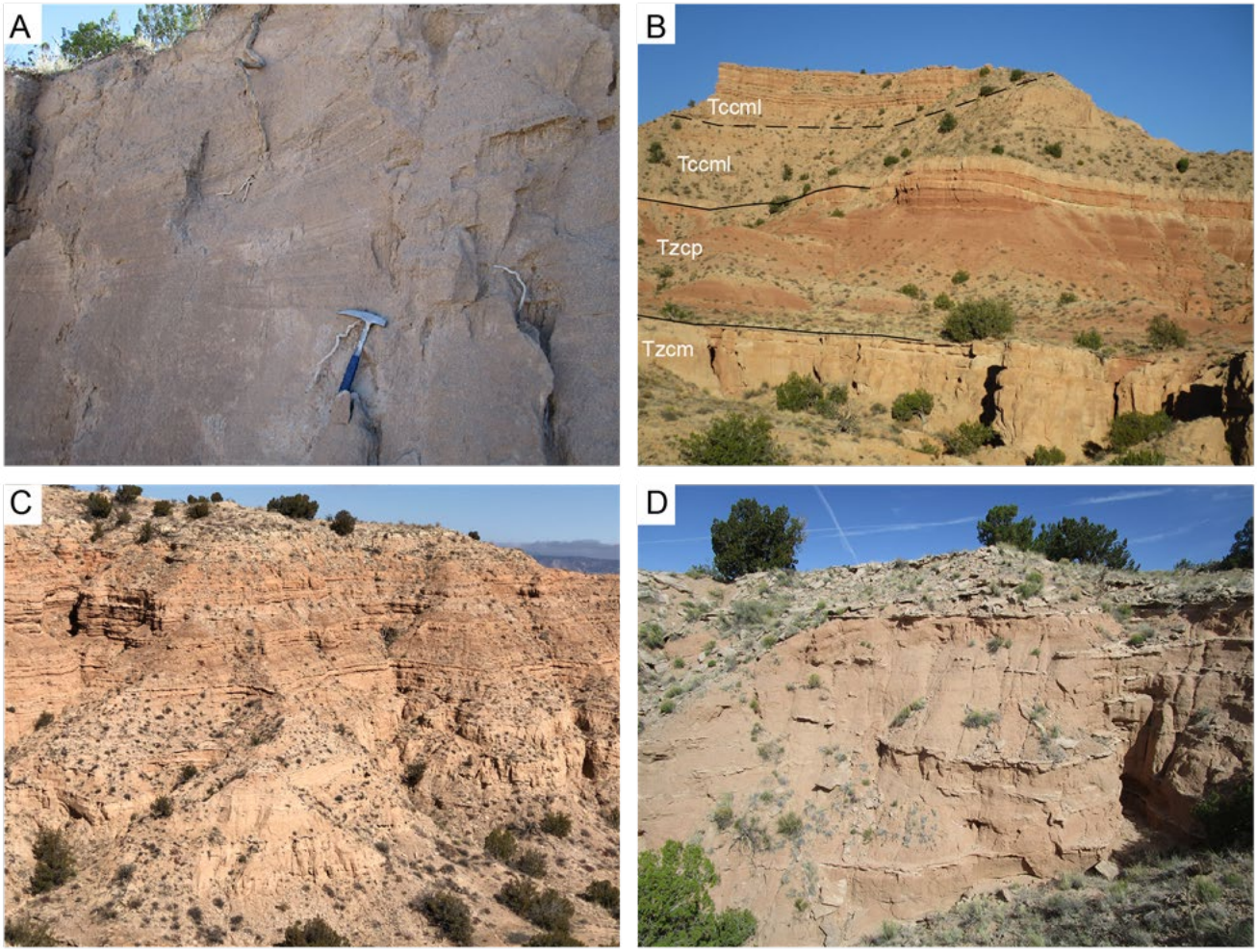

Figure 7. Photographs of the Zia HSU (A–C) and Lower Rio Rancho HSU (D). (A) Outcrop of lower–middle Zia Formation, which corresponds to the Piedra Parada Member of the Zia Formation. Note the tangential foresets above the rock hammer, likely associated with a paleowind-blown dune. Grain size is mostly medium- to coarse-grained. (B) Upward succession at the top of the Zia Formation and overlying Cerro Conejo Formation, located west of the western end of Northern Boulevard. Tzcm = Chamisa Mesa Member of Zia Formation (19.0–18.0 Ma), Tzcp = Cañada Pilares Member of Zia Formation (18.0–17.5 Ma), and Tccml = middle to lower Cerro Conejo Formation (mostly post-15 Ma, possibly 17–15 Ma below the dashed black line). (C) Lower, tabular-bedded Cerro Conejo Formation with relatively common clayey beds; note the downward gradation into the sandier, lower part of the formation (both included in the Zia HSU). (D) Upper, sandy Cerro Conejo Formation, which corresponds to the Lower Rio Rancho HSU.

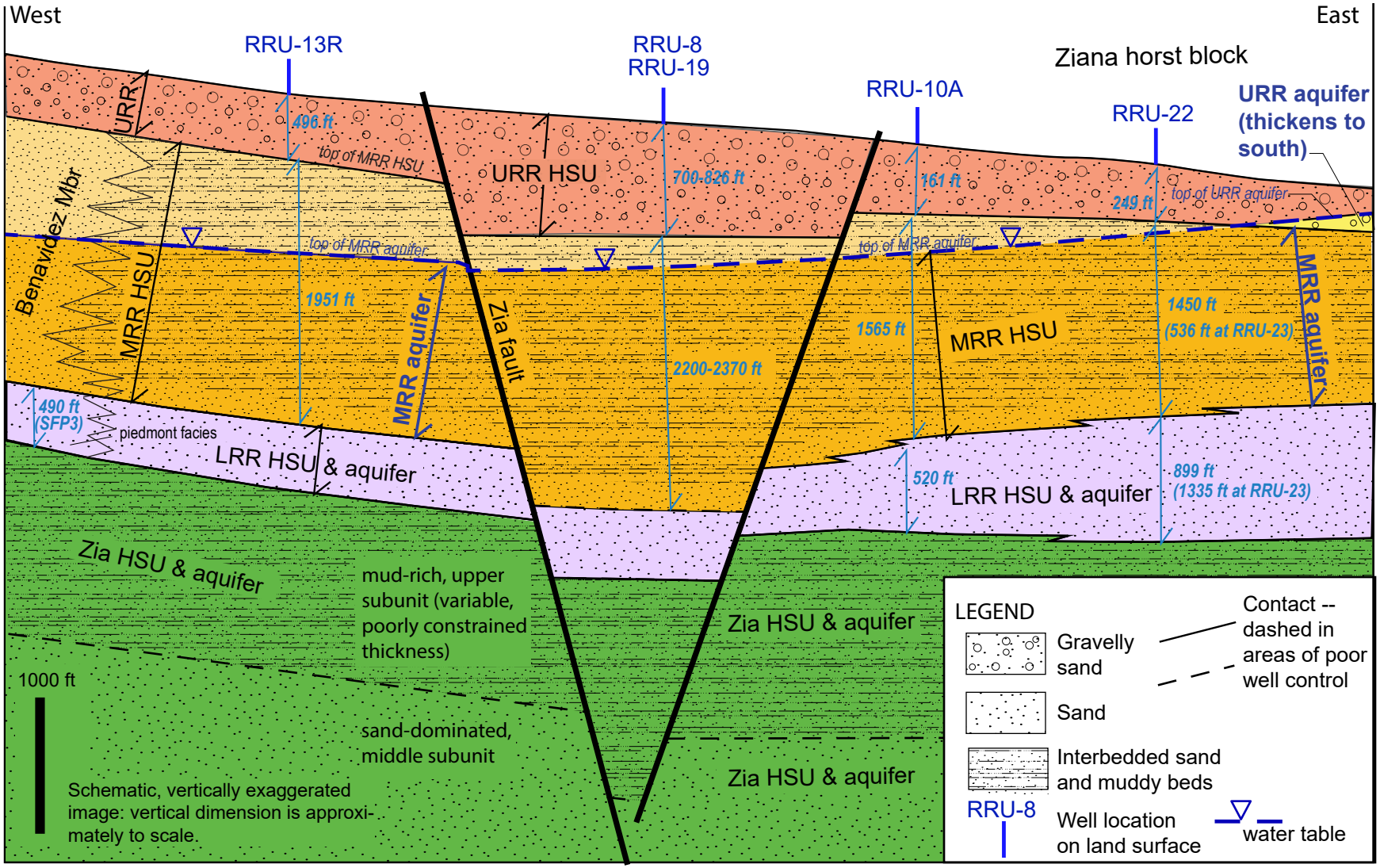

Figure 8. West–east, schematic depiction of lithostratigraphic and hydrostratigraphic unit relations. Approximate thicknesses of the HSUs (saturated plus unsaturated) are shown via the light-blue arrows and text. The potentiometric surface, which approximates the water table, is depicted by the dark-blue line.

Middle Rio Rancho Hydrostratigraphic Unit (Navajo Draw and Loma Barbon Members of Arroyo Ojito Formation, Benavidez unit)

The Cerro Conejo Formation is gradationally overlain by gravel-bearing strata assigned to the Arroyo Ojito Formation (Figs. 6, 8, and 9). Except for the Picuda Peak Member (Connell, 2008a), Arroyo Ojito strata are included in the Middle Rio Rancho HSU. The Arroyo Ojito Formation (>1,300 ft [>400 m] thick) consists of sand, clayey-silty sand, clay-silt, and gravel beds that are mostly tabular-bedded, although coarse channel fills may be lenticular to broadly lenticular. Three lithostratigraphic units make up the Middle Rio Rancho HSU (Fig. 6). To the west lies the Benavidez unit (Koning et al., 2021), which generally lacks clay beds and mostly has a chert-dominated gravel fraction. The Benavidez unit represents deposition by high-energy, ephemeral streams and interfingers eastward with the Navajo Draw Member of the Arroyo Ojito Formation (Koning et al., 2021). The Navajo Draw exhibits a distinctive pale-yellow to pale-brown color (Figs. 9A and 9B) and has a heterolithic gravel fraction dominated by volcanic rocks (to the north) and chert (to the south). This member represents deposition by a fluvial system (probably ephemeral) that drained the southeastern Colorado Plateau and the southeastern San Juan Basin (Connell et al., 1999); the yellow color of the sediment probably reflects erosion of Cretaceous strata in the structurally high area south of Cuba, southwest of the southern end of the Nacimiento Mountains. The Loma Barbon Member (Figs. 9C and 9D) is reddish yellow to strong brown and light yellowish brown, and has a gravel assemblage dominated by granite, volcanic rocks, quartzite, and yellowish-brown or reddish-brown sandstones (Connell et al., 1999). The Loma Barbon Member overlies the Navajo Draw Member and interfingers westward with the Navajo Draw; it does not extend as a recognizable unit west of the Ceja del Rio Puerco. The Loma Barbon is interpreted to reflect deposition on a distal fan and adjoining basin floor by a paleo Jemez River that carried detritus from an exhuming (eroding) Sierra Nacimiento (Connell et al., 1999); its red color may reflect erosion of former Triassic and Permian strata from the top of these mountains. Northeast of the study area, the Loma Barbon Member likely interfingers eastward with volcaniclastic strata shed from the Jemez Mountains (Cochiti Formation of Smith and Lavine, 1996). To the east of the study area, the Loma Barbon Member interfingers with ancestral Rio Grande fluvial strata (Connell et al., 1999). Arroyo Ojito strata are relatively consolidated but only weakly cemented, offset by many faults, and slightly tilted.

Upper Rio Rancho Hydrostratigraphic Unit (Picuda Peak Member of Arroyo Ojito Formation, Ceja Formation)

The Upper Rio Rancho HSU includes the relatively coarse-grained Picuda Peak Member (Arroyo Ojito Formation) and the overlying Ceja Formation (Fig. 6). The Picuda Peak Member is a pinkish-gray to reddish, sandy gravel-gravelly sand unit conformably overlying the Loma Barbon Member (Arroyo Ojito Formation) between the Zia fault and Ziana horst (Figs. 6 and 9E). Its gravel fraction is notably coarser than the underlying Arroyo Ojito strata (Connell et al., 1999, table 2) and is composed of red granite and light-colored gravel eroded from the Pedernal Chert Member of the Abiquiu Formation, with lesser yellowish-brown sandstone, brownish-yellow chert, and quartzite (Connell et al., 1999; Koning and Personius, 2002). Its age is probably latest Miocene–early Pliocene based on basalt clast $^{40}Ar/^{39}Ar$ ages of 8.3–6.5 Ma (Koning and Personius, 2002, table 2), which provide a maximum age of deposition for the unit. This coarse unit was called the Picuda Peak Member of the Arroyo Ojito Formation by Connell (2008a); however, differentiating the top of this unit in well data from our study proved very difficult. This difficulty, in addition to its coarse texture, justifies subsuming the Picuda Peak unit with the relatively coarse-grained, weakly to non-cemented Upper Rio Rancho HSU.

The Plio–Pleistocene Ceja Formation includes three members that interfinger eastward with axial-fluvial facies of the ancestral Rio Grande. The axial-fluvial facies are included in the Sierra Ladrones Formation (Fig. 6). Near the Ceja del Rio Puerco, fine- to medium-grained, pink to light-brown sand and minor clayey mud are assigned to the Atrisco Member. The Atrisco Member is overlain by grayish to tan, unconsolidated, gravelly sand and sandy gravel of the Rio Puerco Member (Fig. 6). The gravel of the Rio Puerco Member is composed of chert, 20–30% quartzite, and minor (<15% each) intermediate-mafic volcanic clasts, sandstone clasts,

and granite clasts. These two members are often recognizable in many wells found in the western study area, but differentiation becomes more difficult to the east. Near the eastern boundary of the study area, reddish, relatively coarse sediment is assigned to the Santa Ana Mesa Member. The high proportion of arkosic sand in the Santa Ana Mesa Member, along with its reddish color, suggests that it was deposited by the Jemez River in the late Pliocene to early Pleistocene. The Ceja Formation is around 300 ft (~100 m) thick.

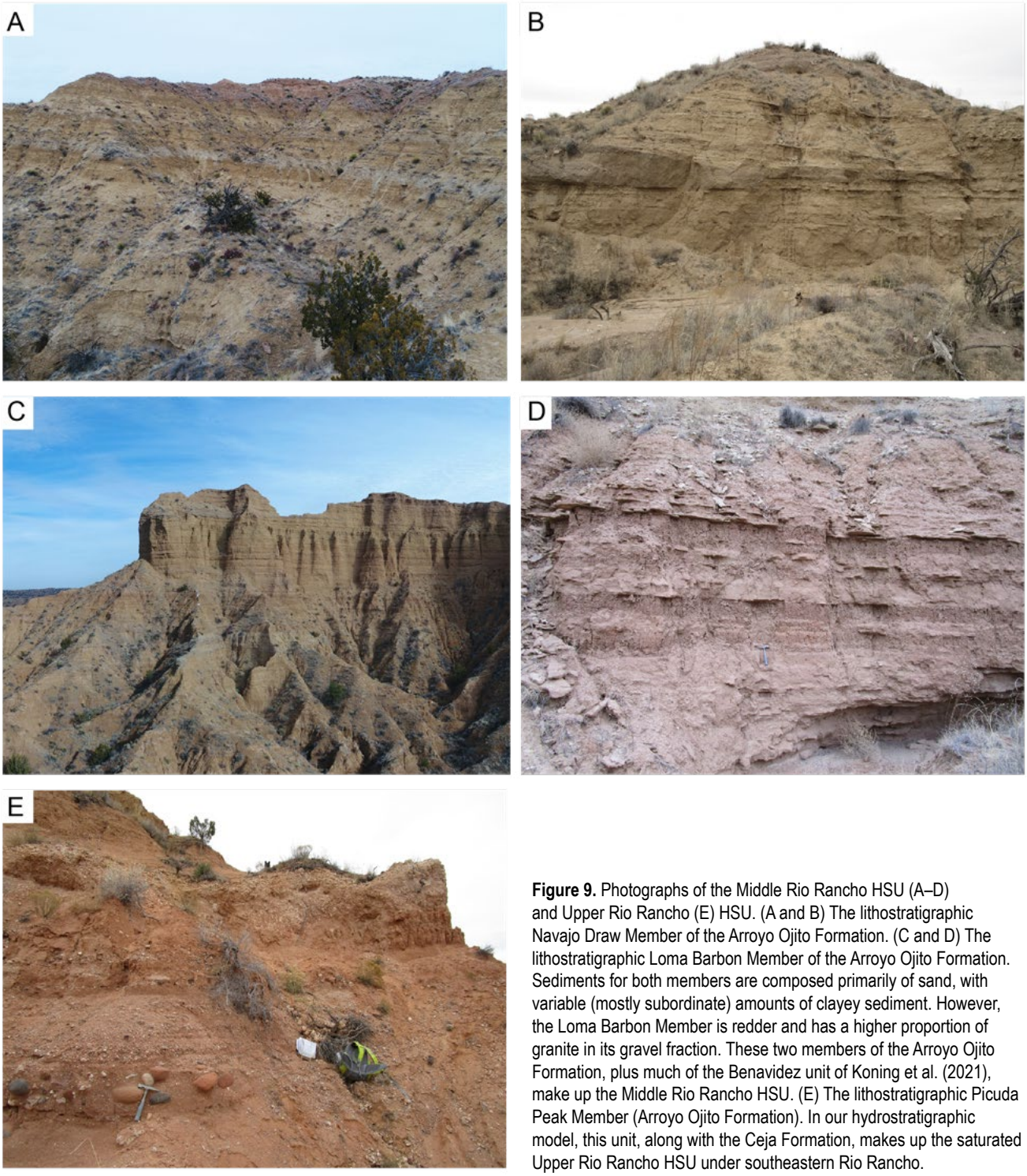

Figure 9. Photographs of the Middle Rio Rancho HSU (A–D) and Upper Rio Rancho (E) HSU. (A and B) The lithostratigraphic Navajo Draw Member of the Arroyo Ojito Formation. (C and D) The lithostratigraphic Loma Barbon Member of the Arroyo Ojito Formation. Sediments for both members are composed primarily of sand, with variable (mostly subordinate) amounts of clayey sediment. However, the Loma Barbon Member is redder and has a higher proportion of granite in its gravel fraction. These two members of the Arroyo Ojito Formation, plus much of the Benavidez unit of Koning et al. (2021), make up the Middle Rio Rancho HSU. (E) The lithostratigraphic Picuda Peak Member (Arroyo Ojito Formation). In our hydrostratigraphic model, this unit, along with the Ceja Formation, makes up the saturated Upper Rio Rancho HSU under southeastern Rio Rancho.

POTENTIOMETRIC SURFACE

We constructed a map of the potentiometric surface in order to constrain the top of saturated HSUs and construct isopach maps of these saturated HSUs. Two terms related to groundwater levels—water table and potentiometric surface—warrant explanation. The **water table** is the elevation (or depth) of saturated sediment in relatively unconfined conditions (i.e., the water is not under pressure). When penetrated by a well, the water level in the well would be approximately the same as the top of the saturated sediment. Under confined (artesian) conditions, however, the level of the water within the well casing could be notably higher than the top elevation of the saturated sediment. The water level in a well, whether under confined or unconfined conditions in the associated aquifer, is called the **potentiometric surface**.

Previous mapping of the potentiometric surface was published by Kernodle (1998), reflecting groundwater conditions in the mid-1990s. We updated this map by compiling more recent groundwater levels (Table 1). The paucity of recent water level data near the northern and western margins of the study area necessitated the use of older (1956–1984) water levels from stock wells. Water level data for dates when a well seemed to be experiencing focused drawdown, presumably due to active pumping, were excluded. Depth-to-water measurements were converted to water level elevations using a digital elevation model.

Contouring of the potentiometric surface was conducted using the following steps in ArcGIS's Spatial Analyst tools. First, a natural neighbor surface interpolation was performed (Natural Neighbor tool in Interpolation toolset) using the well data in Table 1 and spot elevations of the lower Jemez River and Rio Grande; for the latter, we assumed that groundwater depth is near zero at these rivers. Second, the potentiometric surface was contoured (40-ft contour interval) using the Contour tool (Surface toolset). Third, the contours were edited according to topography and were extended manually in the northwestern part of the study area. These contours, the water level elevations in wells, and the elevations of the rivers were used as inputs for the ArcGIS tool called Topo to Raster. This tool was used to produce an XYZ grid file of the potentiometric surface elevation in the northwestern Albuquerque Basin (127.4 m x 127.4 m grid size), which was smoothed utilizing the Focal Statistics tool (Neighborhood toolset in Spatial Analyst), where we used a 90-degree wedge neighborhood setting with a 3-cell search radius.

The Natural Neighbor interpolation is similar to an Inverse Distance Weighted (IDW) interpolation. In an IDW interpolation, measurements that are closest are given more influence on the predicted value than those farther away. Natural Neighbor interpolation differs slightly from IDW because it selects the input points that are closest to an interpolation point, but then creates a convex hull around these points. The interpolation then weights their values by proportionate area. This method tends to create smoother, more realistic potentiometric surfaces that lack dramatic cliffs or drop-offs, which rarely represent real-world geometries. This methodology also removes the need to specify parameters such as radius, the number of neighbors, or weights.

Maps of the depth to the potentiometric surface and potentiometric surface elevation are presented in Figures 10 and 11, respectively. Note that the input data for these maps were not as rigorously screened as the U.S. Geological Survey's potentiometric maps produced for the neighboring city of Albuquerque (e.g., Galanter and Curry, 2019), as exemplified in our inclusion of water levels spanning decades of time. Therefore, this map should be considered as an "approximation" of the potentiometric surface, locally having up to 10–100 ft (3–30 m) of inferred vertical error, especially toward the northwest corner of the study area (i.e., where elevation-contour lines are dashed in Figure 11). The implications of the geometry of the potentiometric surface are discussed in the Results section below.

Table 1. Well data used to construct the potentiometric surface.

Well nomenclature			UTM coordinates (NAD 83)		Groundwater data			
Well label (Rio Rancho database)	**Well label** (this report)	**Well name**	**Easting** (m)	**Northing** (m)	**Date measured** (mo/day/yr)	**Depth** (ft)	**Elevation** (ft)	**Source**[1]
AB-0057	DW-5		356069	3909350	9/2/1994	160.00	5012	PI
AB-0065	HRP	Hunter Ridge Piezometer	348099	3896530	8/15/2016	165.48	4939.52	PI
AB-0066	HRP	Hunter Ridge Piezometer	348099	3896530	8/15/2016	162.49	4942.51	PI
AB-0067	HRP	Hunter Ridge Piezometer	348099	3896530	8/15/2016	148.38	4956.62	PI
AB-0068	HRP	Hunter Ridge Piezometer	348099	3896530	8/15/2016	155.92	4949.08	PI
AB-0069	HRP	Hunter Ridge Piezometer	348099	3896530	8/15/2016	152.16	4952.84	PI
AB-0070	HRP	Hunter Ridge Piezometer	348099	3896530	8/15/2016	151.2	4953.8	PI
AB-0071	Intel 3	Intel 3 Production Well	348793	3898580	4/3/2015	262.3	4952.7	PI
AB-0091	LMS-D	Lincoln D	346634	3902630	6/25/2021	507.08	4928.62	PI
AB-0092	LMS-M	Lincoln M	346634	3902630	6/25/2021	506.69	4929.06	PI
AB-0093	LMS-S	Lincoln S	346634	3902630	6/25/2021	501.26	4935.55	PI
AB-0115	AB-115		343955	3892440	6/17/1997	264.49	4931.51	PI
AB-0120	NMU 1	NM Utilities 1	341713	3895900	12/31/1987	533.00	4857	PI
AB-0169	SAP-W1		349074	3924530	8/16/1985	31.22	5290.78	PI
AB-0179	SV-D	Sierra Vista D	345404	3891310	6/16/2021	178.30	4933.16	PI
AB-0180	SV-M	Sierra Vista M	345404	3891310	6/16/2021	156.79	4955.07	PI
AB-0181	SV-S	Sierra Vista S	345404	3891310	6/16/2021	152.75	4958.26	PI
AB-0185	SAF	Soil Amement Facility	333801	3890770	4/25/1988	922.11	4943.89	PI
AB-0192	SWAB TH 2D	SWAB Test Hole #2	337891	3894400	5/13/1996	797.35	4932.65	PI
AB-0222	WiMill 41	Windmill 41	345523	3921880	1/23/1984	373.30	5221.7	PI
AB-0226	AB-226	ZPW-3	346536	3926520	1/23/1984	85.04	5299.96	PI
NM-01258	NMU-4	New Mexico Utilities 4	341656	3897000	1/26/2010	646.00	4827.5	USGS
NM-01268	NMU-3	New Mexico Utilities 3	344128	3898510	3/20/2015	523.98	4936.02	USGS
NM-03409	NM-3409		342591	3892590	11/4/2015	453.53	4885.47	USGS
RR-0001	RRU-1	Rio Rancho Utilities 1	347949	3899311	5/5/2021	299.26	4954.87	RR
RR-0002	RRU-2	Rio Rancho Utilities 2	347977	3899581	5/5/2021	316.88	4951.29	RR
RR-0003	RRU-3	Rio Rancho Utilities 3	347298	3900891	3/29/2006	423.70	4949.2	RR
RR-0004	RRU-4	Rio Rancho Utilities 4	347513	3902124	5/5/2021	488.47	4929.96	RR
RR-0006	RRU-6A	Rio Rancho Utilities 6A	345169	3903567	12/1/2016	728.59	4874.824	RR
RR-0007	RRU-7	Rio Rancho Utilities 7	344670	3904558	4/15/1988	784.00	4889.35	RR
RR-0008	RRU-8	Rio Rancho Utilities 8	342432	3904769	5/5/2021	930.52	4892.75	RR
RR-0009	RRU-9	Rio Rancho Utilities 9	337737	3910345	3/4/2016	1154.83	4902.263	RR
RR-0012	RRU-11	Rio Rancho Utilities 11	357285	3910031	5/5/2021	96.22	5035.9	RR
RR-0013	RRU-12	Rio Rancho Utilities 12	355343	3909770	12/3/2018	247.85	4988.28	RR
RR-0014	RRU-13	Rio Rancho Utilities 13	335994	3905041	5/5/2021	1112.44	4942.95	RR
RR-0015	RRU-14	Rio Rancho Utilities 14	338728	3903599	8/6/2020	862.84	4905.93	RR
RR-0016	RRU-15	Rio Rancho Utilities 15	347116	3913670	3/26/2003	658.03	5135.97	RR
RR-0017	RRU-16	Rio Rancho Utilities 16	346012	3906730	12/1/2016	609.06	4926.734	RR
RR-0018	RRU-17	Rio Rancho Utilities 17	345389	3899683	3/9/2011	387.87	4922.11	RR
RR-0019	RRU-18	Rio Rancho Utilities 18	351498	3912245	5/5/2021	446.93	5085.9	RR
RR-0020	RRU-19	Rio Rancho Utilities 19	342135	3902344	2/3/2015	808.23	4871.277	RR
RR-0021	RRU-20	Rio Rancho Utilities 20	341354	3906305	4/4/1997	825.00	4988.65	RR
RR-0022	RRU-21	Rio Rancho Utilities 21	348166	3903325	10/5/2008	425.41	4883.22	RR

Table 1 continued on p. 16.

Table 1 (continued). Well data used to construct the potentiometric surface.

Well nomenclature			UTM coordinates (NAD 83)		Groundwater data			
Well label (Rio Rancho database)	Well label (this report)	Well name	Easting (m)	Northing (m)	Date measured (mo/day/yr)	Depth (ft)	Elevation (ft)	Source[1]
RR-0023	RRU-22	Rio Rancho Utilities 22	351048	3905138	5/7/2008	346.46	4939.54	RR
RR-0024	RRU-23	Rio Rancho Utilities 23	348978	3907978	6/22/2021	345.24	5091.76	RR
RR-0025	PHNX	Phoenix	336720	3912076	5/5/2021	1182.75	4970.43	USGS
RR-1399	IMW B	IMWB1	350540	3898451	5/5/2021	17.44	4986.22	NMBGMRSL
RR-1400	IMW B	IMWB2	350540	3898451	5/5/2021	33.18	4970.48	NMBGMRSL
RR-1401	IMW B	IMWB3	350540	3898451	5/5/2021	53.01	4950.65	NMBGMRSL
RR-1402	IMW C	IMWC5	351924	3898900	5/5/2021	56.32	4946.81	NMBGMRSL
RR-1403	IMW C	IMWC6	351924	3898900	5/5/2021	57.60	4945.53	NMBGMRSL
OFR-496-BR	BR	Black Ranch	334383	3898123	6/20/1998	977	4943	SL_OFR496
OFR-496-PR	PR	Paradise Road	335436	3894251	6/23/2001	899	4931	SL_OFR496
	ZPW-2		339539	3923001	8/16/1965	780	4993	NMOSE
	WiMill 41	Windmill 41	345540	3921855	1/23/1984	373	5225	NMOSE
	SAP-W3		349438	3920102	2/1/1984	340	5248	NMOSE
	SAP-W2		348927	3922762	2/1/1984	102	5270	NMOSE

[1] Abbreviations
PI: Plummer, L.N., Bexfield, L.M., Anderholm, S.K., Sanford, W.E., and Busenberg, E., 2004, Geochemical characterization of ground-water flow in the Santa Fe Group aquifer system, Middle Rio Grande Basin, New Mexico: U.S. Geological Survey Water-Resources Investigations Report 2003-4131, 395 p. https://doi.org/10.3133/wri034131
USGS: U.S. Geological Survey well database for New Mexico
RR: Rio Rancho well database, created for Rio Rancho (2019) by the NM Bureau of Geology and Mineral Resources
NMBGMRSL: NM Bureau of Geology and Mineral Resources, Subsurface Library
SL_OFR496: NM Bureau of Geology and Mineral Resources, Subsurface Library and Open-File Report 496
NMOSE: NM Office of the State Engineer, WATERS database

The potentiometric surface elevation map can be used to infer groundwater flow paths; these paths are oriented perpendicular to the contour lines (i.e., along the steepest gradient) toward elevational lows (Fig. 11). The lowest elevations of the potentiometric surface lie in an elongated region between the western part of Paseo del Norte, stretching north toward well RRU-19 near Southern Boulevard. This potentiometric surface nicely corresponds to the "groundwater trough" of Plummer et al. (2004a, 2004c); explanations for its existence are evaluated in the Discussion section below. The map geometry of the low is probably influenced, at least in part, by the pumping of wells NMU1, W-4, RRU-19, and RRU-6A. Its north-south elongation may be controlled by nearby north-striking faults acting as groundwater barriers, which was also postulated by Plummer et al. (2004c). Westward across the Zia fault, for example, the potentiometric surface rises about 40 ft (12 m). To the east of this low, potentiometric contours trend northeast; therefore, under the southeastern part of the study area, groundwater likely flows to the northwest toward this potentiometric surface low from the Rio Grande, consistent with a component of recharge from the Rio Grande. In the northern study area, the potentiometric surface slopes south-southwest away from the Jemez River, but the lack of well control makes the specific geometry of the surface there uncertain. The potentiometric surface forms a "mound" over the Ziana horst, suggesting that its bounding faults act as groundwater flow barriers that both allow groundwater input from the north and keep this groundwater relatively elevated within the horst between these bounding faults. Groundwater may possibly be upwelling near or north of well RRU-23. There does not seem to be a strong slope in the potentiometric surface west of the Zia fault zone, and the exact configuration of the contours there is uncertain. We infer that groundwater contours there are likely oriented north-south due to possible barrier effects related to the San Ysidro and Sand Hill faults; however, more data are needed to test this inference. Lastly, there appears to be a focused low in the potentiometric surface centered at well RRU-9, which is likely due in part to pumping of that well (where water levels are demonstrated to be sensitive to pumping according to consultant reports in Appendix 1) and the relatively fine-grained, lower-permeability sediment there (discussed below).

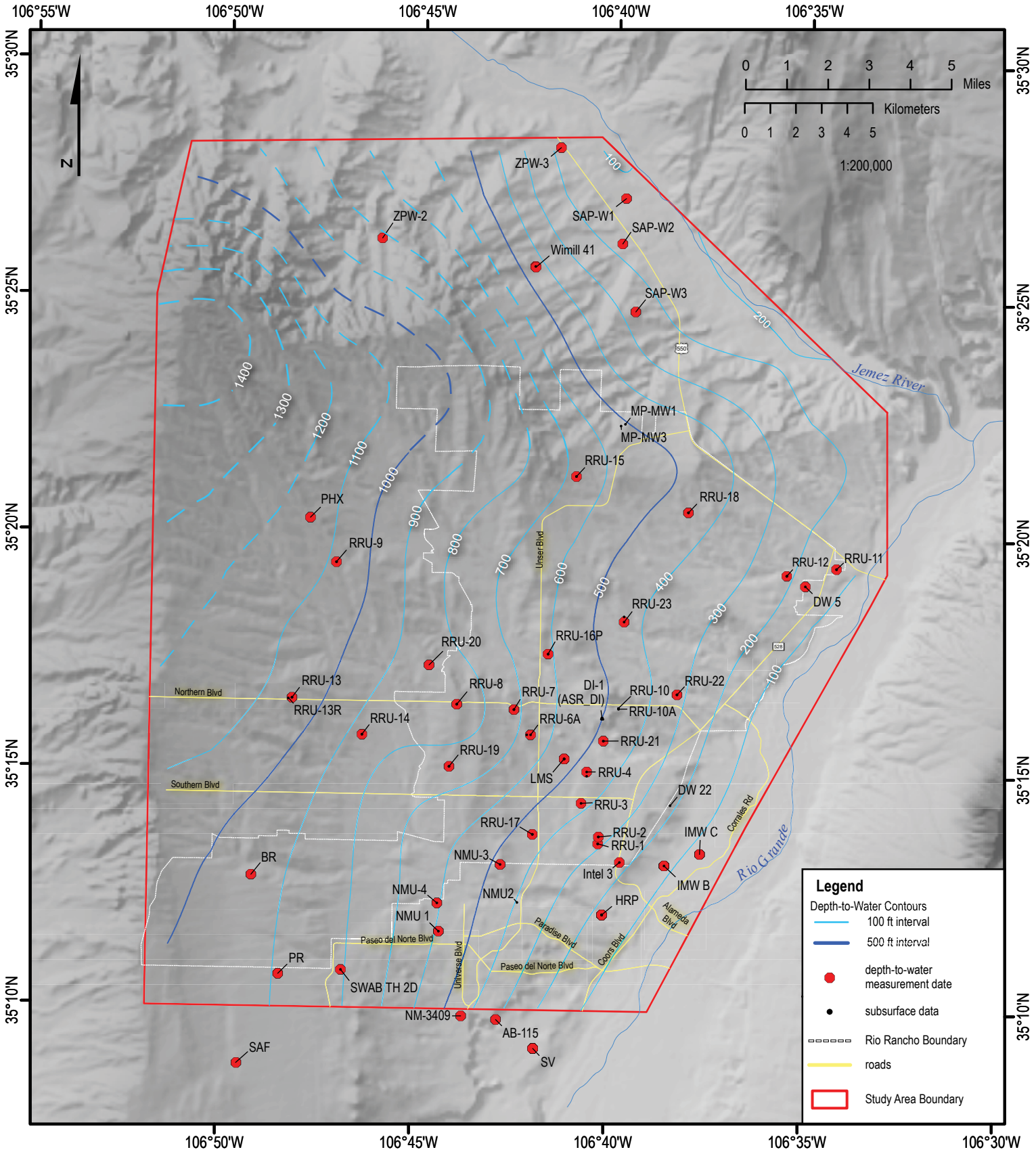

Figure 10. Contours showing depth to the potentiometric surface. Wells used to create the potentiometric surface map are shown as red octagons; wells marked by black dots were also used to construct the 3D hydrostratigraphic model. A list of the associated water wells is provided in Table 1, which also indicates when the groundwater levels were measured. Dashed lines are uncertain.

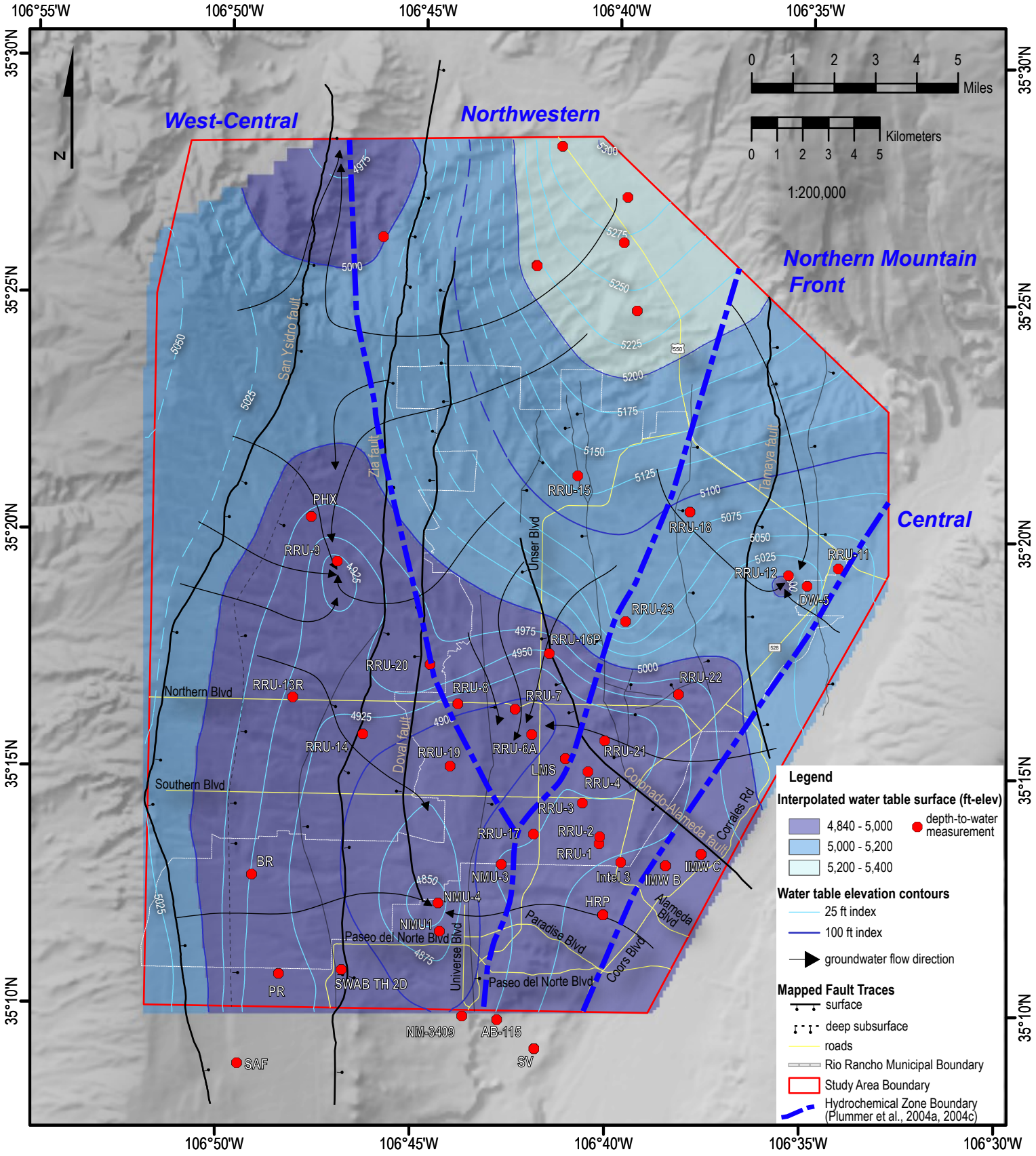

Figure 11. Contours showing the elevation (in feet above mean sea level) of the approximate potentiometric surface. Dashed contour lines indicate relatively high uncertainty. Wells used to create the potentiometric surface map are shown as red octagons. The dashed, thick blue line denotes boundaries between the hydrochemical zones of Plummer et al. (2004a, 2004c).

3D MAPPING OF HYDROSTRATIGRAPHIC UNITS WITHIN THE SANTA FE GROUP AQUIFER

DELINEATION OF HYDROSTRATIGRAPHIC UNITS

To evaluate permeability trends and identify possible "target aquifers," hydrostratigraphic units (HSUs) were formulated for the study area. Our initial scheme for delineating HSUs was based on field observations conducted during extensive geologic mapping by the lead author (Koning et al., 1998; Koning and Personius, 2002; Koning and Jochems, 2014; Koning and Rawling, 2017). The first iteration envisaged the following grouping of lithostratigraphic units (listed in ascending stratigraphic order): Zia Formation; lower–middle Cerro Conejo Formation; upper, sandy Cerro Conejo Formation; lower, sandier Arroyo Ojito Formation; lower–middle, mud-rich Arroyo Ojito Formation; upper, coarser Arroyo Ojito Formation; and Ceja Formation.

To successfully create the 3D subsurface geologic model, these initial hypothesized HSUs needed to be recognized in well data and correlated between wells. For this purpose, we utilized the set of wells listed in Table 2 and Appendix 2, most of which had high-quality wireline data and archived cuttings. Kingdom software was heavily employed in this initial evaluation of HSUs. This powerful software, developed for the oil industry, facilitates subsurface correlation of strata and vertical trends in porosity and clay content. Digital files of wireline (downhole geophysical) data were used to make picks based largely on the proportion of clay, which has a strong influence on permeability and is also measured in many wireline methods. Most wireline data were in hard copy format only, so time and effort were spent digitizing them. Lithologic textures and compositions in a well, based solely on cuttings data, were assigned numeric codes and used in the Kingdom analyses. Cuttings description data were obtained from consultant reports (see Appendix 1), except for several wells whose cuttings were archived in the New Mexico Bureau of Geology's Subsurface Library, which the lead author described in detail (see Appendix 3). Useful wireline curves proved to be resistivity and gamma-ray, density-porosity, and neutron-porosity (Fig. 12). These well logs are compiled in Appendix 4.

Using Kingdom software, Vshale ratios (i.e., the proportion of clay vs. total sediment) were also used to pick and correlate potential HSUs. Vshale ratios were calculated by comparing the magnitude of the gamma-ray signal in inferred clay-dominated intervals versus the magnitude of the gamma-ray signal for relatively clay-free sand formations (note that depth intervals of sand vs. clay were inferred using cuttings and resistivity plus neutron curves; see Appendix 5). Vshale values were assigned from the relative value of the gamma-ray signal between these end-member values. Gamma-ray curves could also be influenced by radiogenic sediment from granite (where gamma rays can be contributed by potassium, thorium, and uranium). But comparison of gamma-ray curves (particularly spectral gamma-ray curves) with cuttings suggested that the proportion of granite versus non-granite cuttings seemed to have little influence on the gamma-ray curves. Rather, the gamma-ray signal mostly reflected the amount of clay in the sediment.

Using Kingdom software, one can plot the various datasets for each well (e.g., various wireline curves plotted as a function of depth, cuttings lithology as a function of depth) and then compare wells side by side along chosen cross-section lines (Fig. 12). One can then determine if certain subsurface intervals can be correlated between wells and note thickness changes that can be ascribed to lateral facies changes or to faults. Sometimes, changing picks in wells resulted in the successful correlation of a given stratigraphic interval. The final lithologic picks per well (listed as elevation in feet) of units that could be correlated in the subsurface are presented in Table 2 and Appendix 4.

Table 2. Well information and HSU elevations for the northwestern Albuquerque Basin.

Well label	Well name	Easting	Northing	Approx surface elev (ft), ±5 ft	Middle Rio Rancho HSU top elev (ft)[3]	Lower Rio Rancho HSU top elev (ft)	Zia HSU top elev (ft)	Middle Rio Rancho HSU top depth (ft)[3]	Lower Rio Rancho HSU top depth (ft)	Zia HSU top depth (ft)	Well total depth (TD, ft)
T1Y	Davis Petroleum Tamara #1-Y	344653	3916523	6125	6120	4722	4260	5	1403	1865	8732
SFP1	Shell Santa Fe Pacific #1	348283	3913459	5753			5551			202	10276
SFP3	Shell Santa Fe Pacific #3	332610	3910494	6299	6004	5154	4668	295	1145	1631	11113
Sasf1	Santa Ana Pueblo Soccer Field #1	357294	3912665	5240							1043
Sap1	Santa Ana Pueblo Well 1	357515	3910828	5145							820
Sap2	Santa Ana Pueblo Well 2	358011	3910574	5105							860
sagc	Santa Ana Pueblo Golf Course	358280	3911497	5712							904
RWP17	Santa Ana Pueblo Range Well 17	356784	3914924	5450	90			5360			580
RRU-1	Rio Rancho Utilities 1[1]	347949	3899311	N/A							
RRU-2	Rio Rancho Utilities 2[1]	347977	3899581	5260							813
RRU-3	Rio Rancho Utilities 3	347298	3900891	5370							828
RRU-4	Rio Rancho Utilities 4	347518	3901955	5416							990
RRU-5	Rio Rancho Utilities 5	348234	3901458	5356							1100
RRU-6A	Rio Rancho Utilities 6A	345169	3903567	5602	4945			657			1476
RRU-7	Rio Rancho Utilities 7	344670	3904558	5650	4956			694			1225
RRU-8	Rio Rancho Utilities 8	342432	3904769	5822	5156			666			2083
RRU-9	Rio Rancho Utilities 9	337737	3910345	6054	5755			299			1540
RRU-10	Rio Rancho Utilities 10	348760	3904606	5500	5337			163			1470
RRU-10A	Rio Rancho Utilities 10A	348764	3904579	5500	5339	3775	3255	161	1725	2245	2520
RRU-11	Rio Rancho Utilities 11	357285	3910031	5137							350
RRU-12	Rio Rancho Utilities 12	355352	3909775	5250	4049			1201			1491
RRU-13	Rio Rancho Utilities 13[1]	335994	3905041	6055							2032
RRU-13R	Rio Rancho Utilities 13R	335848	3905021	6055	5559	3608		496	2447		2530
RRU-14	Rio Rancho Utilities 14	338728	3903599	5770	5041			729			2000
RRU-15	Rio Rancho Utilities 15	347116	3913670	5795	5563	4210		232	1585		1800
RRU-16P	Rio Rancho Utilities 16P	346012	3906730	5536	4968	3910		568	1626		2010
RRU-17	Rio Rancho Utilities 17	345389	3899683	5308	3803			1505			1710
RRU-18	Rio Rancho Utilities 18	351498	3912245	5535	5255	4463		280	1072		2070
RRU-19	Rio Rancho Utilities 19	342135	3902344	5676	4850			826			2070
RRU-20	Rio Rancho Utilities 20	341539	3906296	5810	5511			299			970

Table 2 continued on p. 21.

Table 2 (continued). Well information and HSU elevations for the northwestern Albuquerque Basin.

Well label	Well name	Easting	Northing	Approx surface elev (ft), ±5 ft	Middle Rio Rancho HSU top elev (ft)[3]	Lower Rio Rancho HSU top elev (ft)	Zia HSU top elev (ft)	Middle Rio Rancho HSU top depth (ft)[3]	Lower Rio Rancho HSU top depth (ft)	Zia HSU top depth (ft)	Well total depth (TD, ft)
RRU-21	Rio Rancho Utilities 21	348166	3903325	5322	5172			150			2100
RRU-22	Rio Rancho Utilities 22	351048	3905138	5280	5031	3578	2679	249	1702	2601	2987
RRU-23	Rio Rancho Utilities 23	348908	3908090	5452	5392	4752	3502	60	700	1950	2820
PHX	Phoenix Road Piezometer	336720	3912076	6130	5832			298			1685
PR	Paradise Road Piezometer	335446	3894246	5830	5332			498			1742
BR	Black Ranch Test Well	334395	3898112	5920	5525	3100		395	2820		3035
ASR_DI	Rio Rancho ASR Direct Injection	348117	3904215	5496	5335	3365		161	2131		2140
Bernalillo 4	Bernalillo Well 4	356138	3911578	5146	4092			1054			1220
HRP	Hunters Run Park Piezometer	348113	3896300	5105							1520
Intel 1	Intel Production Well 1	349441	3899735	5267	3585			1682			2050
Intel 2	Intel Production Well 2	349518	3899176	5232	3598			1634			2038
Intel 3	Intel Production Well 3	348777	3898572	5231	3539			1692			2050
LMS	Lincoln Middle School Piezometer	346698	3902538	5450	4650			800			1339
SAF-1	Soil Amendment Facility 1[2]	333810	3891050	5875							

[1] Subsurface data not used to make hydrostratigraphic model due to lack of adequate well logs or proximity to another well with good data.
[2] Subsurface data not used to make hydrostratigraphic model, but well pumping test data utilized in our study.
[3] No value indicates MRR top not encountered in drill hole.

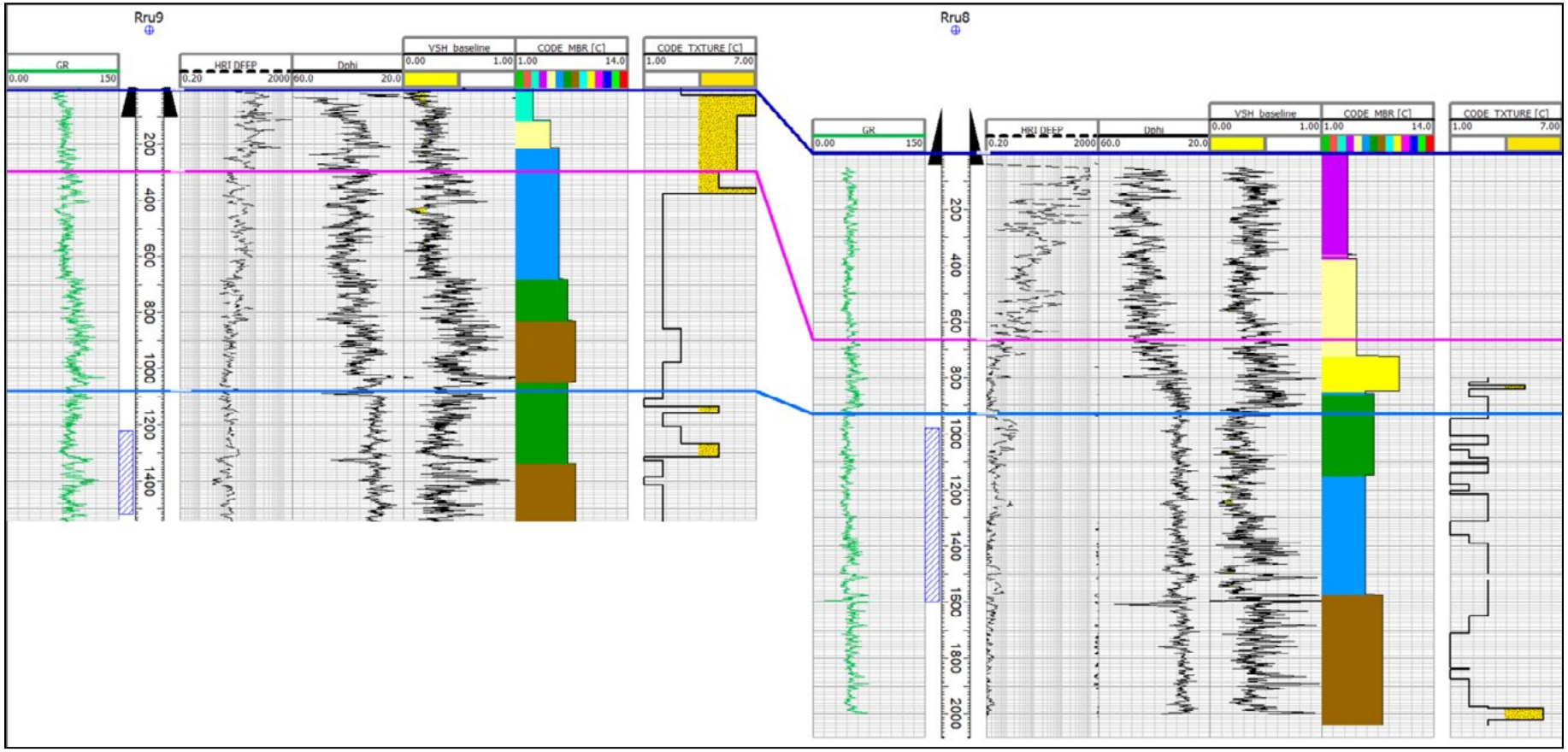

Figure 12. Illustration of well data displayed using Kingdom software. Plotting various wireline data for each well greatly aids in correlating subsurface stratigraphic units. In this example, we plot subsurface data for wells RRU-9 and RRU-8, which are separated by the east-side-down Zia fault. The upper dark-blue line is the top of the Upper Rio Rancho HSU (corresponding to the land surface), the pink line is the top of the Middle Rio Rancho HSU, and the lighter-blue line illustrates the top of the saturated portion of the Middle Rio Rancho HSU. The columns of data for each well are (from left to right) (1) gamma-ray curve (green line), ranging from 0 to 150 API (the standard unit of measurement developed by the American Petroleum Institute for measuring natural gamma-ray logs); (2) the depth of the well (in ft), with the screened interval shown by the blue diagonal lines; (3) deep-induction curves (HRI DEEP), ranging from 0.20 to 2,000 ohm-meters; (4) density-porosity curves (Dphi); (5) the Vshale curve (VSH baseline), which uses the gamma-ray data to depict sands (gamma-ray values <0.25 Vshale, depicted by yellow shades) versus clayey sediment (Vshale values >0.25); (6) "working" subunit assignments based on drill cuttings analysis (CODE MBR); and (7) the coded texture (CODE TXTURE) of the sediment based on drill-cuttings descriptions and wireline well log interpretation. The complete set of logs and an explanation of symbology and codes are given in Appendix 4. Note the following general upward trends in the Middle Rio Rancho HSU in the datasets of RRU-9 and RRU-8: (1) leftward in the gamma-ray, density-porosity, and Vshale data and (2) rightward in the induction data. These upward trends indicate an upward coarsening and a likely increase in porosity in the upper Middle Rio Rancho HSU.

About a dozen Kingdom cross sections were made that allowed us to determine which units could be correlated in the subsurface. Since these units had different geophysical properties related primarily to the proportion of clay, and since clay directly impacts the degree of permeability, we considered these correlative units as potential HSUs; whether these HSUs indeed had unique permeability properties was later tested by compiling hydraulic conductivities derived from pumping test data. The final HSUs are as follows (listed in ascending stratigraphic order, with lithostratigraphic counterparts listed in parentheses): **Zia HSU** (the entire Zia Formation and the overlying lower–middle Cerro Conejo Formation, the latter containing notable muddy beds), **Lower Rio Rancho HSU** (upper, sand-dominated Cerro Conejo Formation and Benavidez unit), **Middle Rio Rancho HSU** (Navajo Draw and Arroyo Ojito Members of the Arroyo Ojito Formation plus the Benavidez unit), and **Upper Rio Rancho HSU** (Picuda Peak Member of the Arroyo Ojito Formation and the Ceja Formation). Note that the lower–middle Zia Formation, corresponding to the sand-dominated Piedra Parada Member, seems to extend across the northern study area (based on its identification in the Santa Fe Pacific No. 1, Santa Fe Pacific No. 3, and Tamara No. 1-Y wells; Table 2) and could be a potential fifth HSU. We lumped this sandy, lowermost Santa Fe Group unit within the Zia HSU because of its great depth and general lack of penetration by existing water wells. The initially hypothesized lower, sandier Arroyo Ojito Formation HSU and lower–middle, muddier Arroyo Ojito HSU could not be successfully correlated across the study area and thus were subsumed into the Middle Rio Rancho HSU (Figs. 6 and 8). In most areas, the Arroyo Ojito Formation coarsened upward, but the lower boundary of this coarsening is too diffuse to correlate between wells.

SUBSURFACE MAPPING METHODS

Mapping HSU Tops (includes both saturated and unsaturated zones)

The final geologic model consists of a set of raster surfaces, each corresponding to the top of one of the four HSUs (Plates 1–4, Appendix 6). These raster surfaces were made using an ArcGIS tool called Topo to Raster, which utilized the elevations of the HSU tops in the 41 studied wells (Table 2) and structural contours as inputs. The well picks were already determined using the previous Kingdom software analyses of lithologic picks and inter-well correlations. Below, we summarize how the structural contours were constructed for the tops of the Zia, Lower Rio Rancho, and Middle Rio Rancho HSUs. More detail about the ArcGIS component of the methodology is given in Appendix 7.

Except for the Upper Rio Rancho HSU, the lithostratigraphic-top equivalent of a given HSU was identified in outcrops north of La Ceja. The top contact of the Upper Rio Rancho HSU corresponds to surface topography and thus did not need to be identified in outcrop. These lithostratigraphic tops (*per HSU unit*) include the top of the Loma Barbon Member or, if absent, Navajo Draw Member of the Arroyo Ojito Formation (Middle Rio Rancho HSU); the top of the Cerro Conejo Formation (Lower Rio Rancho HSU); and the top of the ledge-forming, reddish, middle part of the Cerro Conejo Formation (Zia HSU). The last contact had to be drawn in using aerial imagery, but the other contacts were already mapped (Cather et al., 1997; Koning et al., 1998; Koning and Personius, 2002).

Using data from these earlier maps (compiled in Connell, 2008b), structural contours were drawn southward from the La Ceja outcrops and eastward from Ceja del Rio Puerco outcrops. Attitudes from geologic maps, lithologic picks in wells (Table 2), and locations of major faults were essential for drawing structural contours away from outcrops. Major faults, defined as those with vertical offsets of more than about 300 ft (100 m), were explicitly modeled by drawing structural contours of their associated fault planes, beginning with their mapped ground trace and extending down-dip according to dip values shown on the geologic map of Connell (2008b). Where no dip data existed, we assumed a dip value consistent with those measured on nearby faults. Faults that were incorporated into the 3D hydrogeologic map include the San Ysidro fault, Zia fault, Doval fault, Coronado-Alameda fault, an unnamed east-down fault between the Doval and Coronado-Alameda faults (continuing southward to Universe Boulevard), Arroyo Venada fault (new name), Tamaya fault, and the Santa Ana section of the San Felipe fault. Vertical displacements for a given fault, used to offset the HSU structural contours, were determined by apparent offsets of

strata in the Kingdom software cross sections as well as vertical displacements calculated from offset contacts on the geologic map of Connell (2008b).

Rasters were generated separately for the tops of the Middle Rio Rancho, Lower Rio Rancho, and Zia HSUs. These tops incorporated both the unsaturated and saturated parts of a given HSU and are found in the feature dataset called "HydroStratUnits_tops" (Appendices 5 and 6). For the tops of the Middle Rio Rancho, Lower Rio Rancho, and Zia HSUs, "relative accuracy" polygons were drawn in areas that we judged to contain poor well control (contained in the "AccuracyPolygons" feature dataset in the geodatabase of Appendix 6). For all three HSUs, low-accuracy polygons are present on the hanging wall (east side) of the Tamaya fault. For the Lower Rio Rancho and Zia HSUs, a low-accuracy polygon extends across most of the southern fifth of the study area. Caution should be used when interpreting the data in these areas because the uncertainty in the results is higher there.

Mapping Saturated HSU Tops

Mapping the top of the saturated portions of a given HSU required additional steps. Two zones within an aquifer needed to be considered: (1) the zone where the HSU is completely saturated (extending from the top to the lower contact of the HSU) and (2) the partially saturated zone, which in the study area is locally found on the western and northern periphery of the completely saturated zone of an HSU. In the partially saturated zone, the elevation of the potentiometric surface lies below the top of the HSU.

Working from the Zia HSU upward to the Upper Rio Rancho HSU, we first defined the saturated extent of the base of a given HSU. Then, within that saturated extent, we combined two rasters to obtain the top of the saturated zone: (1) a raster showing the HSU top where it is fully saturated (corresponding to the HSU top in the previous section) and (2) a raster containing the elevation of the potentiometric surface where the HSU is partially saturated. See Appendix 7 for the ArcGIS details related to this procedure.

Creating Isopach Maps

An isopach map shows the thicknesses of a given map unit using color shading and/or contour lines. Two types of isopach maps were created, the details of which are given in Appendix 7. The first incorporates the entire thickness of an HSU, containing both saturated and unsaturated strata. It is created by subtracting a raster containing the elevations of the base of an HSU from a raster containing the elevations of the top of an HSU. The second isopach map only calculates the thickness of the saturated intervals of an HSU. In the associated raster calculations, one subtracts the saturated base of an HSU (corresponding to the saturated top of the underlying HSU) from the saturated top of the HSU. These surfaces are the same as the rasters used to map the saturated tops of HSUs (as discussed in the previous paragraph).

SUBSURFACE MAPPING RESULTS

Extent and Geometry of HSUs

Sixteen plates in this report illustrate the geometry and elevations of the bounding surfaces of the mapped HSUs, in addition to illustrating their thickness variations. Plates 1–8 depict each HSU in its entirety, including both its saturated and unsaturated portions. Plates 9–16 only depict the bounding surfaces and thicknesses of the saturated zone of each HSU. Plate 17 illustrates which HSUs are present at the potentiometric surface. The ArcGIS map package containing the HSU rasters and other features depicted in the plates (such as structural contours) is provided in Appendix 6. Figures 13 and 14 show the elevation-contoured upper surfaces of the Middle and Lower Rio Rancho HSUs, and Figures 15–17 depict the elevation-contoured tops of the saturated zone contained within the Upper, Middle, and Lower Rio Rancho HSUs, respectively. Figures 18 and 19 are isopach maps of the saturated Upper and Middle Rio Rancho HSUs, respectively.

We synthesized these data regarding the subsurface geometry of the HSUs using a 3D block diagram (Fig. 20). The southwestern and southeastern faces of this diagram correspond to the cross-section lines shown in Figure 4 (blue lines labeled A–A´ and B–B´). Figure 21 provides a 3D depiction of the HSU surfaces. Both of these conceptual models (Figs. 20 and 21) illustrate thickness variations between the HSUs (for example, the Lower Rio Rancho HSU is notably thinner than the Middle Rio Rancho HSU), how the HSUs are offset by faults, and the Ziana horst block.

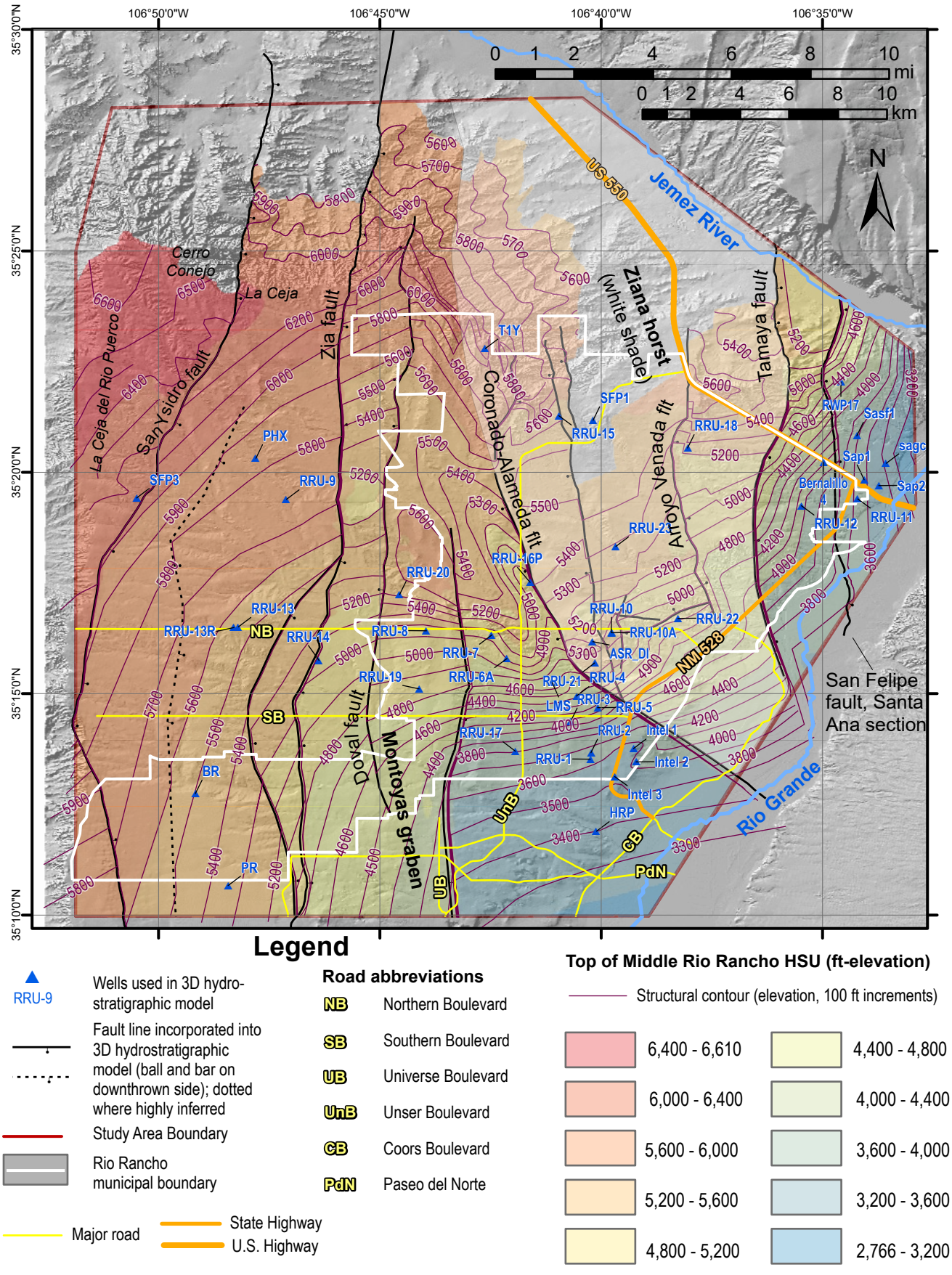

Figure 13. Elevation of the top of the Middle Rio Rancho HSU (in feet); includes both saturated and unsaturated parts of the HSU.

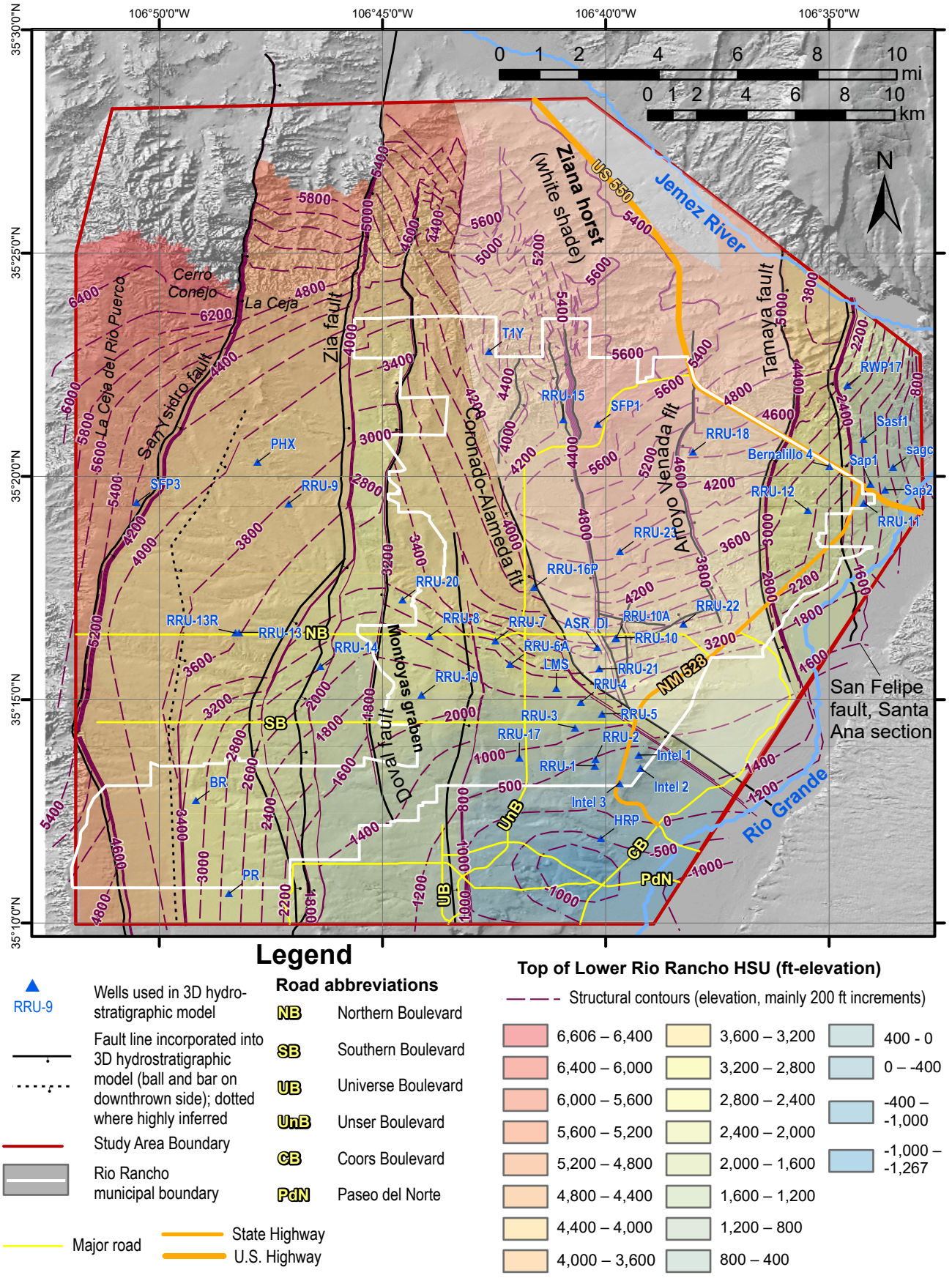

Figure 14. Elevation of the top of the Lower Rio Rancho HSU (in feet); includes both saturated and unsaturated parts of the HSU.

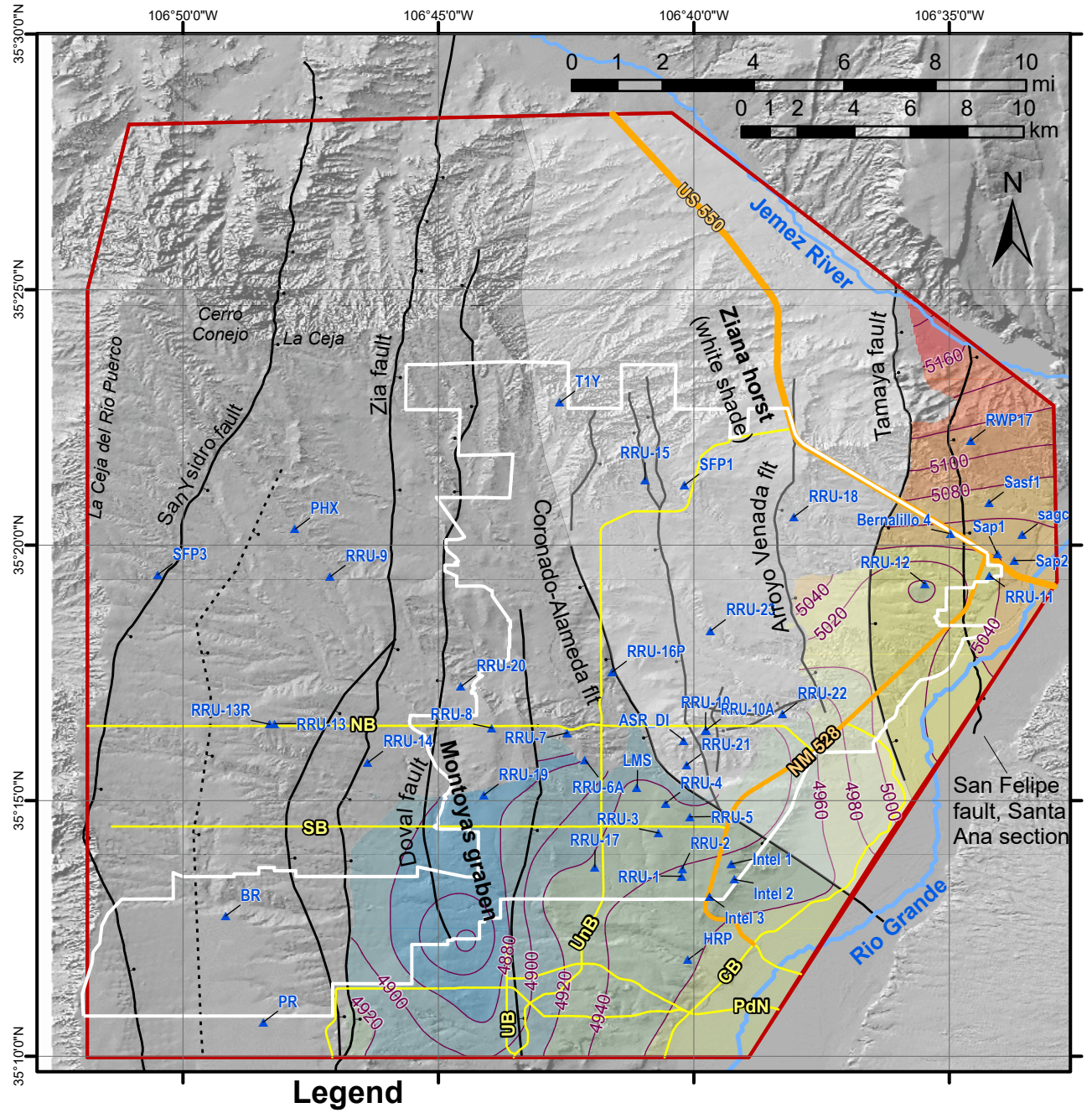

Legend

RRU-9 — Wells used in 3D hydrostratigraphic model

Fault line incorporated into 3D hydrostratigraphic model (ball and bar on downthrown side); dotted where highly inferred

Study Area Boundary

Rio Rancho municipal boundary

Major road

State Highway

U.S. Highway

Road abbreviations

NB	Northern Boulevard
SB	Southern Boulevard
UB	Universe Boulevard
UnB	Unser Boulevard
CB	Coors Boulevard
PdN	Paseo del Norte

Top of saturated Upper Rio Rancho HSU (ft-elevation)

Elevation contour (20 ft increments)
No abrupt offset of contours at faults due to smoothing

5,160 – 5,197	4,960 – 5,000
5,120 – 5,160	4,920 – 4,960
5,080 – 5,120	4,880 – 4,920
5,040 – 5,080	4,838 – 4,880
5,000 – 5,040	

Figure 15. Elevation of the top of the saturated Upper Rio Rancho HSU (in feet).

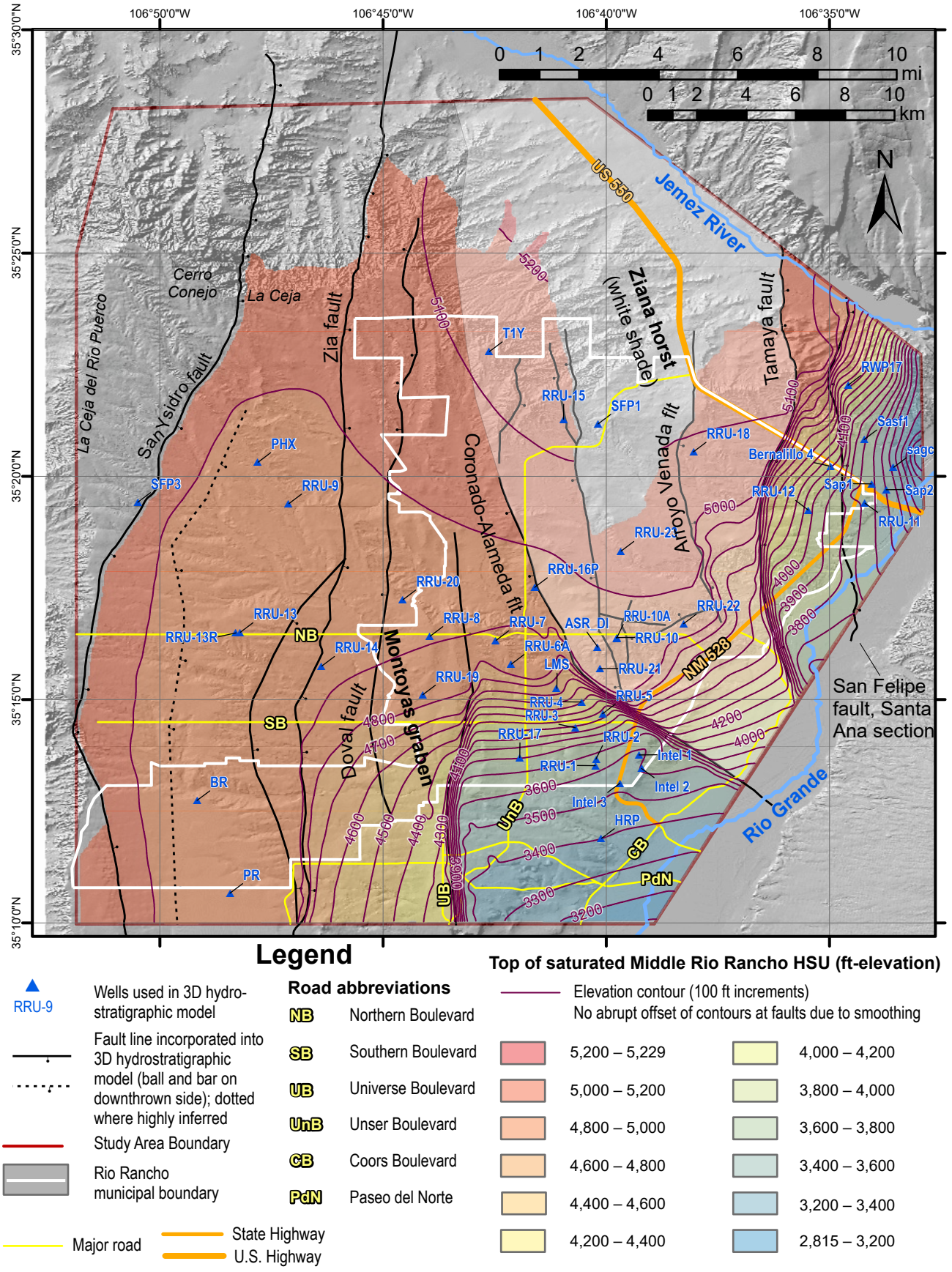

Legend

Top of saturated Middle Rio Rancho HSU (ft-elevation)

RRU-9 — Wells used in 3D hydrostratigraphic model

Fault line incorporated into 3D hydrostratigraphic model (ball and bar on downthrown side); dotted where highly inferred

Study Area Boundary

Rio Rancho municipal boundary

Major road

State Highway

U.S. Highway

Road abbreviations

NB	Northern Boulevard
SB	Southern Boulevard
UB	Universe Boulevard
UnB	Unser Boulevard
CB	Coors Boulevard
PdN	Paseo del Norte

Elevation contour (100 ft increments)
No abrupt offset of contours at faults due to smoothing

5,200 – 5,229	4,000 – 4,200
5,000 – 5,200	3,800 – 4,000
4,800 – 5,000	3,600 – 3,800
4,600 – 4,800	3,400 – 3,600
4,400 – 4,600	3,200 – 3,400
4,200 – 4,400	2,815 – 3,200

Figure 16. Elevation of the top of the saturated Middle Rio Rancho HSU (in feet).

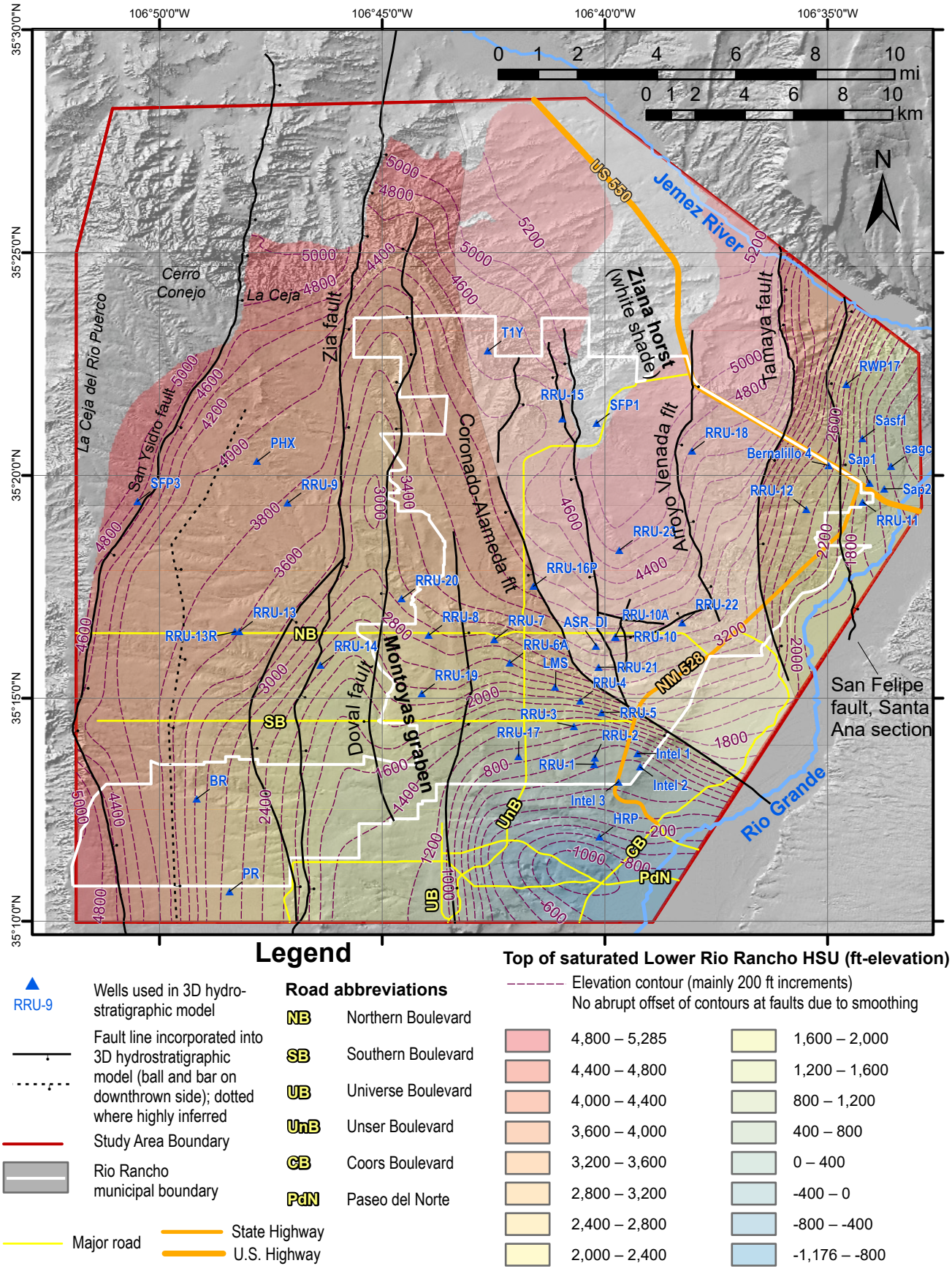

Legend

RRU-9 — Wells used in 3D hydrostratigraphic model

Fault line incorporated into 3D hydrostratigraphic model (ball and bar on downthrown side); dotted where highly inferred

Study Area Boundary

Rio Rancho municipal boundary

Major road

State Highway

U.S. Highway

Road abbreviations

NB	Northern Boulevard
SB	Southern Boulevard
UB	Universe Boulevard
UnB	Unser Boulevard
CB	Coors Boulevard
PdN	Paseo del Norte

Top of saturated Lower Rio Rancho HSU (ft-elevation)

Elevation contour (mainly 200 ft increments)
No abrupt offset of contours at faults due to smoothing

4,800 – 5,285	1,600 – 2,000
4,400 – 4,800	1,200 – 1,600
4,000 – 4,400	800 – 1,200
3,600 – 4,000	400 – 800
3,200 – 3,600	0 – 400
2,800 – 3,200	-400 – 0
2,400 – 2,800	-800 – -400
2,000 – 2,400	-1,176 – -800

Figure 17. Elevation of the top of the saturated Lower Rio Rancho HSU (in feet).

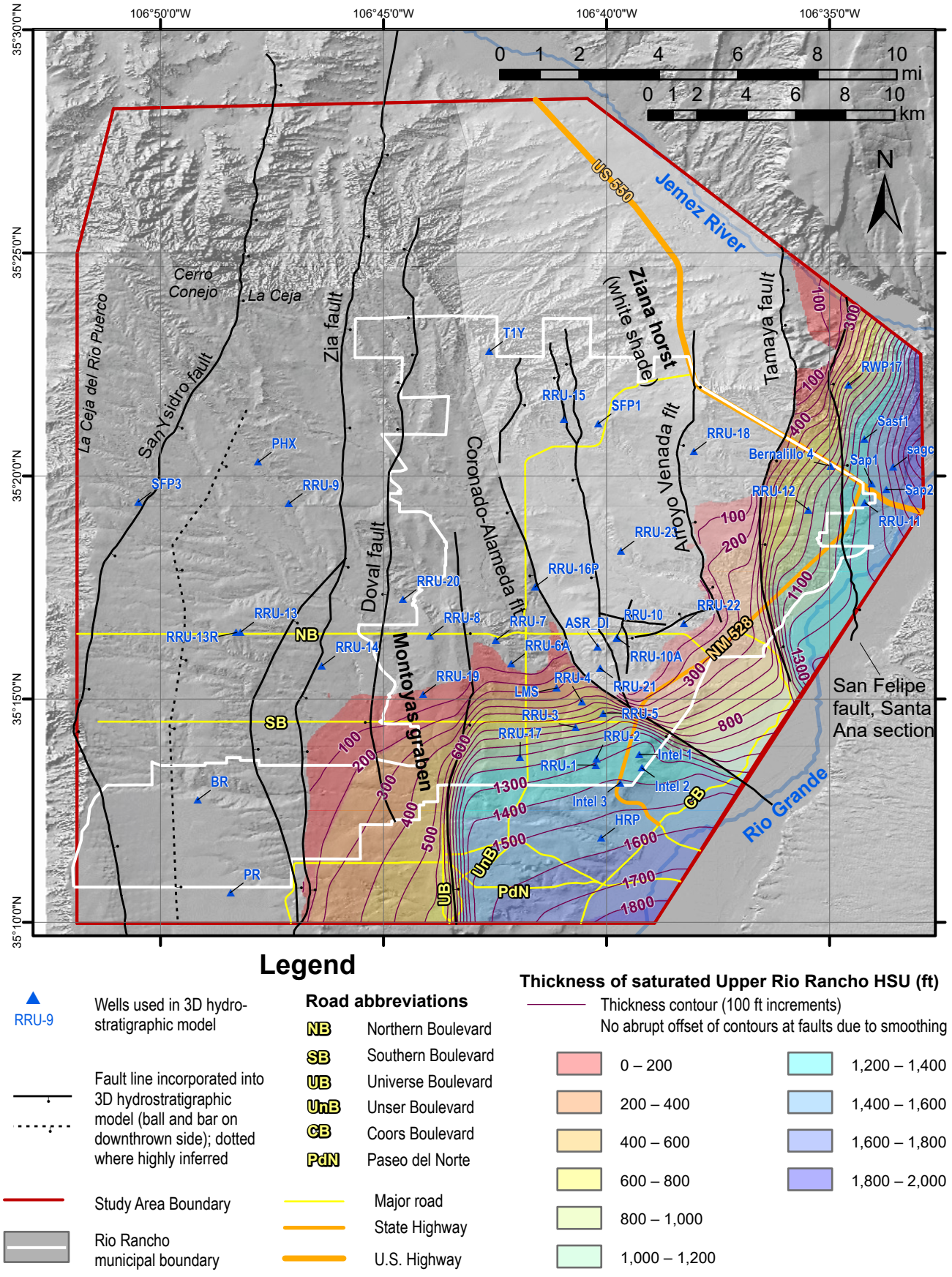

Legend

RRU-9 — Wells used in 3D hydrostratigraphic model

Fault line incorporated into 3D hydrostratigraphic model (ball and bar on downthrown side); dotted where highly inferred

Study Area Boundary

Rio Rancho municipal boundary

Road abbreviations

NB	Northern Boulevard
SB	Southern Boulevard
UB	Universe Boulevard
UnB	Unser Boulevard
CB	Coors Boulevard
PdN	Paseo del Norte

Major road

State Highway

U.S. Highway

Thickness of saturated Upper Rio Rancho HSU (ft)

Thickness contour (100 ft increments)
No abrupt offset of contours at faults due to smoothing

0 – 200	1,200 – 1,400
200 – 400	1,400 – 1,600
400 – 600	1,600 – 1,800
600 – 800	1,800 – 2,000
800 – 1,000	
1,000 – 1,200	

Figure 18. Thickness of the saturated part of the Upper Rio Rancho HSU (in feet).

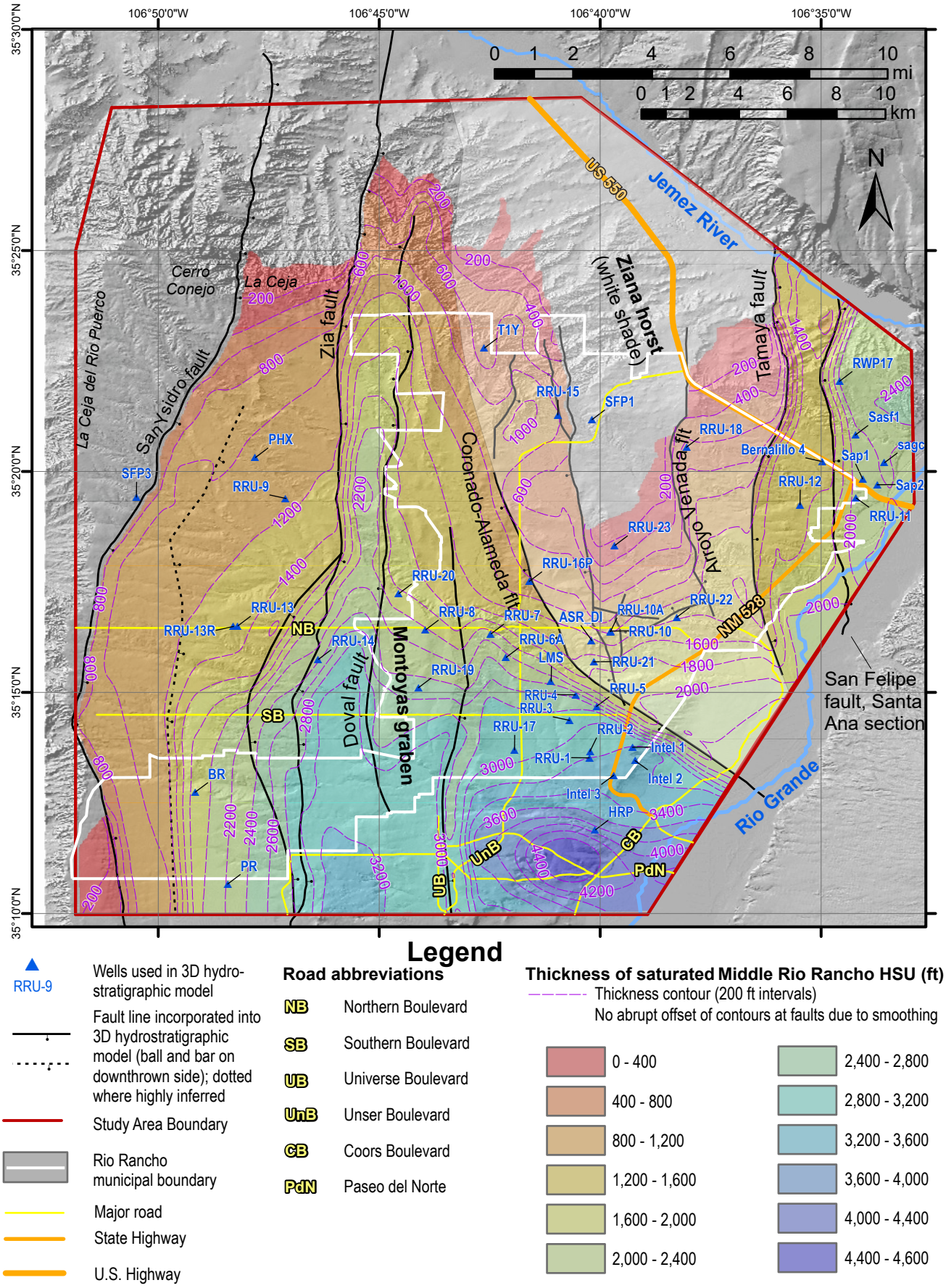

Legend

RRU-9 — Wells used in 3D hydrostratigraphic model

Fault line incorporated into 3D hydrostratigraphic model (ball and bar on downthrown side); dotted where highly inferred

Study Area Boundary

Rio Rancho municipal boundary

Major road

State Highway

U.S. Highway

Road abbreviations

NB	Northern Boulevard
SB	Southern Boulevard
UB	Universe Boulevard
UnB	Unser Boulevard
CB	Coors Boulevard
PdN	Paseo del Norte

Thickness of saturated Middle Rio Rancho HSU (ft)

Thickness contour (200 ft intervals)

No abrupt offset of contours at faults due to smoothing

0 - 400	2,400 - 2,800
400 - 800	2,800 - 3,200
800 - 1,200	3,200 - 3,600
1,200 - 1,600	3,600 - 4,000
1,600 - 2,000	4,000 - 4,400
2,000 - 2,400	4,400 - 4,600

Figure 19. Thickness of the saturated part of the Middle Rio Rancho HSU (in feet).

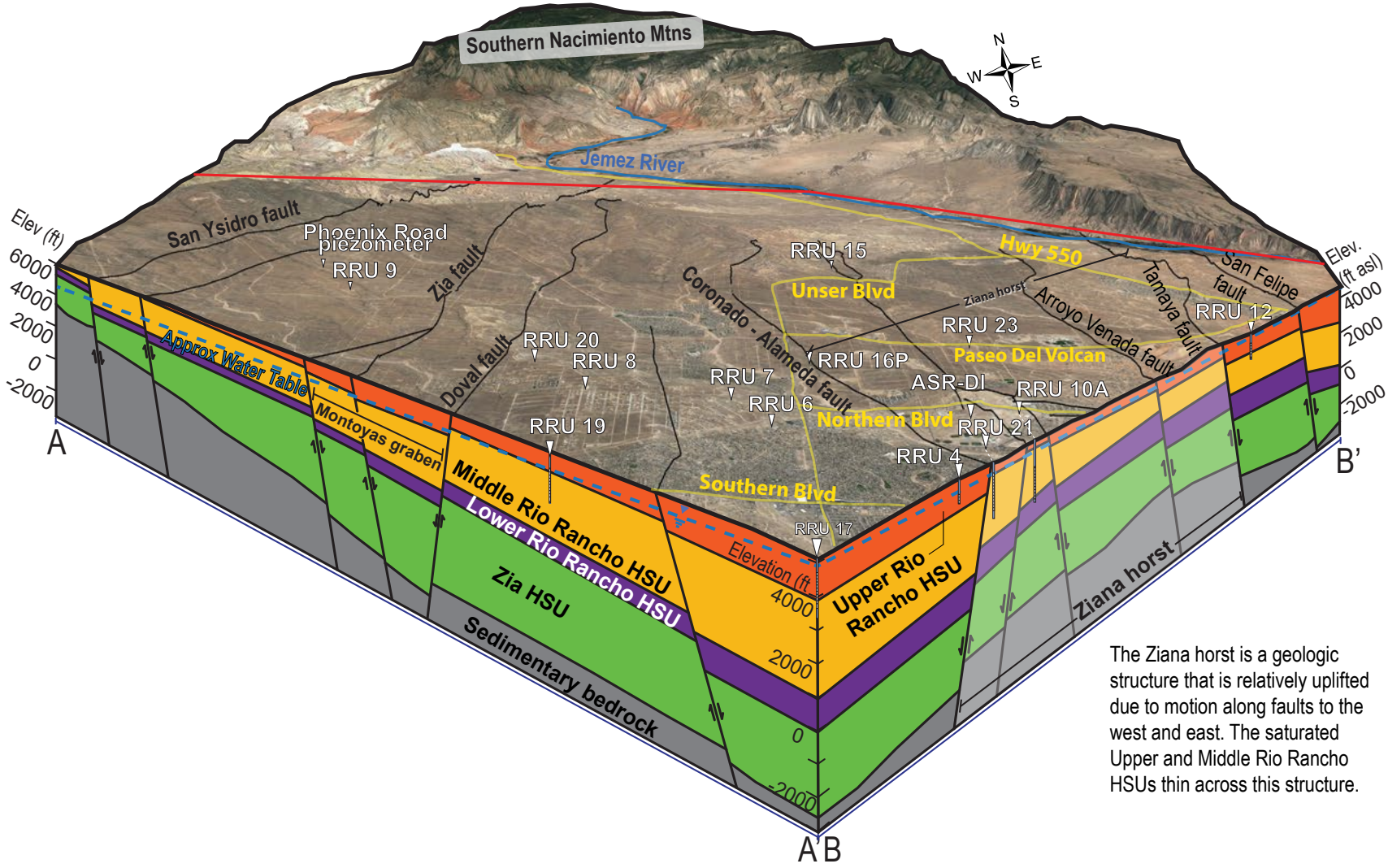

The Ziana horst is a geologic structure that is relatively uplifted due to motion along faults to the west and east. The saturated Upper and Middle Rio Rancho HSUs thin across this structure.

Figure 20. Three-dimensional block diagram of the hydrogeologic subsurface model under the northwestern Albuquerque Basin. View is to the NNE. The faces of the block diagram correspond to the cross-section lines shown in Figure 4. The four colored layers are the HSUs designated in this study (top to bottom): the Upper, Middle, and Lower Rio Rancho HSUs and the Zia HSU. Faults are depicted by thick black lines on the surface and subsurface; the relative sense of vertical motion along a fault is shown by arrows. Surface locations of wells correspond to the white triangles. The subsurface extent and screen depth of a well projected to a cross-section line (face of the diagram) is shown by a vertical line, and the screen depth is indicated by the closely spaced horizontal lines.

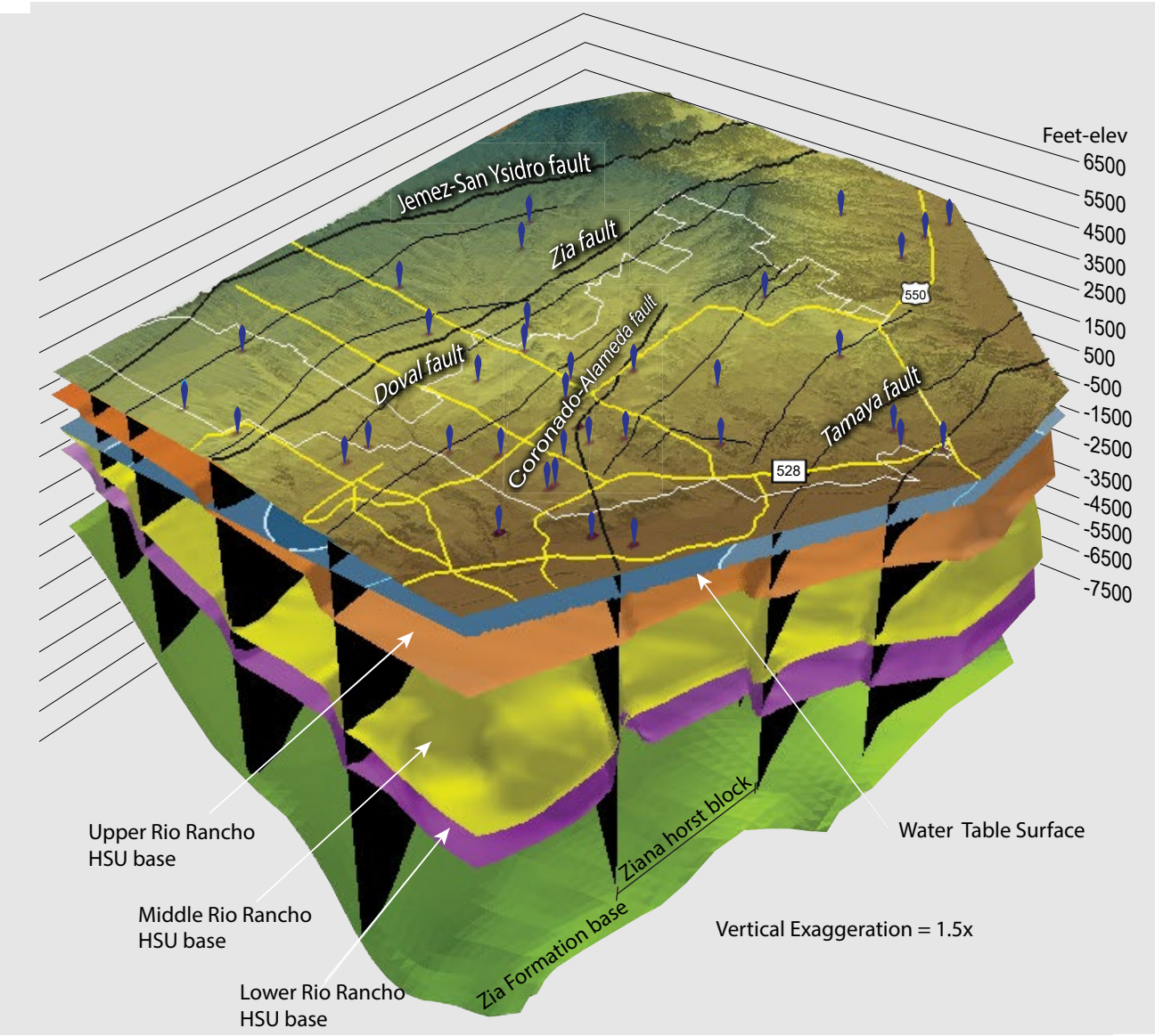

Figure 21. Three-dimensional depiction of the HSU surfaces under the northwestern Albuquerque Basin. The uppermost surface is a shaded-relief map of surface topography on which the following features are shown: roads (yellow lines), Rio Rancho municipal boundary (white line), and faults (black lines). The underlying HSU surfaces are color-coded and labeled. Subsurface fault planes are depicted by black, vertical to very steeply dipping panels (planes). The sloping water table surface is shown in blue.

Hydrogeologic Implications

Here we discuss important hydrogeologic features in the study area, starting in the northwest and moving counterclockwise.

Western Faults

The San Ysidro and Zia faults play major roles in the hydrogeology on the west side of the study area. About 100–1,000 feet (30–300 m) of east-down, vertical displacement of HSU surfaces occurs across these two structures. The top of the Lower Rio Rancho HSU (corresponding to the base of the Middle Rio Rancho HSU) is commonly offset more than the top of the Middle Rio Rancho HSU (Figs. 13 and 14). The saturated Middle Rio Rancho HSU is generally only present on the east side of the San Ysidro fault and thickens notably east of the Zia fault, where it is about 3,000 ft (~900 m) thick south of Southern Boulevard (Fig. 19).

Montoyas Graben

Between the Zia fault and the Ziana horst lies a structurally depressed area, referred to as the Montoyas graben (after the nearby Arroyo de los Montoyas), bisected by the west-down Doval fault (Figs. 16, 17, and 19; Arroyo de los Montoyas shown in Fig. 1). East of the Doval fault, map data (Connell, 2008b) indicate north-northwest strikes and west-southwest dips, so the eastern part of the graben is modeled as an approximately 3°, west-southwest-dipping homocline. Approximately 100 to a few hundred feet (30 to ~100 m) of west-down offset is inferred to occur along the Doval fault, so the deepest part of the Calabacillas subbasin is modeled as a narrow (~2 mi [3 km] wide) arm bracketed between the Doval and Zia faults (Figs. 3, 14, and 17). It is in this arm that the saturated Middle Rio Rancho HSU is estimated to be 2,000 ft (600 m) thick (Fig. 19).

The Montoyas graben merges with the Calabacillas subbasin near the southern end of the Doval fault, at the western end of Paseo del Norte (Figs. 3, 14, and 17). The saturated zone of the Upper Rio Rancho HSU is present only south of Southern Boulevard, where it increases southward in thickness to roughly 500–600 ft (150–180 m) on the immediate footwall (west side) of an unnamed fault that runs parallel to Universe Boulevard (Fig. 18). This fault is inferred largely from an aeromagnetic lineament (Connell, 2008b) and the top-of-bedrock surface of Grauch and Connell (2013). The amount of throw across this fault is uncertain, so there is considerable uncertainty in how much the saturated Upper Rio Rancho HSU thickens across it. The underlying saturated Middle Rio Rancho HSU is estimated to be about 3,000 ft (900 m) thick on the immediate west side of this unnamed fault and roughly 3,000–4,000 ft (900–1,200 m) thick in the area east of this unnamed fault, but the thickness on the east side is poorly constrained. Note that the sandy Lower Rio Rancho HSU may not extend as far south as this area, in the sense of being unique compared to the Zia HSU in texture and permeability (Fig. 17, Plates 3 and 6), based on the uncertain presence of the Lower Rio Rancho HSU at the bottom of the Black Ranch test well (Table 2, well labeled BR in Figs. 14–19).

Southeast Corner of the Study Area

Data from abundant wells indicate relatively steep southward dips of the Upper/Middle Rio Rancho HSU contact near the eastern end of Southern Boulevard. The related structure was referred to as the Loma Colorado Transition Zone by Hawley and Whitworth (1996). This structure defines the southern end of the Ziana horst (see below) and results in the Upper and Middle Rio Rancho HSUs being thicker to the south (Figs. 18 and 19).

Based on this structure and the top-of-bedrock surface of Grauch and Connell (2013), we infer that the Santa Fe Group aquifer is thickest in the southeast corner of the study area, in the vicinity of the intersection of Coors Boulevard and Paseo del Norte (Figs. 18 and 19). Here, the saturated Upper Rio Rancho HSU is 1,500–1,800 ft (450–550 m) thick, and the underlying saturated Middle Rio Rancho HSU is inferred to be greater than 4,000 ft (>1,200 m) thick. The saturated Upper Rio Rancho HSU decreases in thickness to the north, between the unnamed fault near Universe Boulevard and the Coronado-Alameda fault (Fig. 18), pinching out northward about midway between Southern and Northern Boulevards along the aforementioned Loma Colorado Transition Zone. The Zia HSU is also probably thick in the southeast corner (Plate 8). As noted earlier, we are not certain how far southward of Southern Boulevard the sandy Lower Rio Rancho HSU extends as a unit distinguishable from the Zia HSU (Fig. 17, Plate 3). Except for the Lower Rio Rancho HSU, the thickest saturated HSUs, and correspondingly the highest aquifer transmissivities, are interpreted to exist in the southeast corner of the study area.

Coronado-Alameda Fault

The fault that bounds the west and southwest sides of the Ziana horst is inferred to be a continuation of the Coronado-Alameda fault (Connell, 2008b). That such a southwest-down normal fault is present is well-supported by our lithologic picks and inter-well correlations in the area west of New Mexico State Road 528 (northern Coors Boulevard) and north of Southern Boulevard. Based on these correlations, we interpret several hundred feet of southwest-down vertical displacement on the Coronado-Alameda fault, increasing to the southeast (Figs. 13, 14, and 20). The saturated Upper Rio Rancho HSU is interpreted to increase in thickness by 400–800 ft (120–250 m) across this structure (from NE to SW), and thus the fault should be considered an important hydrogeologic feature that forms the northeast side of the relatively thick, saturated Upper Rio Rancho HSU (Fig. 18).

Ziana Horst

The Ziana horst (referred to as the Ziana anticline in Black and Hiss, 1974) extends southeasterly across the east-central part of the study area (Figs. 3, 4, and 13–21). It is bounded mainly by the west-southwest-down Coronado-Alameda fault and a series of east-down faults that includes the Arroyo Venada, Tamaya, and San Felipe faults. To the north of Rio Rancho, the Coronado-Alameda fault appears to die out northward, and the western margin of the Ziana horst is mainly a west-southwest-dipping homocline merging westward with the eastern Montoyas graben. Many internal, relatively small-displacement faults are present within the delineated horst block, and they form a particularly complex network near Rio Rancho High School between the eastern ends of Northern and Southern Boulevards (Fig. 4). To reconcile geometries during the structural contouring of HSU tops, we reinterpreted the mapping of the two innermost faults of the Ziana horst (cf. Personius et al., 2000; Connell, 2008b). The western of the two faults (unnamed) continues northward from previously mapped faults near wells RRU-21 and RRU-10; our contouring effort east of well RRU-16P necessitated this fault being west-down there, and we connect it to previously mapped west-down faults near wells RRU-15 and SFP-1 (Figs. 2 and 13–19). The eastern of the two inner faults is a large east-down fault immediately west of well RRU-18 (Fig. 4), which we call the Arroyo Venada fault (new name), the majority of which was mapped earlier by Personius et al. (2000). An ash located at the bottom of well RRU-18 (2,070–2,080 ft [~630 m] depth) chemically correlates with an 11.3 Ma Trapper Creek B Ash (Appendix 8). This ash is more or less at the same stratigraphic level as the 11.19 ± 0.10 Ma Trapper Creek ash seen in outcrop along U.S. Route 550 (sample MRGB-19BN of Koning and Personius, 2002), and together these ashes provide a stratigraphic datum for mapping the top of the Lower Rio Rancho HSU across this fault. Our structural contouring of this datum indicates approximately 600 ft (~180 m) of east-down vertical displacement on the Arroyo Venada fault and several hundred feet (hundreds of meters) of structural relief from a south-down structural ramp on the eastern hanging wall of the fault. The structural relief caused by these features must have occurred after the emplacement of the 11.3–11.2 Ma Trapper Creek ashes.

On the Ziana horst, the tops of the HSUs strike east-northeast and dip south-southeast (e.g., Figs. 13 and 14). Furthermore, the Upper and Middle Rio Rancho HSUs pinch out to the north-northwest on this horst (Plates 5–8). This results in a north-northwest pinch-out of the saturated parts of these particular HSUs (Figs. 15, 16, 18, and 19). The saturated Upper Rio Rancho HSU is generally restricted to the southeast of New Mexico State Road 528 (Fig. 18). The saturated Middle Rio Rancho HSU extends only about 4 mi (6 km) north of wells RRU-10 and RRU-10A on the footwall (west side) of the Arroyo Venada fault (Fig. 19). However, it continues several miles northward on the west side of the unnamed fault extending from well RRU-10 to well RRU-15, where the saturated HSU is 600–1,000 ft (180–300 m) thick and thickens to 800–1,500 ft (250–450 m) west of the Coronado-Alameda fault (Fig. 19). Between the Arroyo Venada and Tamaya faults, the saturated Middle Rio Rancho HSU is only a few hundred feet (~100 m) thick near U.S. Route 550, but it increases southward to be greater than 1,000 ft (>300 m) thick near New Mexico State Road 528 (Fig. 19).

Bernalillo Area, East of the Tamaya Fault

Because of their long lengths, we assume several hundred feet of vertical offset for both the Tamaya and San Felipe faults (Santa Ana section). This is consistent with the interpretation that none of the studied wells east of the San Felipe fault fully penetrate the Upper Rio Rancho HSU (Table 2, Appendix 2). Due to this lack of penetration, tops and saturated thicknesses for the HSUs east of the San Felipe fault, in the Bernalillo area, are uncertain.

ASSESSING PERMEABILITY DIFFERENCES BETWEEN AND WITHIN HSUS

We used two approaches to assess permeability differences between HSUs. The first approach entailed detailed mapping of selected vertical outcrop faces associated with a given HSU, and the second involved compiling pumping test data reflective of permeability, namely hydraulic conductivities and specific capacities.

OUTCROP MAPPING

Strata that make up the four HSUs are visible at the surface about 13 mi (20 km) to the northwest of the city of Rio Rancho, allowing for direct study of the lithologic character of these HSUs in the badlands of the Zia Pueblo south of U.S. Route 550 (Fig. 5). Direct study of the outcrops in this area allows for a comparative, local assessment of the lithologic differences between various stratigraphic intervals of the Santa Fe Group aquifer (i.e., between selected parts of HSUs), and presumably these differences would also exist to the southeast in the subsurface. Collectively, these data can be used to assess which HSUs may provide more favorable groundwater yields or hydraulic conductivities. Comparable outcrop analog studies for assessing aquifer permeability properties include those of Aigner et al. (1996), Al-Ajmi et al. (2011), Becker et al. (2019), Biteman et al. (2004), Busch et al. (2022), Davis et al. (1993), Gaud et al. (2004), Hornung and Aigner (2006), Howell et al. (2014), Keller et al. (2019), and Klingbeil et al. (1999). Only outcrops correlative to the upper Zia HSU and Middle Rio Rancho HSU provided adequate vertical faces extensive enough for outcrop mapping, so we restricted our mapping to these two units. Various data relating to this effort, including lithologic texture maps of outcrop faces, are contained in Appendix 9.

Methods

At six sites (ZP-1 through ZP-6), whose locations are depicted in Figure 2, we used an uncrewed aerial vehicle (UAV) to photograph illustrative outcrops for both the middle Cerro Conejo and lower–middle Arroyo Ojito Formations. Highly overlapping photographs with GPS coordinates taken from the UAV were stitched together using structure-from-motion software (Drone2Map) to produce 3D point clouds of the near-vertical cliff faces that expose the units of interest. The stitched photographs were mapped (in 2D) using ArcGIS software to calculate the relative proportions of sand versus clayey sediment as well as sand amalgamation ratios (length of sand-against-sand contacts vs. total contact length). The 3D models of the outcrop were used to measure lengths and thicknesses of sand bodies (models are available from the lead author, provided associated permission is granted by Zia Pueblo).

Results

Appendix 9 contains data and a discussion related to the outcrop mapping effort. Table A9-01 gives the outcrop locations, and Tables A9-02 and A9-03 tabulate the measurement data from the annotated outcrops of the 2D exposures. The annotated versions of the high-resolution stitched images of the outcrop mapping are in a folder in Appendix 9 (OutcropPhotos_Annotated). In the tables and annotated photographs of Appendix 9, the upper Zia Formation HSU corresponds to the middle Cerro Conejo Formation. The stratigraphic lithologic intervals of the Middle Rio Rancho HSU include the Navajo Draw and Loma Barbon Members of the Arroyo Ojito Formation. Note that the two outcrop faces we studied in the Loma Barbon Member are from the lower part of this lithostratigraphic unit.

Compared to the analyzed Middle Rio Rancho HSU, the upper Zia HSU has a higher proportion of sand (93–100% vs. 76–91% in the Middle Rio Rancho HSU) and a lower proportion of clayey beds (<10% vs. 9–24% in the Middle Rio Rancho HSU; Table 3). Sand amalgamation ratios (Table 3)

are also notably higher for the upper Zia HSU (0.7–1.0) compared to the Middle Rio Rancho HSU (0.2–0.7), implying more connectivity of sandstones that would facilitate groundwater flow. Data from two sites suggest that the Loma Barbon Member has shorter clay body and sand body lengths compared to the Navajo Draw Member. Although the lower part of the exposed Loma Barbon Member (analyzed by this method) has around 10% clays, qualitative observations of outcrops and wells indicate that the Loma Barbon Member generally coarsens upsection, so the clay percentage likely decreases upsection. Length measurements for sands are of limited practical value for comparing the upper Zia HSU to the Middle Rio Rancho HSU because they generally correspond to outcrop length. Clay lengths in the upper Zia HSU are longer than those in the Middle Rio Rancho HSU by a factor of 3 to 4, based on comparison of four sites. The shorter clay lengths in the Middle Rio Rancho HSU would suggest possibly higher connectivity between sand intervals in the Middle Rio Rancho HSU than implied by the sand amalgamation ratios (Table 3). Average sand body thicknesses are around 16 ft (5 m) in both the upper Zia HSU and Middle Rio Rancho HSU, although locally in the upper Zia HSU they are as much as 55 ft (17 m). Collectively, these outcrop data suggest that the upper Zia HSU has lithologic characteristics (particularly sand vs. clay proportions and sand amalgamation ratios) conducive to slightly higher permeability and groundwater yields. However, because the Zia HSU is buried to a greater extent than the Middle Rio Rancho HSU in the Rio Rancho area, it is expected to be more compacted and perhaps more cemented, and this will adversely affect its permeability. Overestimation of actual permeability in subsurface strata has been documented in previous outcrop analogue studies due to lower degrees of cementation and compaction in outcrops compared to subsurface (well samples) (Busch et al., 2022). Furthermore, we only studied outcrop faces representing limited stratigraphic intervals of either the upper Zia HSU or the Middle Rio Rancho HSU, so extrapolating results to the entire hydrostratigraphic unit could very well be misleading.

Table 3. Results of the HSU outcrop study on Zia Pueblo.

Site	HSU[1]	Lithostratigraphic unit[1]	Sand %	Clayey sediment %	Sand amalgamation ratio	Avg sand body length (m)[2]	Avg clayey body length (m)	Avg sand body thickness (m)
ZP_01	Upper Zia	Tccml	93	7	0.89	324	n/a	5
ZP_02	MRR	Taobl	90	10	0.5	n/a	n/a	n/a
ZP_03-east[3]	Upper Zia	Tccml	94	6	0.7			
ZP-03-west[3]	Upper Zia	Tccml	100	0	0.98			
ZP-03-all	Upper Zia	Tccml				497	434	17
ZP_04	MRR	Taobl	91	9	0.69			
ZP_05-east[3]	MRR	Taon	76	24	0.27			
ZP_05-west[3]	MRR	Taon	84	16	0.22			
ZP_06	MRR	Taobl	90	10	0.49			
ZP_04, 06	MRR	Taobl				98	99	5
ZP_05-all	MRR	Taon				306	134	5

SUMMARY		
HSU	**Avg sand body thickness (m)**	**Avg sand amalgamation ratio**
Middle Rio Rancho (MRR)	5 (n=2)	0.43 (n=5)
Upper Zia	11 (n=2)	0.86 (n=3)

[1] Abbreviations: MRR = Middle Rio Rancho HSU, Tccml = middle to lower part of Cerro Conejo Formation, Taobl = lower Loma Barbon Member of Arroyo Ojito Formation, Taon = Navajo Draw Member of Arroyo Ojito Formation, n/a = data not available because of paucity of clay beds (ZP-01) or because a 3D model was not made (ZP-02).
[2] Length measurements for sands are of limited practical value because they generally correspond to outcrop length. See Appendix 9 for full dataset.
[3] Note that some sites are divided into eastern and western parts.

DETERMINING SAND VERSUS CLAYEY SEDIMENT FOR HSUS USING WELL DATA

Methods

Well Wireline Analyses

Rio Rancho is fortunate to have at least 41 wells with adequate lithologic data (i.e., archived cuttings or wireline geophysical logs) to construct structural contours of the HSU contacts (Table 2, Appendix 2). Of these, digital data (LAS) files were available for 25 wells (Appendix 2). The wireline logs commonly contain induction (or electric resistivity), spontaneous potential (SP), gamma-ray, neutron-porosity, and density-porosity data. Some wells have formation analysis logs, which use the previously listed wireline data to calculate sand versus shale versus calcium carbonate content, as well as effective porosity as a function of depth.

Using these wireline data combined with available cuttings data, we delineated sand, clay, and clayey sand intervals for 22 of these wells (Appendix 5). In terms of procedure, various well logs were placed on a large gridded canvas in Adobe Illustrator and adjusted so that they lined up side by side in terms of depth. The utilized well logs included induction (or electric resistivity) plus SP, gamma-ray plus neutron-porosity, caliper plus density-porosity, and formation analysis (the latter was only available for wells RRU-6A, RRU-9, RRU-10, and RRU-14 through RRU-20). Curves of gamma-ray and conductivity, digitized as part of the work by Riesterer et al. (2004), were also placed on the canvas. Using standard wireline interpretation methods to recognize subsurface lithologies, uniquely colored rectangles were drawn in Adobe Illustrator that corresponded to sand versus clay intervals. "Muddy sand" was assigned to depths not designated as sand or clay. The stack of colored rectangles enabled rapid visual assessment of vertical changes in lithology in a given well. The depth ranges of each colored rectangle were tabulated in an Excel spreadsheet. The proportions of clay, muddy sand, and sand were then calculated and compiled for each HSU (Table 4, Appendix 5).

Note that this lithologic breakout was conducted from the water table to the bottom of the well. Thus, the lithologic summaries only pertain to the saturated zones of an HSU; in the case of the Middle Rio Rancho HSU, which coarsens upward, this results in an underestimation of the sand content compared to using the entire HSU (including the saturated and unsaturated zones). Also, we only delineated lithologies to the bottom of the Cerro Conejo Formation in deep oil exploratory wells.

Vshale Analyses

Assuming that higher percentages of sand correlate with higher permeability (Gaud et al., 2004, fig. 3; Fetter, 2018), an indirect method of assessing permeability changes is noting vertical or horizontal changes in the percentage of sand bodies in an HSU. As an ancillary to the aforementioned sand percentage dataset, determined through detailed investigation and analysis of several wireline logs (Table 4, Appendix 5), we used only gamma-ray data to calculate net-to-gross ratios of sand bodies relative to the saturated HSU thickness in a given well. This ratio can be viewed as a sand body percentage and is calculated using Kingdom software from downhole gamma-ray logs. From the gamma-ray log, a Vshale curve is calculated using the end members of pure sand (approximate minimum of gamma-ray values) and pure clay (approximate maximum of gamma-ray values). The corresponding equation (Tearpock and Bischke, 2002) is:

$$Vshale = (GR-GRCLN)/(GRSHL-GRCLN)$$

where GR is the gamma-ray log value at a measured depth, GRCLN is the minimum gamma-ray value (clean sand) along the studied depth of the well, and GRSHL is the maximum gamma-ray value (clay or shale) along the studied depth of the well. For this study, sand bodies were recognized as such where the Kingdom Vshale value was 0.25 or less.

Results

Well Wireline Analyses

We used all available downhole wireline logs coupled with a study of archived cuttings to manually delineate sand, clay, and clayey sand intervals for 22 wells in the study area. The proportions of sand versus clayey sand versus clay are tabulated in Table 4. Figure 22 summarizes the results of these analyses.

These data show that the Lower Rio Rancho HSU has the most favorable lithologic permeability proxies, followed by the Upper Rio Rancho HSU.

Table 4. Compilation of lithologic texture thicknesses per well (saturated part of HSU only).

		Total thicknesses (ft)				Fraction of total			Sand/clay proportions	
Well	HSU[1]	Clay	Muddy sand	Sand	All strata	Clay	Muddy sand	Sand	Sand/ clay	Clay/ sand
RRU-6A	MRR	151	247	510	908	0.17	0.27	0.56	3.38	0.30
RRU-7	MRR	75	133	270	478	0.16	0.28	0.56	3.60	0.28
RRU-8	MRR	210	388	527	1125	0.19	0.34	0.47	2.51	0.40
RRU-9	MRR	99	184	182	465	0.21	0.40	0.39	1.84	0.54
RRU-10A	MRR	176	577	477	1230	0.14	0.47	0.39	2.71	0.37
	LRR	10	113	405	528	0.02	0.21	0.77	40.50	0.02
RRU-12	URR	179	298	539	1016	0.18	0.29	0.53	3.01	0.33
	MRR	99	96	83	278	0.36	0.35	0.30	0.84	1.19
RRU-13R	MRR	187	622	467	1276	0.15	0.49	0.37	2.50	0.40
	LRR	0	3	73	76	0.00	0.04	0.96	All sand	0.00
RRU-14	MRR	103	338	506	947	0.11	0.36	0.53	4.91	0.20
RRU-15	MRR	103	338	506	947	0.11	0.36	0.53	4.91	0.20
Fault in unsaturated zone	LRR	28	48	105	181	0.15	0.27	0.58	3.75	0.27
RRU-16P[2]	MRR	50	319	633	1002	0.05	0.32	0.63	12.66	0.08
MRR may be faulted	LRR	5	100	336	441	0.01	0.23	0.76	67.20	0.01
RRU-17	URR	102	433	621	1156	0.09	0.37	0.54	6.09	0.16
	MRR	158	201	115	474	0.33	0.42	0.24	0.73	1.37
RRU-18	MRR	42	201	415	658	0.06	0.31	0.63	9.88	0.10
	LRR	49	85	891	1025	0.05	0.08	0.87	18.18	0.05
RRU-19	URR	5	21	83	109	0.05	0.19	0.76	16.60	0.06
	MRR	260	293	773	1326	0.20	0.22	0.58	2.97	0.34
RRU-20[3]	MRR	13	39	33	85					
RRU-21	MRR	242	736	740	1718	0.14	0.43	0.43	3.06	0.33
RRU-22	URR	8	8	37	53	0.15	0.15	0.70	4.63	0.22
	MRR	221	530	700	1451	0.15	0.15	0.70	4.63	0.22
	LRR	4	55	841	900	0.00	0.06	0.93	210.25	0.00
	Zia	55	109	235	399	0.14	0.27	0.59	4.27	0.23
RRU-23	MRR	65	148	116	329	0.20	0.45	0.35	1.78	0.56
	LRR	113	312	915	1340	0.08	0.23	0.68	8.10	0.22
	Zia	294	346	322	962	0.31	0.36	0.33	1.10	0.22
Phoenix Rd	MRR	113	133	272	518	0.22	0.26	0.53	2.41	0.22
Paradise Rd	MRR	156	406	294	856	0.18	0.47	0.34	1.88	0.22
Hunters Ridge Piezometer	URR	110	780	442	1332	0.08	0.59	0.33	4.02	0.22
Bernalillo 4	URR	127	201	626	954	0.13	0.21	0.66	4.93	0.20
ASR_Dir_Injection	MRR	210	608	720	1538	0.14	0.40	0.47	3.43	0.29
Per HSU										
	URR	**531**	**1741**	**2348**	**4620**	**0.11**	**0.38**	**0.51**	**4.4**	**0.2**
	MRR	**2879**	**6585**	**8398**	**17862**	**0.16**	**0.37**	**0.47**	**2.9**	**0.3**
	LRR	**209**	**713**	**3566**	**4488**	**0.05**	**0.16**	**0.79**	**17.1**	**0.1**
	Zia	**349**	**455**	**557**	**1361**	**0.26**	**0.33**	**0.41**	**1.6**	**0.6**

[1] Abbreviations: URR = Upper Rio Rancho HSU, MRR = Middle Rio Rancho HSU, LRR = Lower Rio Rancho HSU, Zia = Zia HSU
[2] Faulting very likely excises strata.
[3] Insufficient data for proportion calculations.

The sand-versus-clay ratio in the Lower Rio Rancho HSU is 17.1 and the Upper Rio Rancho HSU is 4.4, whereas the Middle Rio Rancho and upper Zia HSUs are close to 3 and 2, respectively (Fig. 22). The proportions of clay and clayey sand in the Lower Rio Rancho HSU are at least half of those in the other three HSUs. The proportions of clay and sand (relative to total) in the Upper Rio Rancho HSU (Table 4) are 0.11 and 0.51, respectively, while those of the Middle Rio Rancho HSU are 0.16 and 0.47, implying higher permeabilities for the Upper Rio Rancho HSU based on these lithologic proxies.

Going into this project, we hypothesized that sand would decrease and clay would increase to the southeast, parallel to paleostreamflow (paleoflow data from Cather et al., 1997; Koning et al., 1998; Connell, 2008a, 2008b; Koning and Jochems, 2014; Koning and Rawling, 2017). However, such a trend is not obvious in most of the lithologic texture data, at least not in the saturated zones of the Upper Rio Rancho and Middle Rio Rancho HSUs (Figs. 23 and 24). For the saturated part of the Upper and Middle Rio Rancho HSUs, the proportions of clay, muddy sand, and sand obtained from these analyses were plotted as pie charts on a map of the central study area (Fig. 23). For a given well, the proportion of sand versus clay in the Upper Rio Rancho HSU is consistently much higher than that in the Middle Rio Rancho HSU, indicating a vertical trend in the data. To test our hypothesis regarding a downstream- or upstream-oriented lateral trend in the Middle Rio Rancho HSU, we orthogonally projected the sand and clay percent data of a well (Fig. 23) to a line trending 315° (upstream), as shown in Figure 24. The wells are divided into three sets according to the major structural zone in which they lie: west of the Zia fault, within the Montoyas graben, and on the Ziana horst. The strongest lateral trend showing coarsening in the Middle Rio Rancho HSU along a 315° trend corresponds to wells on the Ziana horst. A weaker trend is seen west of the Zia fault, where sand increases along a 315° direction, but clay percentage is steady. Note that the rightward increasing separation (vertically) of the trend lines in both datasets corresponds to slightly higher sand-versus-clay ratios in an upstream direction. There is no notable trend in the Montoyas graben. The east-to-west increase of fine strata in the saturated zone between wells RRU-14 and RRU-13R (Fig. 23) may be due to the combination of two factors in the coarsening-upward Arroyo Ojito Formation: (1) a westward-decreasing groundwater potentiometric surface and (2) down-dropping, on the east side of the Zia fault, of coarser-grained strata in the upper part of the Arroyo Ojito Formation. The lack of a strong upstream coarsening trend may be attributed to the extent of the study area being relatively minor compared to the entire length of the paleostream drainages, which is difficult to quantify because paleodrainage extent is not constrained to the northwest.

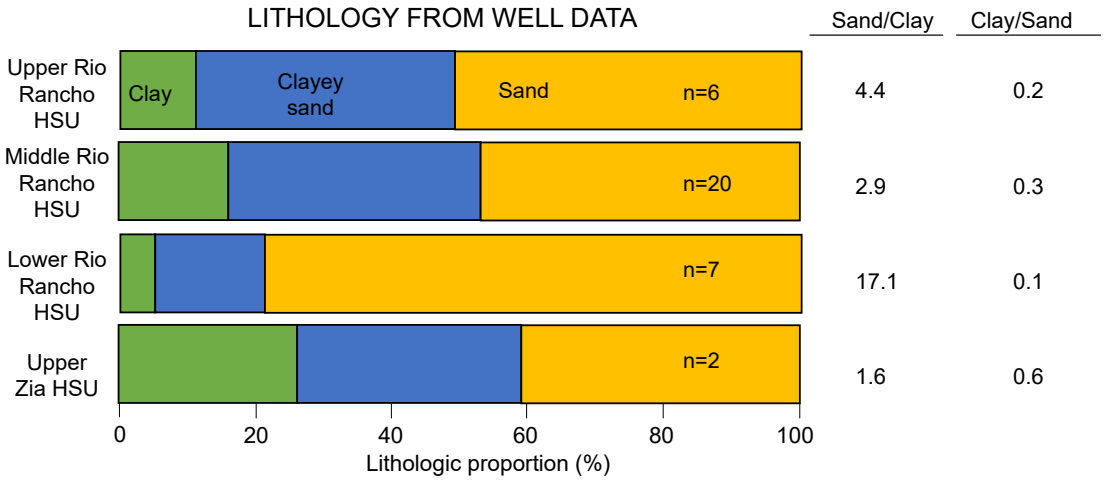

Note: Lithology determined using all available well data, rather than just gamma-ray (Vshale ratios).

Figure 22. Results of lithologic analyses for 22 wells in the study area, determined manually using all available well data. The bar plot enables a comparison of the proportions of clay, clayey sand, and sand for the four HSUs. The sand-versus-clay and clay-versus-sand ratios (excluding "clayey sand") are shown to the right of the bar plot. Associated data (i.e., subsurface picks of clayey vs. sandy intervals per well) are compiled in Appendix 5 and restricted to the saturated zone in an HSU.

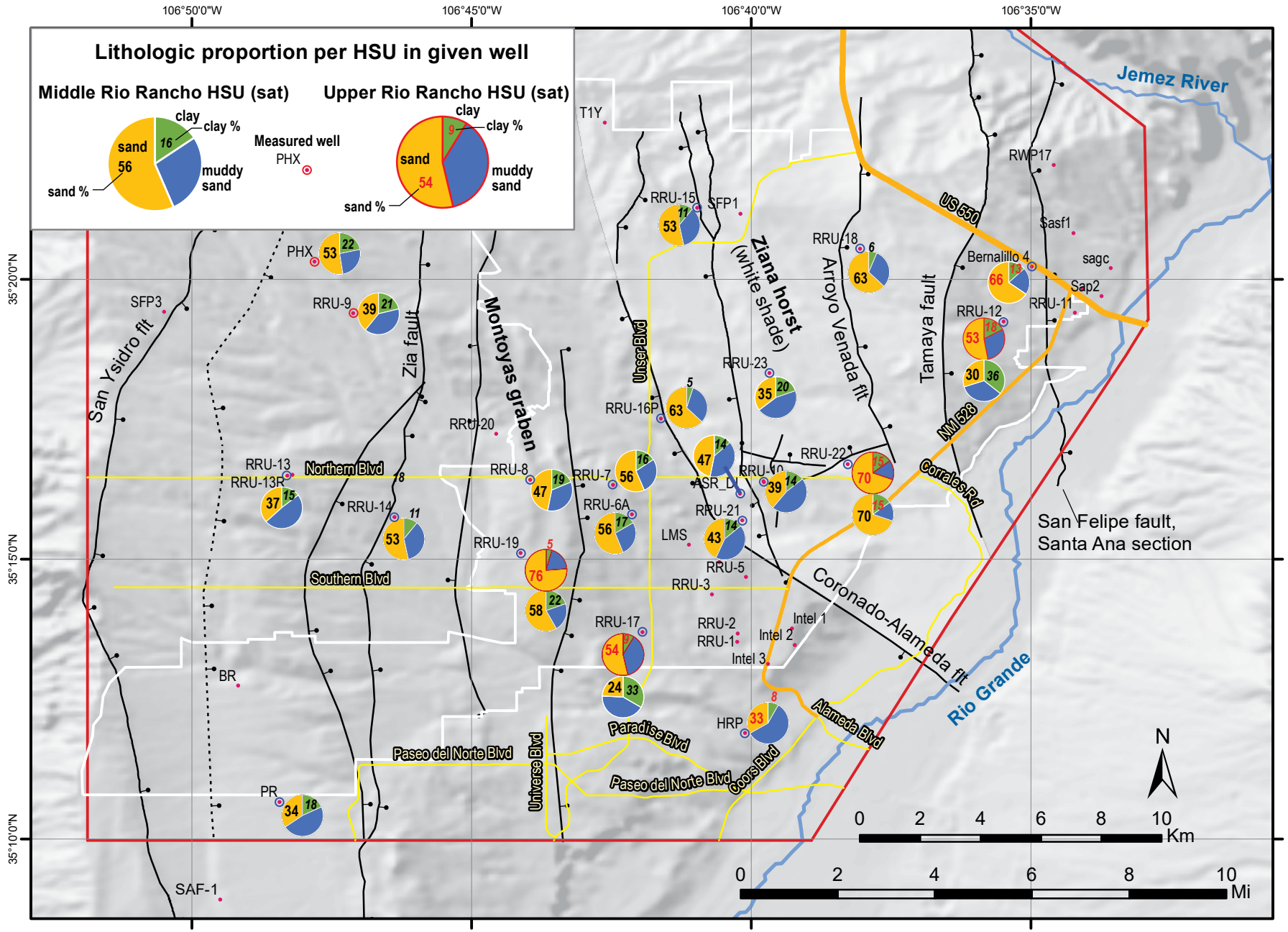

Figure 23. Pie graphs showing the proportion of clay, muddy sand, and sand per HSU in a given well. The values of the proportions for the sand and clay are plotted near the graph. The approximate average paleoflow direction is to the southeast (Cather et al., 1997; Koning et al., 1998; Connell, 2008a, 2008b; Koning and Jochems, 2014; Koning and Rawling, 2017). Associated data (i.e., subsurface picks of clayey vs. sandy intervals per well) are compiled in Appendix 5 and restricted to the saturated zone in an HSU.

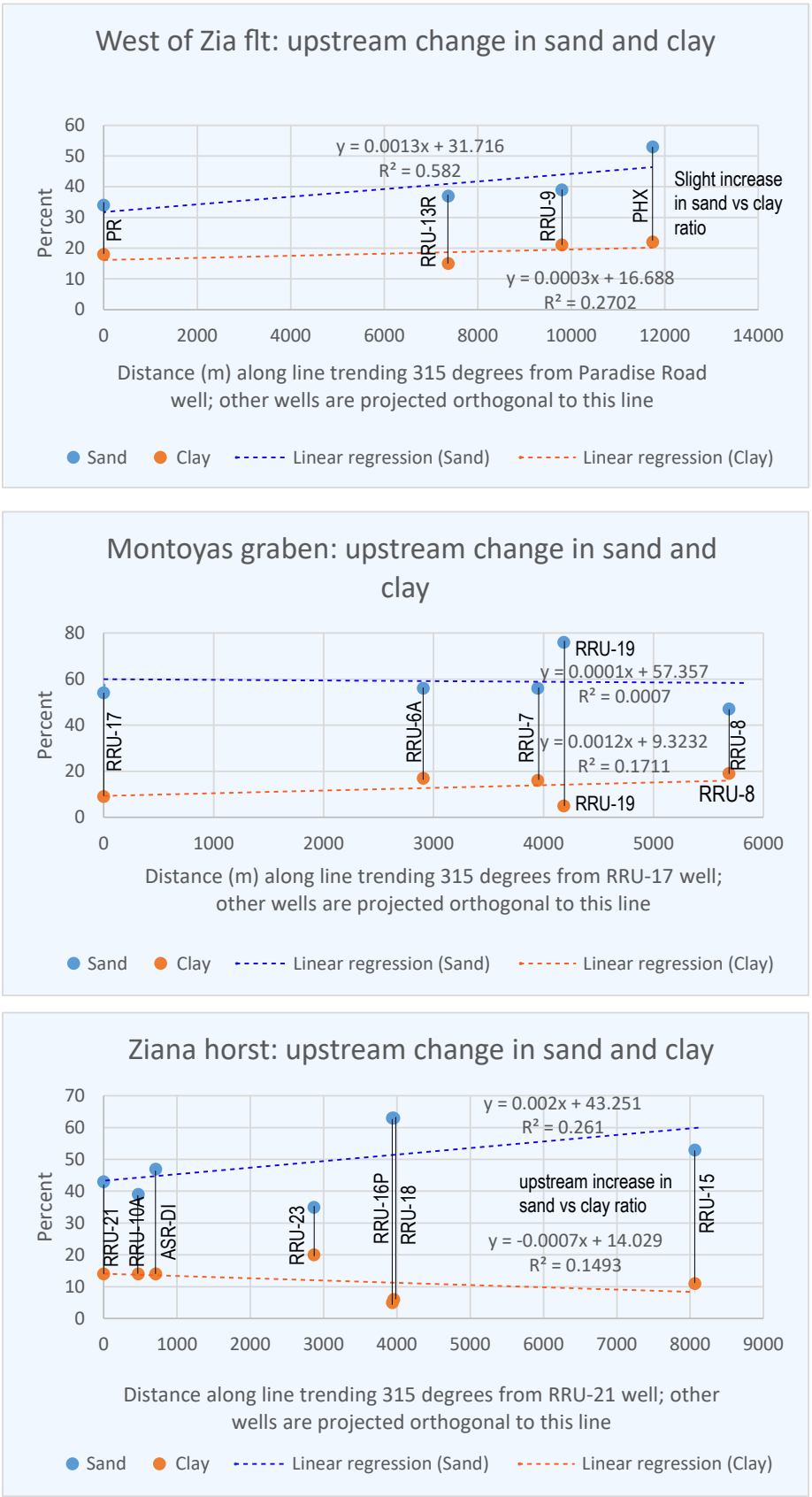

Figure 24. Plots of percent sand (blue dots) and clay (orange dots) per well. Data are projected orthogonally to a line oriented 315° from a specified well. Note the lack of an upstream-downstream trend in the sand and clay percentages in the Montoyas graben (center plot). There is a suggestion of a slight northwestward upstream increase in sand west of the Zia fault. On the Ziana horst, there is a suggestion of a northwestward upstream increase in sand and an upstream decrease in clay. Lithologic picks are compiled in Appendix 5 and pertain to the saturated zone of an HSU.

Storage zone thickness equates to sand body thickness and is shown via a box-and-whisker plot at the top of Figure 25. The Lower Rio Rancho HSU has the highest storage zone thicknesses (10 ft [3 m] median vs. 6 ft [1.8 m] median in the Upper Rio Rancho HSU). The median value of storage zone thickness is higher in the Upper Rio Rancho HSU than in the Middle Rio Rancho HSU (6 ft [1.8 m] vs. 4 ft [1.2 m]), and about 50% of the data in the Upper Rio Rancho HSU have higher thickness values than about 75% of the data in the Middle Rio Rancho HSU (Fig. 25, top plot). One can also consider a modified definition of the storage zone thickness, where the storage zone consists of both sand and muddy sand that lie in between relatively impermeable clay beds (Fig. 25, lower plot). Using this definition, the Lower Rio Rancho HSU generally has higher storage zone values compared to the Upper Rio Rancho HSU (although the medians are relatively similar at 24 median vs. 22 median), and the Upper Rio Rancho HSU has higher values and ranges than the Middle Rio Rancho HSU (22 median vs. 8 median). The Middle Rio Rancho and upper Zia HSUs have comparable storage zone thicknesses using either definition, which contrasts with the outcrop mapping results that indicated a higher contrast (upper right of Fig. 25). Because of the larger sampled stratigraphic intervals associated with the well data compared to the outcrop faces, we prefer the interpretation that permeability-related proxies are similar between the upper Zia and Middle Rio Rancho HSUs (i.e., compare the two units in the two plots in Fig. 25).

DETERMINING SAND VERSUS CLAYEY SEDIMENT FOR HSUS USING VSHALE ANALYSES AND DENSITY-POROSITY ANALYSES

Where adequate gamma-ray curves were available, net-to-gross sand body ratios were calculated for each saturated HSU, where sand bodies were delineated using a Vshale ratio of ≤0.25. These ratios equate to the proportion of sand bodies (relative to the total sediment) for an HSU in a well. For these same sand bodies in a given well (where Vshale ≤0.25), we also calculated porosity using density-porosity wireline data (Appendix 2).

Results of the Vshale and density-porosity analyses for the saturated zones of the HSUs are shown in Table 5. Figure 26 plots the net-to-gross ratios for the saturated zones of the Middle and Lower Rio Rancho HSUs, depicted as bubble plots on a map of the study area. Figure 27 plots the net-to-gross ratios for the saturated and unsaturated zones of the Middle Rio Rancho HSU. A net-to-gross value of 1.0 means all of the considered thickness is sand, and lesser values are the fractional value of sand out of a total of 1.0. For example, a net-to-gross ratio of 0.2 means 20% sand.

Where both the Middle Rio Rancho and Lower Rio Rancho HSUs are penetrated by a well, the proportion of sand is greater in the Lower Rio Rancho HSU compared to the Middle Rio Rancho HSU (Fig. 26). The averaged value of sand net-to-gross ratios (Table 5) is greater in the Lower Rio Rancho HSU (0.52 ± 0.20) compared to the stratigraphically higher Middle Rio Rancho HSU (0.29 ± 0.16) and Upper Rio Rancho HSU (0.34 ± 0.24) (errors correspond to one standard deviation; note the overlap between HSUs). This is consistent with data presented above that show the Lower Rio Rancho HSU has greater sand proportions than the Middle Rio Rancho HSU.

Within a given HSU, there is an unexpectedly wide range of lateral variability, as illustrated in Table 5 and in the lithologic proportions of the Middle and Lower Rio Rancho HSUs depicted in Figures 26 and 27. The Middle Rio Rancho HSU exhibits a coarsening-upward trend in most wells, but the sand body ratios in the saturated zone can differ by as much as 0.1–0.2, even for wells on the same fault-bounded block that lie within about a mile (1.6 km) of each other (e.g., Phoenix monitoring well vs. RRU-9, RRU-7 vs. RRU-6A, RRU-10 vs. RRU-10A in Fig. 26). When one considers both the saturated and unsaturated zone for the Middle Rio Rancho HSU, there is somewhat less variability between adjacent wells (cf. the Middle Rio Rancho HSU data in Figs. 26 and 27). This difference may be due to the saturated zone occupying different stratigraphic levels in some adjacent wells, creating more variability in the net-to-gross ratios in Figure 26. But even when both the saturated and unsaturated zones are considered, there is generally not a noteworthy south-southeastward fining trend over most of the study area (Fig. 27), parallel to the paleoflow direction (paleoflow data from Cather et al., 1997; Koning et al., 1998; Connell, 2008a, 2008b; Koning and Jochems, 2014; Koning and Rawling, 2017).

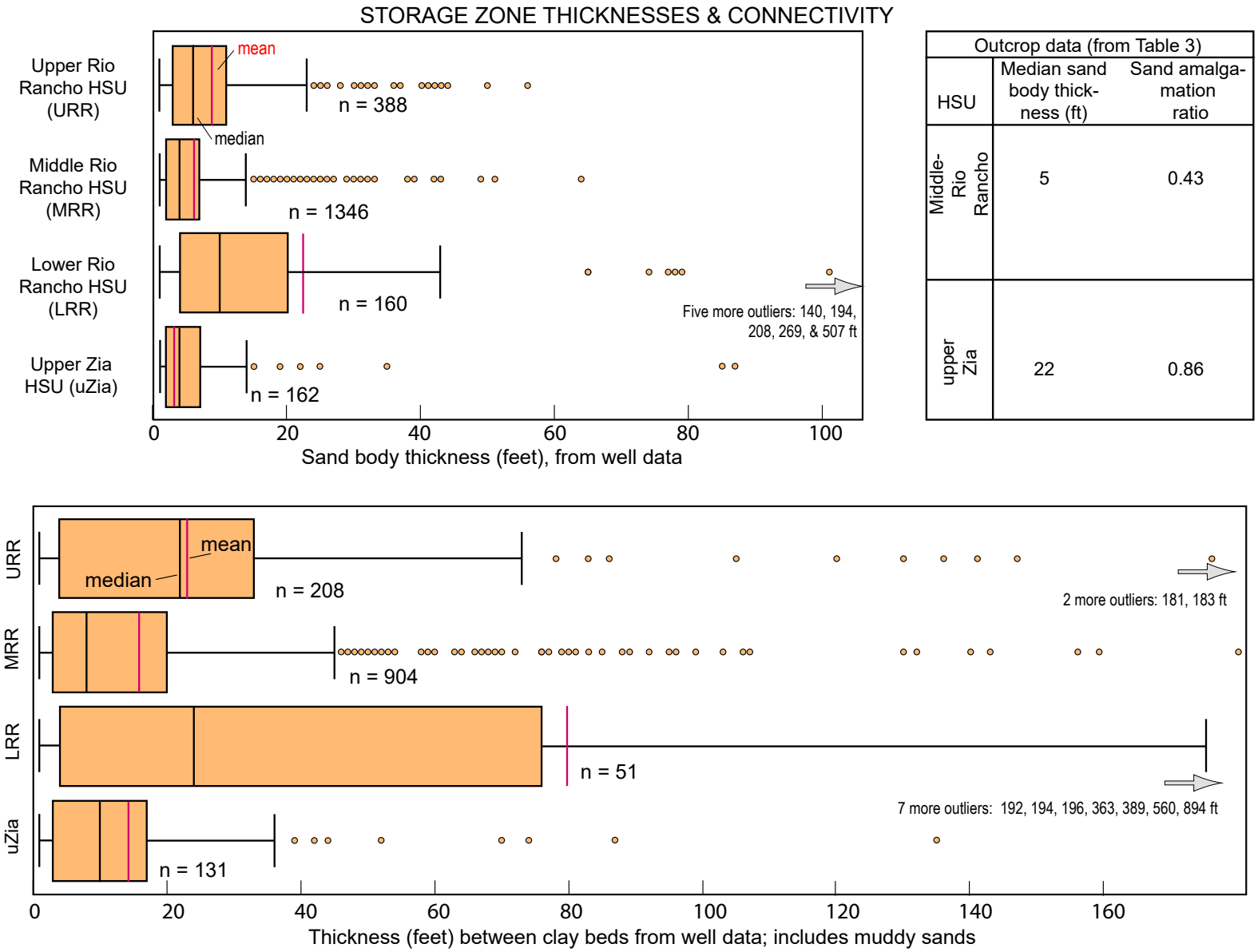

Figure 25. Box-and-whisker plot of storage zone thickness. The top plot depicts thickness data for sand bodies (excluding muddy sand and clay), and the bottom plot shows thickness data for undivided sands and muddy sands lying between clay beds. In these plots, the boxes represent the range of values of the thicknesses between the 25th and 75th percentiles. The "whiskers" on either side of the boxes are the minimum and maximum of the data (excluding the outliers). Outliers are plotted as circles and are defined as being more than 1.5 times the interquartile distance (i.e., the distance between the 25th and 75th percentiles) relative to the 75th percentile value. The black vertical line is the median of the data, and the red vertical line shows the mean of the data. For comparison, data from outcrop mapping (median sand body thickness and sand amalgamation ratios) are shown in the upper right of the figure. The associated lithologic data are compiled in Appendix 5 and pertain to the saturated zone of an HSU.

Table 5. Sand body versus total sediment ratios (net-to-gross) in wells using Vshale values (sand body cut-off of Vshale ≤0.25) and density-porosity compilations.

Well label	Easting (m)[1]	Northing (m)[1]	NGR_sand[2] (fractional value), saturated zone	Arith_Mean_ Dphi[3] (%), saturated zone	Arith_Mean Dphi_Vsh_0.25[4] (%), saturated zone	Arith_Mean Dphi_ Vsh_0.25[4] (%), saturated + unsaturated zones
Upper Rio Rancho saturated HSU						
PHX	336720	3912076				41.0±2.0
PR	335446	3894246				36.8±2.4
RRU-6A	345169	3903567				43.23±5.1
RRU-7	344670	3904558				41.5±3.0
RRU-8	342432	3904769				44.3±4.1
RRU-9	337737	3910345				41.7±9.3
RRU-14	338728	3903599				35.5±5.2
RRU-15	347116	3913670				40.5±4.9
RRU-16P	346012	3906730				44.0±3.4
RRU-17	345389	3899683	0.42	33.0±2.7	33.3±2.5	38.1±14.8
RRU-18	351498	3912245				40.3±2.9
RRU-19	342135	3902344	0.64	33.4±1.8	32.8±1.8	38.5±14.1
RRU-20	341539	3906296				40.3±2.9
RRU-21	348166	3903325				62.0±24.4
Be4	356138	3911578	0.15			
Br	334367	3898211	0.15			
Upper Rio Rancho Average[5]			**0.34±0.24**	**33.2±2.3**	**33.1±2.2**	**41.9±7.0**
Middle Rio Rancho saturated HSU						
PHX	336720	3912076	0.4	27.7±4.3	27.4±4.5	31.5±7.6
PR	335446	3894246	0.29	26.0±5	25.9±3.8	26.0±4.0
RRU-6A	345169	3903567	0.46	31.1±2.7	31.9±2.5	32.0±2.6
RRU-7	344670	3904558	0.14	27.2±2.3	28.7±1.9	28.7±1.9
RRU-8	342432	3904769	0.26	30.9±2.6	32.0±2.1	32.2±2.7
RRU-9	337737	3910345	0.17	30.34±3.0	30.5±2.5	37.3±5.7
RRU-10	348760	3904606	0.21	33.2±3.5	33.1±2.6	33.7±3.6
RRU-10A	348764	3904579	0.12			
RRU-13R	335848	3905021	0.2			
RRU-14	338728	3903599	0.18	33.7±10.0	37.5±14.6	40.1±16.0
RRU-15	347116	3913670	0.41	31.3±2.7	32.2±2.6	33.4±3.3
RRU-16P	346012	3906730	0.32	32.3±2.6	33.2±2.8	33.2±2.7
RRU-17	345389	3899683	0.25	29.2±2.4	30.6±2.3	30.7±.2
RRU-18	351498	3912245	0.1	31.8±2.4	32.6±2.1	32.8±2.4
RRU-19	342135	3902344	0.42	30.8±2.9	32.0±2.2	32.0±2.2
RRU-20	341539	3906296	0.46	31.4±2.9	31.1±2.3	32.8±2.5
RRU-21	348166	3903325	0.39	29.7±2.4	30.3±2.3	30.5±2.4
RRU-22	351048	3905138	0.4			
RRU-23	348978	3908183	0.17			
Be4	356138	3911578	0.01			
T1Y	344653	3916523	0.73			
Middle Rio Rancho Average[5]			**0.29±0.16**	**30.4±3.4**	**31.3±3.5**	**32.4±4.1**
Lower Rio Rancho saturated HSU						
RRU-10A	348764	3904579	0.4			
RRU-13R	335848	3905021	0.55			
RRU-15	347116	3913670	0.29	30.5±3.0	31.3±1.8	31.3±1.8
RRU-16P	347949	3899311	0.61	34.0±2.7	34.2±2.8	34.2±2.8
RRU-18	347977	3899581	0.34	32.2±3.2	32.9±2.3	32.9±2.3
RRU-22	351048	3905138	0.7			
RRU-23	348978	3908183	0.49			
SFP3	332610	3910494	0.4			
T1Y	344653	3916523	0.92			
Lower Rio Rancho Average[5]			**0.52±0.20**	**32.2±3.0**	**32.8±2.1**	**32.8±2.1**

[1] Easting and northing are UTM coordinates in meters (m) (zone 13, NAD83).
[2] NGR = "Net-to-gross" sand, which is equivalent to the proportion of sand out of the total sediment in a well.
[3] Dphi = Density-porosity value; arithmetic mean calculated for all sediment types in the well.
[4] Dphi_Vsh_0.25 = Density-porosity value; arithmetic mean calculated for just the sand bodies (where Vshale is ≤0.25).
[5] Standard deviation is plotted after the ± symbol. In the three Dphi columns, the standard deviation listed after the ± symbol for the "Average" row is the average of the column's standard deviations.

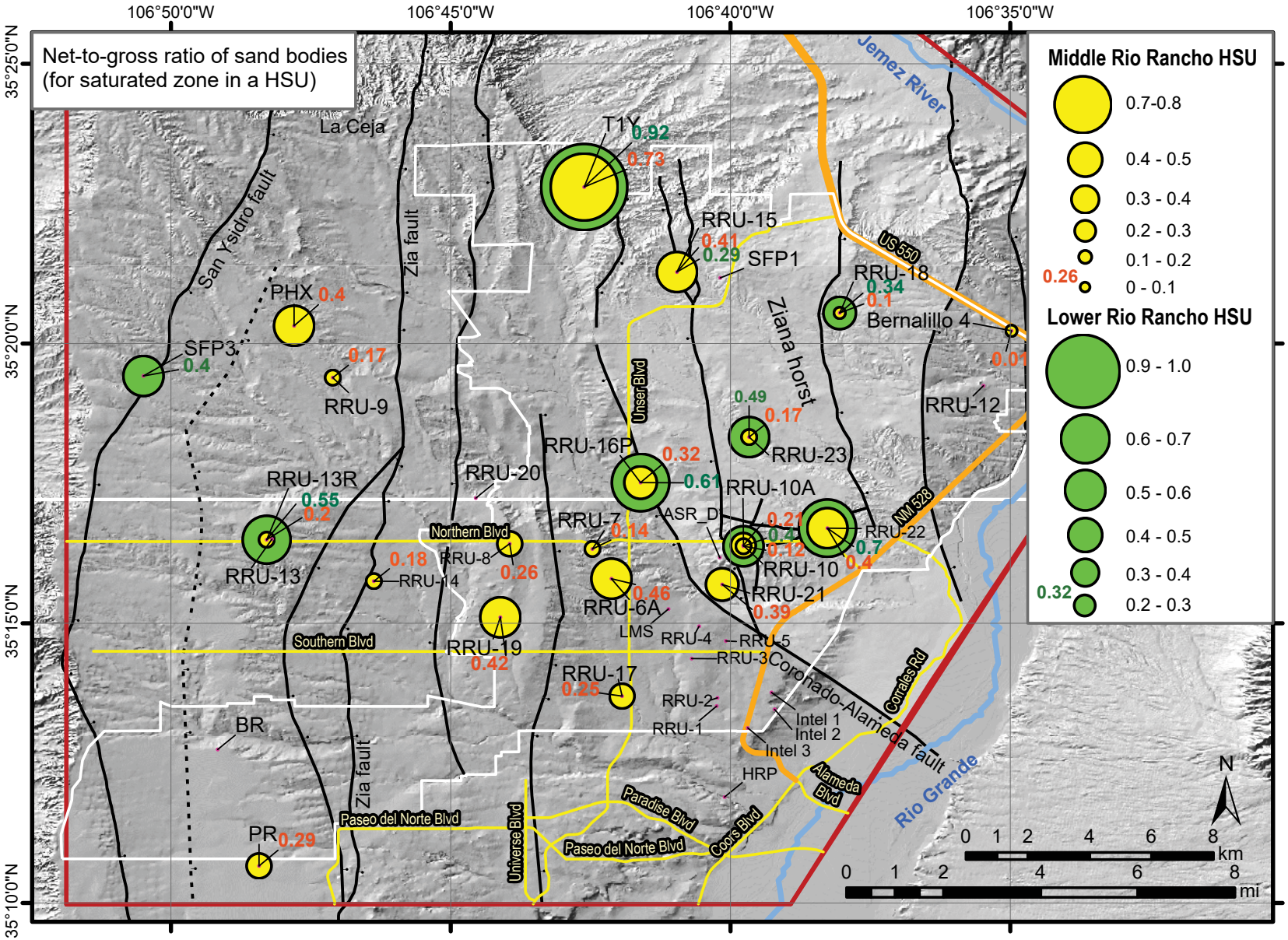

Figure 26. Bubble plot of net-to-gross ratios of sand bodies in the saturated zone for the Middle and Lower Rio Rancho HSUs for the portion of the HSU penetrated by a given well. Values are depicted using scaled yellow and green circles (for the Middle and Lower Rio Rancho HSUs, respectively). This analysis is conceptually equivalent to calculating the proportion of sand bodies in the penetrated HSU. Note that "sand" is defined by a Vshale value ≤0.25. Input data are given in Table 5.

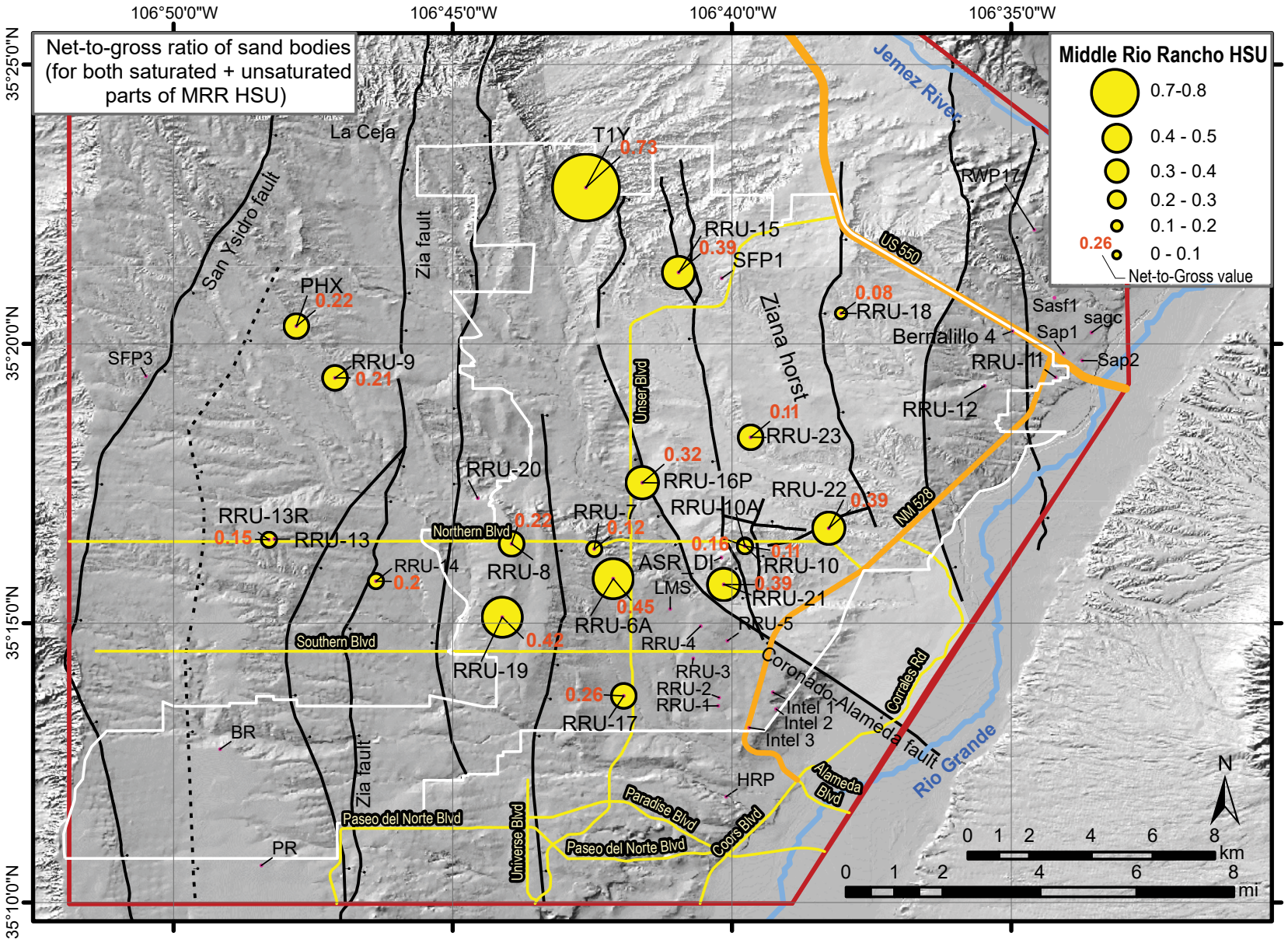

Figure 27. Bubble plot of net-to-gross ratios of sand bodies in both the saturated and unsaturated zones for the Middle Rio Rancho HSU. Values are depicted using scaled yellow circles. This analysis is conceptually equivalent to calculating the proportion of sand bodies in the penetrated HSU. Note that "sand" is defined by a Vshale value ≤0.25. Input data are given in Table 5.

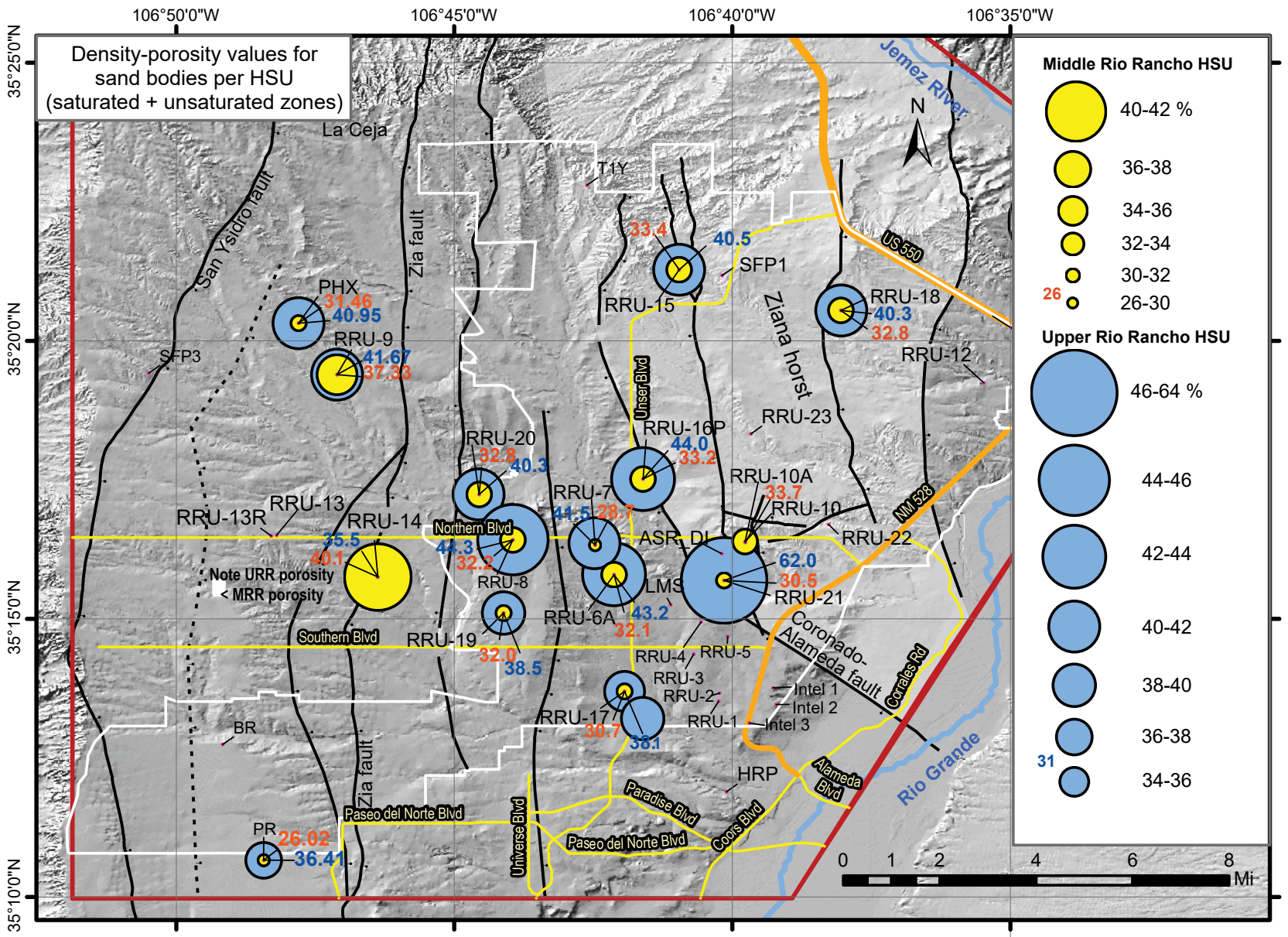

Figure 28. Bubble plots illustrating arithmetic means of density-porosity data for sand intervals in wells penetrating the Middle and Upper Rio Rancho HSUs (scaled yellow and blue circles, respectively). Sand intervals are defined using Vshale values ≤0.25. Except for well RRU-14, the Upper Rio Rancho HSU has consistently higher values than the Middle Rio Rancho HSU. Input data are given in Table 5.

However, there is a suggestion (based on wells RRU-9, RRU-23, RRU-18, RRU-15, PHX, and T1Y) that northward coarsening in the Middle Rio Rancho HSU occurs from the approximate latitude of RRU-9 north to La Ceja. Perhaps that locale reflects the position of paleofans, whereas downstream (to the south-southeast), the paleo depositional environment approximated a gently sloping bajada or basin floor.

Using Kingdom software, density-porosity values were calculated for the saturated zones in each HSU per well utilizing wireline data we digitized from sources listed in Appendices 1 and 2. Arithmetic means were calculated for all strata in an HSU per well as well as for just the sand fraction. For the sand fraction, arithmetic means were calculated for depth intervals where the Vshale ratio was ≤0.25 (Table 5). Although they lie within the 1-standard deviation error range, these data suggest higher porosities for the Upper and Lower Rio Rancho HSUs than the Middle Rio Rancho HSU. When density-porosities are compiled for both the saturated and unsaturated zones in a given well for only the sand bodies, the difference between the Upper and Middle Rio Rancho HSUs is noteworthy (Fig. 28). We interpret this difference as reflecting less compaction and less cementation of sand bodies in the Upper Rio Rancho HSU compared to the Middle Rio Rancho HSU (e.g., Haneberg, 1996; Busch et al., 2022). Since the proportion of sand versus clayey sediment is only slightly higher (~5%) in the Upper Rio Rancho HSU versus the Middle Rio Rancho HSU (Table 4), we infer that the difference in density-porosity values is largely due to differences in compaction and cementation. Collectively, the lower clay content, lesser compaction, and lesser cementation in the Upper Rio Ranch HSU compared to the Middle Rio Rancho HSU explain why the Upper Rio Rancho HSU exhibits generally higher hydraulic conductivity values (Figs. 29 and 30), as discussed below.

DIRECT PERMEABILITY ANALYSIS

We used three approaches to measure vertical and lateral changes in permeability: compilation of hydraulic conductivity and specific capacities from pumping tests, the Kozeny-Carman model, and the Berg model. Note that pumping tests sample the saturated part of an entire screened interval in a given HSU, whereas the Kozeny-Carman and Berg models calculate hydraulic conductivity as a function of depth in an HSU per well.

Input information for the Kozeny-Carman and Berg models includes sand grain sizes and effective porosity. Sand grain sizes were obtained from sieve tests conducted during the drilling of the Rio Rancho production wells (previously tabulated in consultant reports associated with a given well; Appendix 1). We did not have empirical data on effective porosity, so we instead substituted porosity measured by the density-porosity tool in wireline logs (not available for all wells). Effective porosity represents the connected pores in a sand that allow through-going water flow. Because the porosity measured by the density-porosity tool is very likely higher than the effective porosity, **the permeability values we obtained from these two models would theoretically be higher than the actual values. Thus, it is important to note that we use the permeabilities from the Kozeny-Carman and Berg models only in a comparative sense, that is, to compare lateral trends in permeability within a given HSU.** Another potential problem with the Kozeny-Carman and Berg models is that the sand-size data come from a limited number of sieve analyses, consisting of 10–20 samples within a particular HSU.

Methods

Pumping Test Hydraulic Conductivity Compilations per HSU

We compiled hydraulic conductivity and specific capacity measurements from pumping tests (Table 6). These data were available for the Rio Rancho production wells (RRU-1 through RRU-23, except RRU-18 and RRU-20), the Bernalillo No. 4 well, and the three Intel production wells. Pumping test data were also available from wells in the extreme southwest of the study area, including the Black Ranch test well and the Soil Amendment Facility well (BR and SAF-1, respectively, in Fig. 29); the latter is located 1 mi (1.6 km) south of the southern boundary of the study area. Where more than one pumping test was conducted on a well, corresponding to different depth intervals of a particular HSU, the average of the hydraulic conductivities was used; this was done for the Black Ranch test well (BR), which had hydraulic conductivities of 12 and 5.4 ft/day in the Middle Rio Rancho HSU, and for well RRU-13R, which had values of 1.2 and 0.8 ft/day in the Middle Rio Rancho HSU (Table 6).

Table 6. Well hydraulic conductivity (K), total dissolved solids (TDS), and age data.

Well label	Well name	HSU	K from pumping tests (ft/day)[1]	K from Kozeny-Carman model (ft/day)	K from Berg model (ft/day)	Specific capacity (gpm/ft)[1]	Storativity	TDS (ppm)[2]	C-14 age (ka)[3]
RRU-1	Rio Rancho Utilities 1	URR	21.2			3.7		412	
RRU-2	Rio Rancho Utilities 2	URR	3.2			5.7		360	2.8
RRU-3	Rio Rancho Utilities 3	URR	10.7			10.5		300	
RRU-4	Rio Rancho Utilities 4	URR	6.3			8.3		376	14.8
RRU-5	Rio Rancho Utilities 5	URR	9.4			7.5			
RRU-6A	Rio Rancho Utilities 6A	MRR	4.9	1.4	2.32	11	0.00002	274	
RRU-7	Rio Rancho Utilities 7	MRR	2.1			2.5		190	
RRU-8	Rio Rancho Utilities 8	MRR	5.2			13.3		260	18.2
RRU-9	Rio Rancho Utilities 9	MRR	1.1	0.48	1.56	4.6		322	23.1
RRU-10	Rio Rancho Utilities 10	MRR	2.0			5.9		388	19.3
RRU-10A	Rio Rancho Utilities 10A	MRR-LRR	2.5*			14.4*	*	900	
RRU-11	Rio Rancho Utilities 11	URR	20.7			5		1100	
RRU-12	Rio Rancho Utilities 12	URR-MRR	3.9*			11.94	0.0008*	461	11.9
RRU-13	Rio Rancho Utilities 13	MRR	1.9			11		282	30.9
RRU-13R	Rio Rancho Utilities 13R	MRR	1.0[8]	1.9		2.5		291[7]	
RRU-14	Rio Rancho Utilities 14	MRR	2.9	1.1	4.17	13.3	0.0013	274	
RRU-15	Rio Rancho Utilities 15	MRR	5.4			4.6	0.00004	530	14.2
RRU-16P	Rio Rancho Utilities 16P	MRR		0.68	14.5	5.9			
RRU-16P	Rio Rancho Utilities 16P	MRR-LRR	1.8*				0.0001*	466	
RRU-17	Rio Rancho Utilities 17	URR	9.1			39.5	0.00001	330	
RRU-18	Rio Rancho Utilities 18	MRR-LRR		0.24	2.12			1248	
RRU-19	Rio Rancho Utilities 19	MRR	2.8	0.39	0.6	11.9	0.00001	462	
RRU-21	Rio Rancho Utilities 21	MRR	3.6	0.35	0.63	16.2	0.0001	412	
RRU-22	Rio Rancho Utilities 22	LRR-Zia	*					5207	
RRU-23	Rio Rancho Utilities 23	LRR	21[4]			18.7	0.0017	1400[4]	
BR	Black Ranch Test Well	MRR	8.7[8]					370	
ASR_Di[5]	Rio Rancho ASR Direct Injection	MRR						405[9]	
Bern 4	Bernalillo No.4 Well	URR	2.6			13.3			
HRP	Hunter Ridge Piezometer	URR							5.7
NM Util 4	NM Utilities 4	URR-MRR	2.8*			14.5*	*		23.9
Intel 1	Intel Production Well 1	URR	8.4			26.5	0.001	280[7]	
Intel 2	Intel Production Well 2	URR	9.3			22		299	4.8[6]
Intel 2B	Intel Monitoring Well 2B	URR							
Intel 3	Intel Production Well 3	URR	10			26.6	0.0013	260[7]	
LMS	Lincoln Middle School Piezometer	URR						205[10]	15.4
NMU-1	New Mexico Utilities 1	URR?						326[12]	18.8
NMU-2	New Mexico Utilities 2	URR						376[12]	6.0
NMU-3	New Mexico Utilities 3	URR						414[12]	17.2
NMU-4	New Mexico Utilities 4	URR-MRR	2.8					351[12]	23.9
SAF-1	Soil Amendment Facility	MRR	7					624[12]	28.1
SWAB	SWAB Test Holes 1 and 2	MRR							21.3
MP-MW1	Mariposa MW1[11]	LRR						680	
MP-MW3	Mariposa MW3[11]	LRR						478	

[1] Data from reports listed in Appendix 1; NMU-4 is from Riesterer et al. (2004).
[2] TDS data are from Riesterer et al. (2004) unless noted otherwise.
[3] Groundwater ages from table 10 of Plummer (2004c): "adjusted ^{14}C calendar years (ka)." ka = thousands of years. For HRP, SWAB, and LMS, all sampled depths (n=3 for each) were averaged.
[4] Table 8 of Riesterer and Drakos (2008).
[5] Data from Marley, B., July 21, 2009, Biannual Report for OSE Permit No. USR 3 - Rio Rancho Direct Injection Aquifer Recharge Demo Project: unpublished consultant report to the NM Office of the State Engineer by Daniel B. Stephens and Associates.
[6] Data from Riesterer et al. (2004).
[7] See associated report listed in Appendix 1.
[8] Pumping test is the average of two screened intervals: 12 and 5.4 ft/day for the BR well and 1.2 and 0.8 ft/day for the RRU-13R well.
[9] Average TDS of these values: 410, 460, 400, 360, 410, and 390 ppm.
[10] Average TDS of these values from three depth intervals: 189, 203, 222 feet.
[11] Location of MP-MW1: 349033 m E, 3915713 m N; location of MP-MW3: 348863 m E, 3915644 m N. Data from Marley, B., January 30, 2009, USR 1 Biannual Report 2009 to 2017: unpblished consultant report to the NM Office of the State Engineer.
[12] Calculated from Plummer (2004c) using major ions and SiO_2, NO_3, and F.
* Blue-tinted cells were not included in box-and-whisker plots because <80% of screen length is from a single HSU. In the case of the Intel wells, we attributed the pumping test data as all being from the Upper Rio Rancho HSU, even though 20–30% of the screens were in the Middle Rio Rancho HSU, because the MRR was notably finer-grained than the URR.

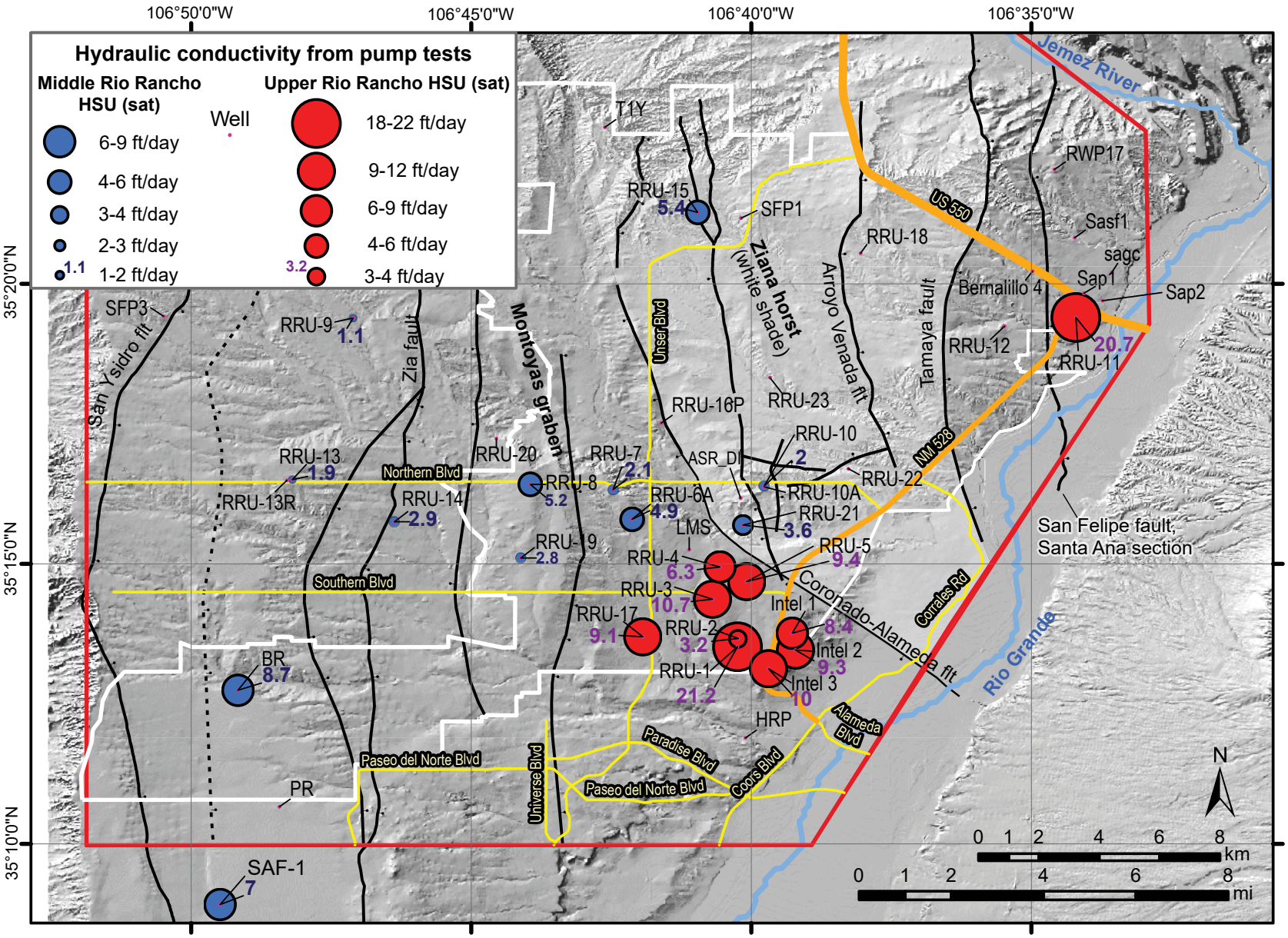

Figure 29. Map showing spatial distribution of hydraulic conductivities calculated from pumping tests. Pumping tests in the Upper Rio Rancho HSU versus the Middle Rio Rancho HSU are shown in red and blue shades and fonts, respectively.

We selected the pumping tests for wells that had screened depths corresponding uniquely to a given HSU or were screened more than 80% within a given HSU. In the case of the Intel wells, we attributed the pumping test data as all being from the Upper Rio Rancho HSU, even though 20–30% of the screens were in the Middle Rio Rancho HSU. This is because the Middle Rio Rancho HSU was notably finer-grained than the Upper Rio Rancho HSU in the well logs, and we therefore assumed that the pumping test mostly reflected the Upper Rio Rancho HSU. We could not use wells RRU-10A, RRU-12, RRU-16P, RRU-22, and NM Util 4 because their screens extended significantly across multiple aquifers. Only one well, RRU-23, had a pumping test from a screened interval wholly within the Lower Rio Rancho HSU.

Kozeny-Carman Model

The Kozeny-Carman model calculates a theoretical hydraulic conductivity based on a referential grain size and effective porosity. It is based on a conceptual flow model that contains a bundle of capillary tubes of equal length (Kozeny, 1927) that was later modified to account for the tortuosity of flow around individual grains (Carman, 1937, 1939). The resulting equation is known as the Kozeny-Carman equation (equation 14 of Urumović and Urumović, 2016):

$$K = CF*[0.0625*D_g^2 *[(n_e^3/(1-n_e)^2]]$$

where K is the hydraulic conductivity, CF is a correctional factor, D_g is the sand grain size, and n_e is the effective porosity.

We assumed that the effective porosity is approximated by the porosities obtained by the density-porosity tool. Based on the results and recommendations of Urumović and Urumović (2016), we used the geometric mean of the sand grain size derived from sieve analyses. We also used a correctional factor to account for temperature-based changes in water density and viscosity (CF = 0.7 + 0.03 × groundwater temperature in °C). The temperature of the groundwater was calculated from the local geothermal gradient and the depth of the sample. Local geothermal gradients were obtained mainly by plotting a regression line of bottom-hole temperature versus bottom-hole depth data from the Rio Rancho production wells. Near well RRU-23, the geothermal gradient was calculated mostly using the temperature log for that well. Calculations of hydraulic conductivity using the Kozeny-Carman model were performed at 1-ft (0.3-m) depth intervals using Kingdom software; the 1-ft depth calculations for a given HSU were then averaged to provide a representative value for a given HSU in a well (Table 6).

Berg Model

The Berg model (1975) links effective porosity, grain size, and grain sorting to permeability. Nelson (1994) interprets that it is a usable means of estimating permeability in unconsolidated to weakly consolidated sands (where porosity values are not much less than 30%) and clean, quartzose sandstone. The equation (3a of Nelson, 1994) is:

$$k \text{ (in darcys)} = 5.1 \times 10^{-6} \phi \text{ (effective porosity in percent)}^{5.1} \; D^2 \; e^{-1.385p}$$

where k is permeability, ϕ is porosity in percent, D (mm) is the median grain diameter, and p is a sorting term.

The median grain diameter is approximated by the 50th percentile in the sieve analyses. The porosity term (p) is the difference of the 90th percentile and 10th percentile in the sand-sieve analyses (expressed in phi units, where phi = $-\log_2$ of the difference in these percentiles). As with the Kozeny-Carman model, we assumed that the effective porosity (n_e) is approximated by the porosities obtained by the density-porosity tool. Since the effective porosity is lower than the density-porosity values, the results overestimate the true hydraulic conductivities. However, we used the results for comparative purposes, particularly in assessing whether there is lateral variation in a given HSU.

Results

There are clear differences in the pumping test hydraulic conductivities and specific capacities for the Upper Rio Rancho versus Middle Rio Rancho HSUs. Hydraulic conductivities at a given well per HSU unit are depicted as bubble plots in Figure 29, where the width of the circle is scaled to the hydraulic conductivity value. Note how the Upper Rio Rancho HSU data are notably larger than the Middle Rio Rancho HSU data. Both hydraulic conductivity and specific capacity data derived from pumping tests are shown in the box-and-whisker plots of Figure 30. For the Upper Rio Rancho HSU, the median value is 9.25 ft/day, and the first quartile (25th percentile) is 7 ft/day. The median value for

the Middle Rio Rancho HSU is 3.25 ft/day, whereas 75% of its values (up to the 75th percentile) lie at ≤5.35 ft/day, below the 25th percentile of the Upper Rio Rancho HSU (Fig. 30).

Standard deviations are plotted relative to the mean of the data in the upper plot of Figure 30 (pumping test-derived hydraulic conductivities). Note that there is overlap between the Upper Rio Rancho HSU data within one standard deviation below the mean and the Middle Rio Rancho HSU data within one standard deviation above the mean. A similar overlap in the standard deviations of specific capacity and well production data, presented in Riesterer et al. (2004), was used to justify that there was no meaningful difference in permeability-related performance between wells screened in the Upper Rio Rancho HSU and those screened in the Middle Rio Rancho HSU. We acknowledge the overlap but argue that our hydraulic conductivity data (Fig. 30) indicate a notably increased probability of encountering higher-permeability strata in the Upper Rio Rancho HSU compared to the Middle Rio Rancho HSU. Also, permeability-related data (including lithologic proxies) plotted for individual wells strongly indicate a higher likelihood of more favorable permeability in the Upper Rio Rancho HSU compared to the Middle Rio Rancho HSU (e.g., Figs. 23, 25, 26, and 28).

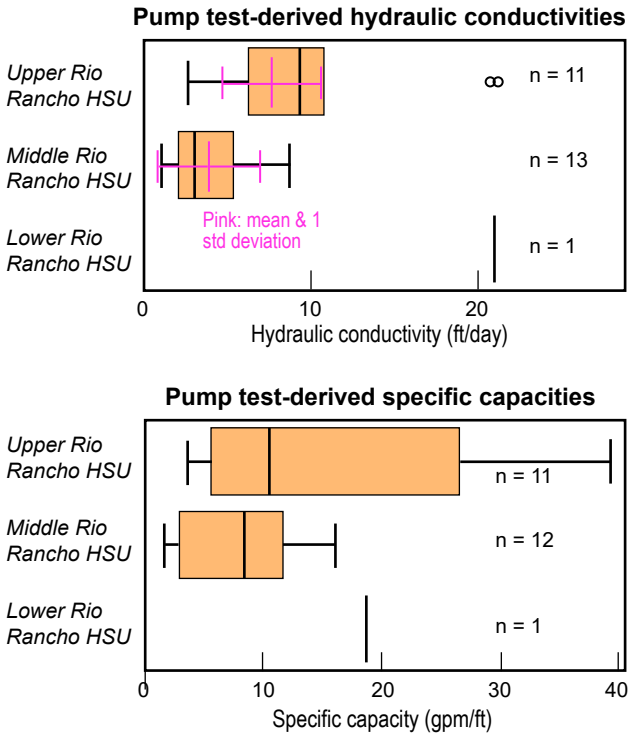

Figure 30. Box-and-whisker plots of hydraulic conductivity and specific capacity data for the Upper, Middle, and Lower Rio Rancho HSUs. In these plots, the boxes represent the range of values for the hydraulic conductivities and specific capacities between the 25th and 75th percentiles. The vertical black line in each box is the median value, and the "whiskers" on either side of the boxes are the minimum and maximum of the data (excluding the outliers). Outliers are plotted as circles and are defined as being more than 1.5 times the interquartile distance (i.e., the distance between the 25th and 75th percentiles) relative to the 75th percentile value. The pink lines show the standard deviation relative to the mean of the hydraulic conductivity data (note that the mean is plotted as a long, vertical bar).

Visual inspection of the map-plotted hydraulic conductivity data indicates that two wells in the southwest corner of the study area returned relatively high hydraulic conductivities for the Middle Rio Rancho HSU (Fig. 29). In terms of geology, these higher results could possibly be due to more tongues of medium-coarse sand related to the Benavidez unit, which would be expected to increase toward the west and southwest because this unit is mapped only in the Rio Puerco Valley (Koning and Jochems, 2014; Koning and Rawling, 2017; Koning et al., 2021). Such zones of coarser-grained sand were noted locally in the Arroyo Ojito Formation in the Black Ranch test well (Appendix 3). The Benavidez unit is a piedmont-slope deposit that transported relatively coarse-grained material off of the southeastern Colorado Plateau (Koning et al., 2021). It interfingers eastward with the upper Cerro Conejo Formation and the Navajo Draw Member of the Arroyo Ojito Formation (Figs. 6 and 8), which is a fluvial deposit containing higher proportions of finer sand and mud (Connell et al., 1999; Koning and Jochems, 2014).

Compared to hydraulic conductivity data, there is more overlap when specific capacity data are presented as box-and-whisker plots (Table 6, Fig. 30). However, the Upper Rio Rancho HSU does exhibit a range of values higher than the Middle Rio Rancho HSU, with the higher 50% of data for the Upper Rio Rancho HSU being higher than the lower 75% of data for the Middle Rio Rancho HSU. Also, the median value of the specific capacity data is 10.5 gpm/ft for the Upper Rio Rancho HSU and 8.45 gpm/ft for the Middle Rio Rancho HSU.

Of the three studied HSUs, we only had enough data for the Middle Rio Rancho HSU to evaluate lateral permeability differences using the Kozeny-Carman and Berg models (Figs. 31 and 32). As a reminder, these models calculate a theoretical hydraulic conductivity using sand-sieve analyses of

10–20 sand samples taken from cuttings at a given well. Using the sand sample depth-interval values (typically in increments of 10 ft [3 m]), density-porosity values were extracted from a window centered on the corresponding depths from the wireline logs (e.g., ~5 ft [~1.5 m] on either side of the sample depth if the sampling interval was 10 ft [3 m]). However, plotting the results of these analyses with hydraulic conductivities derived from pumping tests shows very poor correlation, with R^2 values of <0.2 (Figs. 33a and 33b). Thus, we do not feel confident in using these particular data to make any interpretations regarding lateral permeability trends in the Middle Rio Rancho HSU. We explain this poor correlation by inferring that (1) the 10–20 sieve samples taken of the Middle Rio Rancho HSU per well are insufficient in number to adequately characterize this HSU and/or (2) in actuality, because the sieve sample is not intact, it does not adequately represent even the 10-ft-thick (3 m) sampled interval because the drilling process homogenizes the sand and clayey beds and eradicates stratification-related controls of permeability. For example, it may be the case that a high-yielding sand bed is thinner than the 10-ft (3 m) sieve sample interval, and its unique properties are not adequately sampled. A higher number of samples or analyses of intact core would probably have yielded a better correlation with the pumping test data.

The only well log-associated parameter that seemed to correlate, albeit weakly, with pumping test-derived hydraulic conductivities was the net-to-gross sand bodies, which had an R^2 of 0.56 (Fig. 33c). "Net-to-gross" corresponds to the percentage of sand bodies in a given thickness interval—in our case, the thickness of a given HSU. Although this correlation is intuitive, it does not account for cementation, which can notably reduce the permeability of a sand body (perhaps accounting for the relatively low R^2 value of 0.56). This correlation of net-to-gross sand values with pumping test-derived hydraulic conductivities allowed us to use the net-to-gross (percentage) of sand bodies as a weak proxy for relative permeability changes, which is useful in areas that lack pumping test data. Net-to-gross ratios of sand bodies are plotted in Figures 26 and 27.

Assuming there is a correlation between higher sand net-to-gross values and overall permeability, the following vertical and lateral trends in net-to-gross values of sand bodies are noteworthy. First, where data from both the Middle and Lower Rio Rancho HSUs are available in a single well, the net-to-gross values of the Lower Rio Rancho HSU are greater than those of the Middle Rio Rancho HSU. In Figure 26, one can see how the green circles (representing the Lower Rio Rancho HSU) are larger than the yellow circles (representing the Middle Rio Rancho HSU). Second, for the Middle Rio Rancho HSU, net-to-gross values of sand bodies are variable across the study area, but there is a suggestion (based on six data points) that the northernmost part of the saturated Middle Rio Rancho HSU may be slightly more permeable based on a northward increase in sand body net-to-gross values (Figs. 26 and 27). Specifically, the net-to-gross values for the saturated zone are 0.1–0.2 at wells RRU-9, RRU-23, and RRU-18, but values for wells more than 0.6 mi (1 km) to the north of these wells range from 0.4 to 0.7 (wells PHX, T1Y, and RRU-15 in Table 5 and Fig. 26). This northward increase is present, but more subtle, in the map showing the net-to-gross values of both the saturated and unsaturated zones of the Middle Rio Rancho HSU (Fig. 27).

In summary, tabulation of sands versus clays and the sand body net-to-gross data (Figs. 23, 24, 26, and 27) indicate that there is no strong NNW-SSE lateral trend in sand proportion, which may be viewed as a proxy for permeability, within the study area. Suggestions of coarsening to the north-northwest are most apparent outside of the Montoyas graben (Fig. 24), as discussed above. It is also unclear whether this trend exists in the assessment of direct calculations of hydraulic conductivity using pumping test data (Fig. 29), possibly because fewer wells were used in the hydraulic conductivity compilation. Most of our analyses of lateral permeability trends were conducted on the saturated part of the Middle Rio Rancho HSU. However, due to the sloping potentiometric surface (Fig. 11), variable well depths, and faulting within this HSU, the specific stratigraphic layers of the Middle Rio Rancho HSU that are saturated vary from well to well, and this might affect the results. However, even when the unsaturated zone is taken into consideration in net-to-gross ratios (Fig. 27), there is still no strong lateral trend, and only a suggestion of lateral coarsening north of latitude 35°20′0″. Based on these data, there is little incentive to prioritize future well drilling to the north-northwest due to possible lateral increases in permeability in that direction.

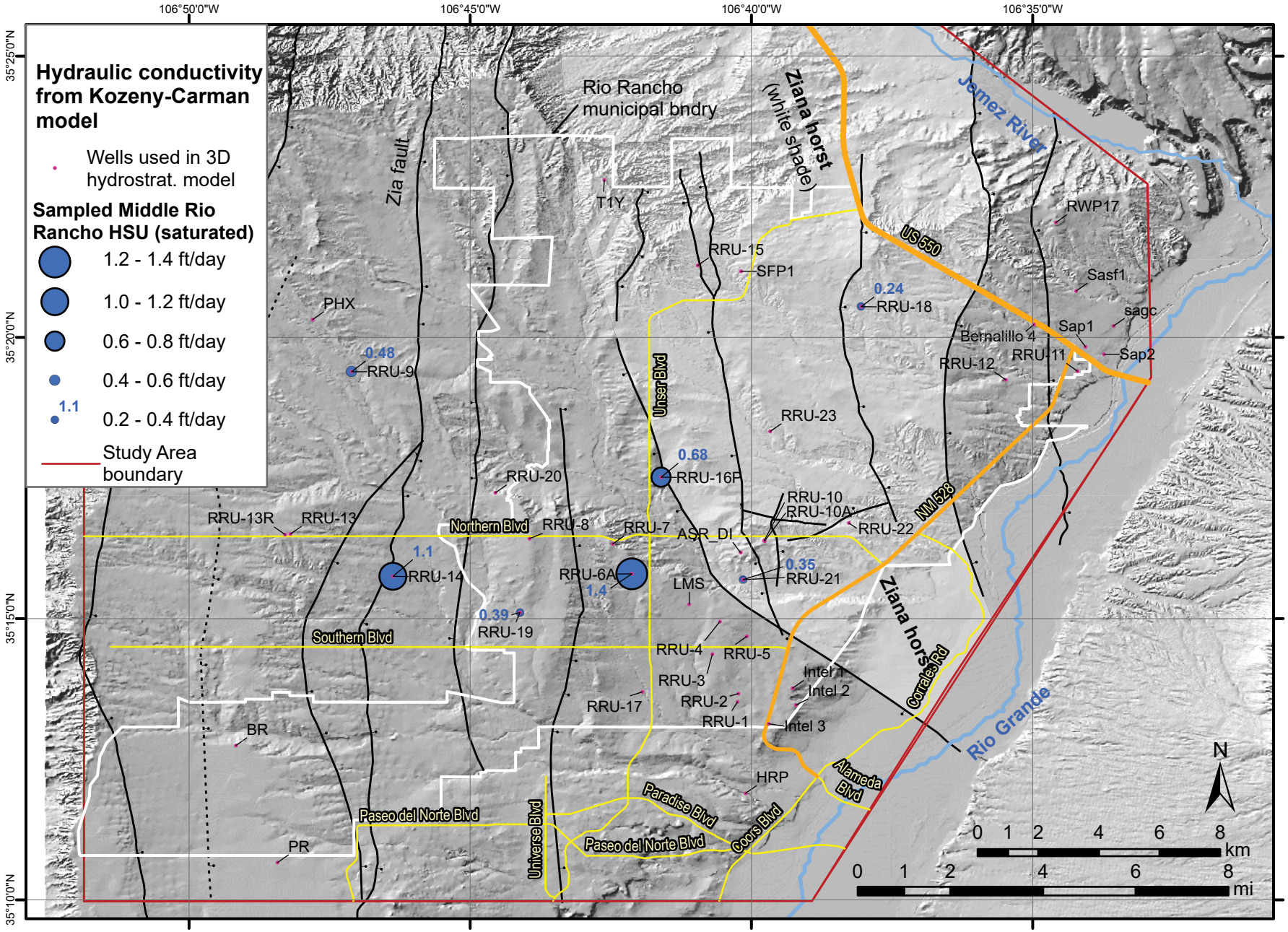

Figure 31. Hydraulic conductivity from the Kozeny-Carman model, plotted as scaled blue circles for saturated strata of the Middle Rio Rancho HSU. No spatial trends are evident.

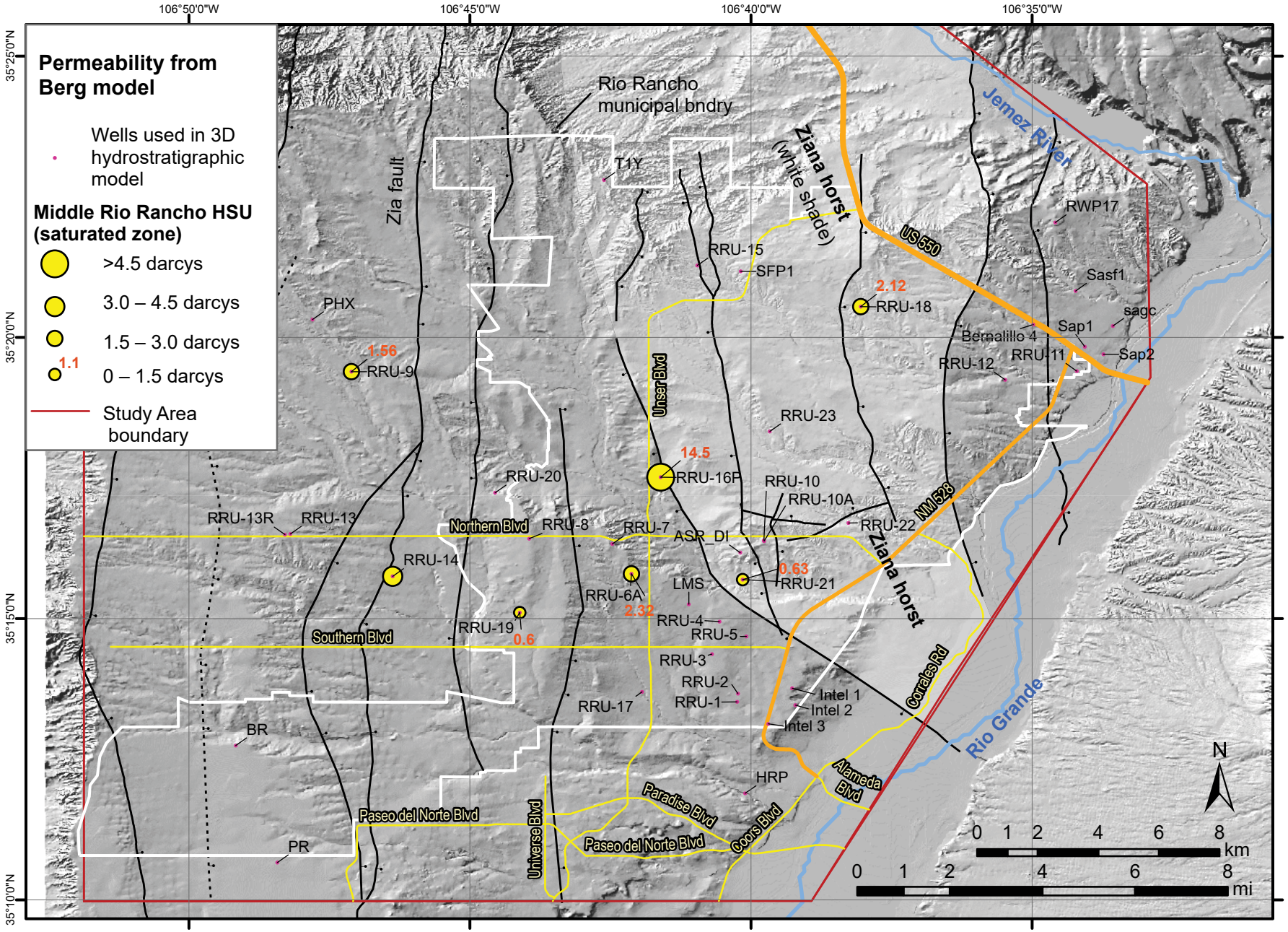

Figure 32. Permeability from the Berg model, plotted as scaled yellow circles for saturated strata of the Middle Rio Rancho HSU. No spatial trends are evident.

Comparison of permeability methods with hydraulic conductivity from pump test data. The corresponding regression equation and R^2 value are shown for each analysis.

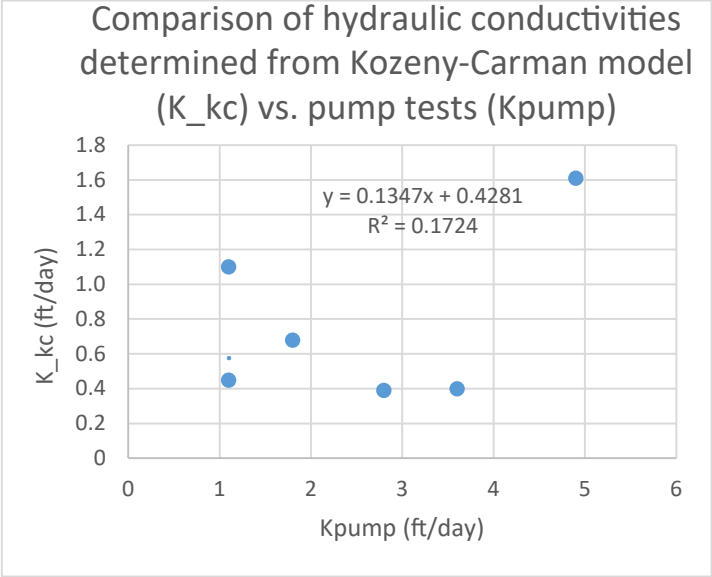

Fig. 33a (right). The hydraulic conductivity values determined from the Kozeny-Carman model (plotted as an arithmetic mean per well) have poor correlation with those determined from pumping tests (R^2 of 0.17) of the same well. We thus have little confidence in applying the Kozeny-Carman model results to the entire aquifer.

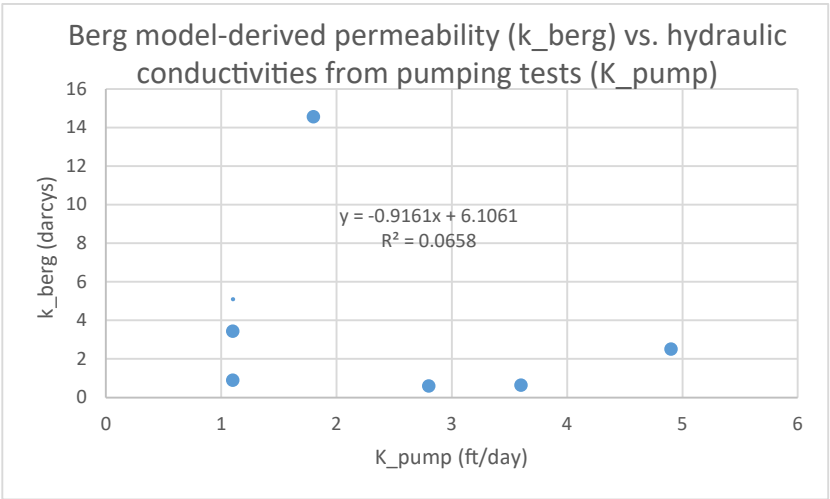

Fig. 33b (left). The permeability values determined from the Berg model also have poor correlation with those determined from pumping tests (R^2 of 0.07). We thus have little confidence in applying the Berg model results to the entire aquifer.

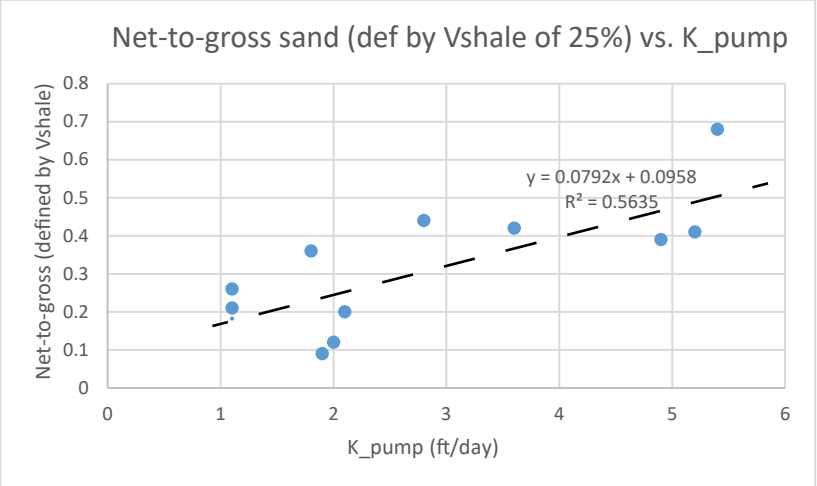

Fig. 33c (left). When comparing the percentage of sand bodies in an aquifer, there is moderate correlation with pumping test data (K_pump; R^2 of 0.56). The percentage of sand bodies was calculated using the Vshale curve in Kingdom software, and is expressed as a net-to-gross ratio.

Figure 33. Comparison of various permeability methods versus hydraulic conductivity derived from pumping tests, as calculated per well. Upper plot: Hydraulic conductivity values from the Kozeny-Carman model are plotted against pumping test data. There is no correlation between the two datasets. Middle plot: Permeability values from the Berg model are plotted against pumping test data. Again, there is no correlation between the two datasets. Lower plot: Net-to-gross ratios of sand are plotted against hydraulic conductivity data derived from pumping tests; in this comparison, there appears to be a positive correlation. Note that "sand" is defined by a Vshale value ≤0.25. All data are from the Middle Rio Rancho HSU.

PRELIMINARY EVALUATION OF WATER QUALITY AND AGE

TOTAL DISSOLVED SOLIDS DATA

We compiled water quality data from water chemistry analyses of samples from Rio Rancho's wells, particularly its main pumping wells (Appendix 1). Total dissolved solids (TDS) was chosen as an approximate proxy for overall water quality. Note that this simplistic exercise should be considered only a preliminary investigation into the water quality and geochemistry of the northwestern Albuquerque Basin, allowing for a comparison of updated knowledge of stratigraphy and structure (this report) with previous, detailed interpretations by Plummer et al. (2004a, 2004c).

The TDS data we compiled (Table 6) are plotted in Figure 34, where the Ziana horst is shaded in white. Note that the Coronado-Alameda fault delineates two TDS zones, one to the southwest and one to the northeast. To the southwest of the fault, TDS values are quite low, ranging from 205 to 462 parts per million (ppm, which is equivalent to milligrams per liter [mg/L]; Table 6), and are sampled from wells screened in either the Upper or Middle Rio Rancho HSU. Within this western, low-TDS zone, TDS values are slightly higher to the west of the Zia fault, but overall are quite acceptable (282–370 ppm; Table 6).

TDS values are higher on the northeast side of the Coronado-Alameda fault, corresponding to the Ziana horst, where they range from 388 to 1,400 ppm (Fig. 34, Table 6). Due to the northward pinch-out of the Upper Rio Rancho HSU and southward dip of the HSUs, sampled aquifers in this area consist of the Middle and Lower Rio Rancho HSUs and the Zia HSU (Fig. 34). A well along the Coronado-Alameda fault (RRU-16P) had moderately high TDS values of 466 ppm.

Water samples east of the Ziana horst (i.e., east of the Tamaya fault) returned variable concentrations of TDS. Well RRU-12, screened across both the Upper and Middle Rio Rancho HSUs and located 1 mi (1.6 km) east of the Tamaya fault and 0.3 mi (0.5 km) west of the San Felipe fault, had TDS values of 461 ppm (Table 6, Fig. 34). Interestingly, well RRU-11, located 0.4 mi (0.6 km) east of the San Felipe fault and screened wholly within the Upper Rio Rancho HSU, had particularly high TDS values of 1,100 ppm. Unless there is surface-based contamination, the high TDS values for that well suggest the possibility of focused upwelling of relatively salty water along the nearby San Felipe fault.

Although considerably more work is needed to fully understand the geologic influences on groundwater chemistry, these data indicate a spatial correspondence of saltier groundwater on and adjacent to the Ziana horst, particularly north of Northern Boulevard. Even the shallower aquifers in the northern part of the horst (such as the Middle Rio Rancho HSU sampled in RRU-15) have relatively high TDS (530 ppm) compared to elsewhere in the study area (Table 6, Fig. 34).

PRELIMINARY RADIOCARBON AGE ANALYSES

We compiled data from previous radiocarbon (carbon-14, or ^{14}C) age analyses that were conducted on groundwater in the northwestern Albuquerque Basin (Plummer et al., 2004c). Radiocarbon ages are approximations of groundwater age; they are subject to complications due to the dissolution of older carbon in calcium carbonate cements in the Santa Fe Group. Mixing of groundwater from different sources of different ages can also occur. Still, when used in a relative sense, these ages can support or discredit hypotheses regarding groundwater flow paths and source areas because younger ages are typically expected to be present closer to recharge areas.

The radiocarbon data we compiled from 15 wells (Table 6) are plotted in Figure 35, where the Ziana horst is shaded in white. The youngest groundwater ages—15.4–2.8 thousand years ago (ka)—are associated with the Upper Rio Rancho HSU in the main part of the city of Rio Rancho (southern study area), south of the Coronado-Alameda fault and east of Unser Boulevard. Groundwater ages from the Middle Rio Rancho HSU range from 30.9 to 14.2 ka. In the southern study area, slightly younger Middle Rio Rancho HSU ages (17.2–15.4 ka) are east of the inferred fault that projects north from Universe Boulevard; in this area, groundwater flow is southwestward or westward away from the Rio Grande and toward the groundwater trough of Plummer et al. (2004a, 2004c) in the south-central part of the study area (Fig. 35). The oldest groundwater ages come from west of the inferred fault that projects north from Universe Boulevard, including samples from RRU-9 (23.1 ka), RRU-13 (30.9 ka), NNMU-4 (23.9 ka), and the SWAB test holes (21.3 ka). These data suggest long flow paths for recharge to the Santa Fe Group aquifer southwest of the Ziana horst and west of the longitude approximating Universe Boulevard.

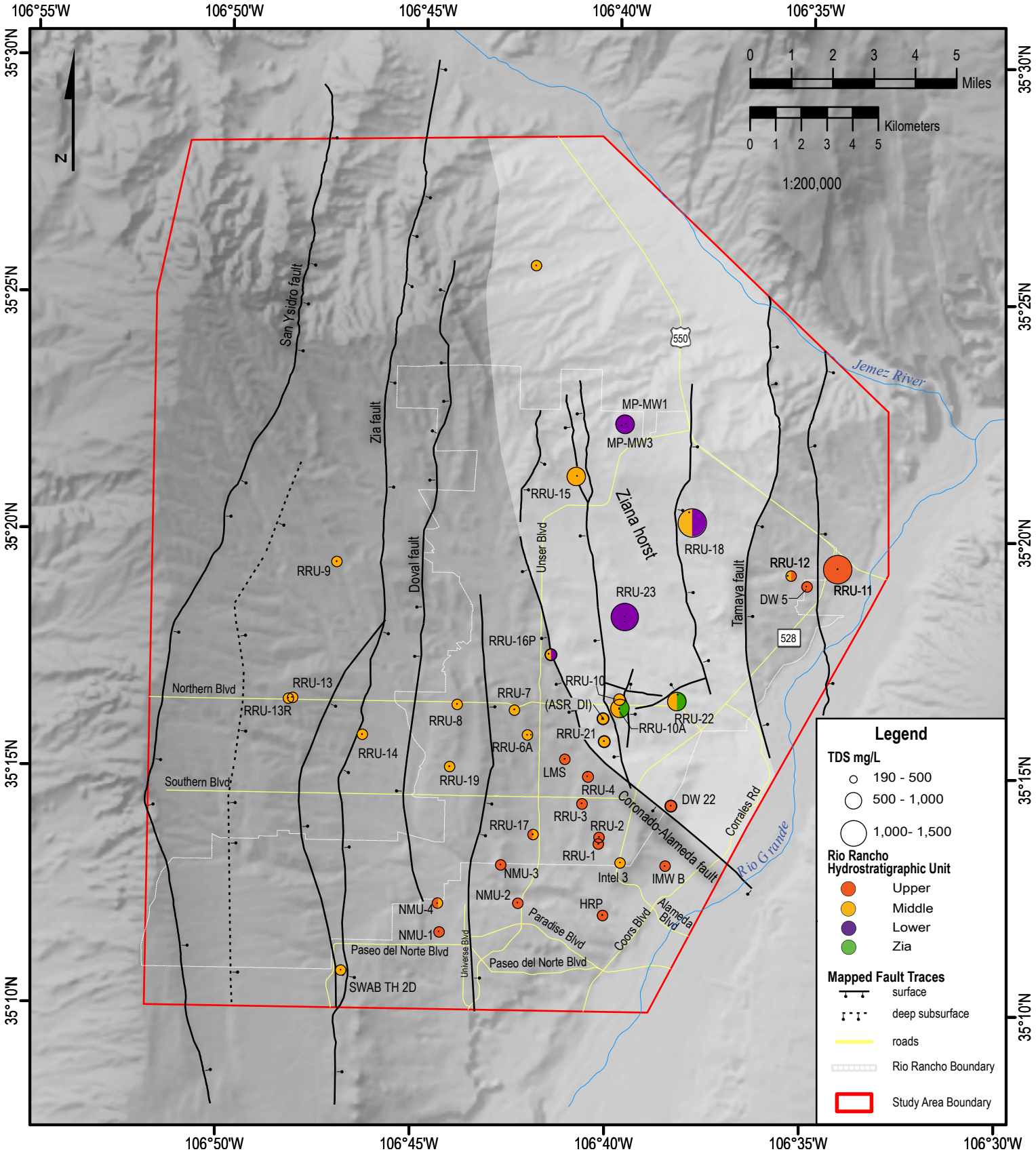

Figure 34. Map of TDS values obtained from well samples (Table 6). Locations of labeled wells are indicated by colored circles, where the colors are coded according to the HSU, and the circle diameters are scaled according to the TDS value. Note that two colors within a circle means a TDS value is interpreted to reflect two HSUs, based on comparison of screen depths with the depths of HSU boundaries in a given well.

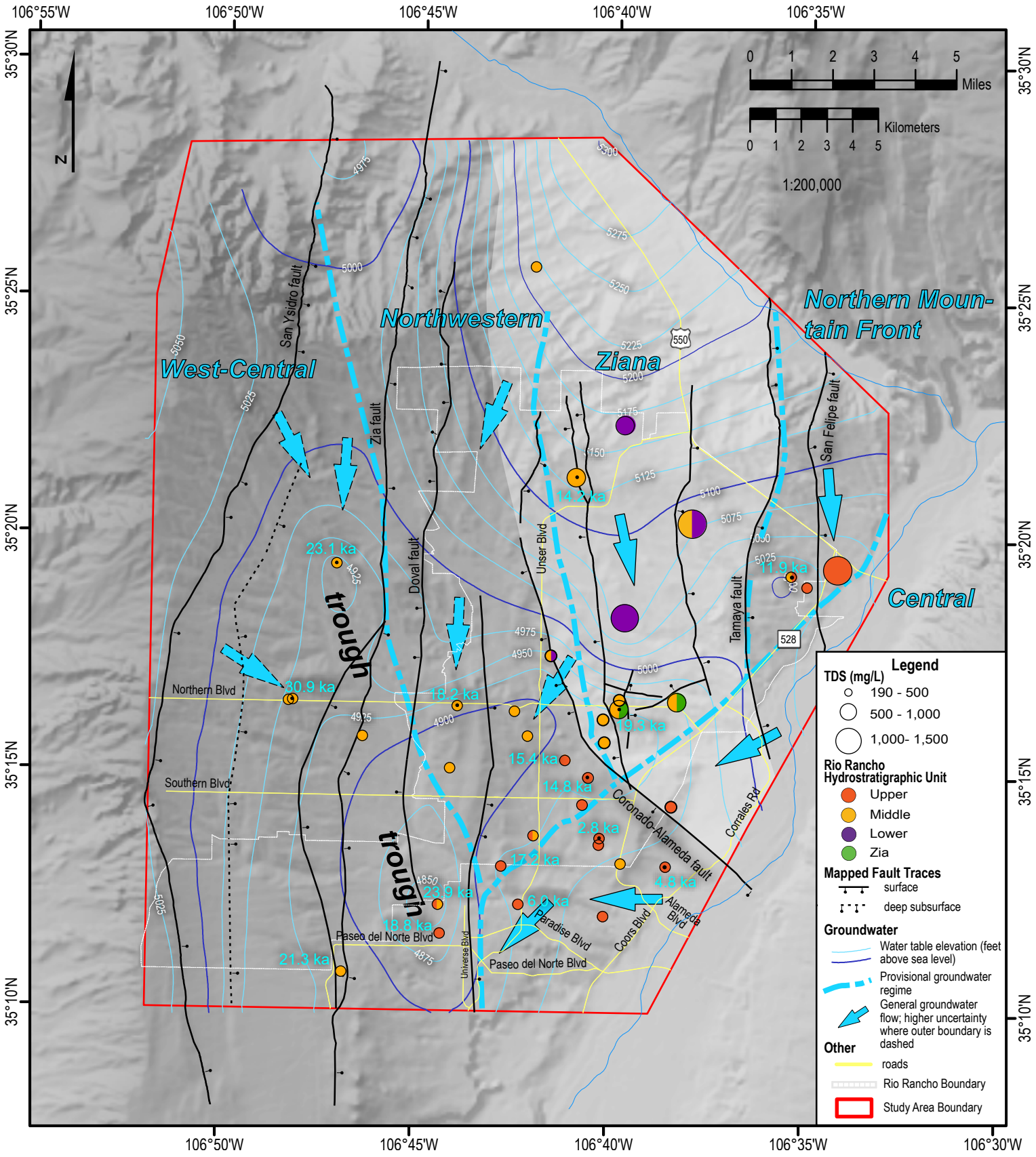

Figure 35. Map of TDS values obtained from well samples (as in Figure 34), but with radiocarbon ages of groundwater and approximate groundwater flow. Ages (in ka) are shown in light-blue text (Table 6). Groundwater flow is denoted by arrows; margins are dashed where flow direction is uncertain. Dashed, thick blue lines separate hydrogeologic regimes postulated in this report based on a synthesis of hydrochemical data (Plummer et al., 2004a, 2004c) with groundwater flow and structural data.

DISCUSSION

COMPARISON WITH PREVIOUS HYDROCHEMICAL WORK

Work by Plummer et al. (2004a, 2004b, 2004c) used a variety of geochemical data to map out various groundwater hydrochemical zones in the upper 2,000 ft (610 m) of the Santa Fe Group aquifer system. The hydrochemical zones of interest to our study include the West-Central, Northwestern, Northern Mountain Front, and Central zones (west to east, shown in Fig. 11). The West-Central zone has relatively moderate specific conductance and old radiocarbon groundwater ages; it is interpreted to have been recharged at relatively higher elevations and/or during a time of cooler climates. This water likely traveled southward to the western study area via long, deep flow paths sourced in the Jemez Mountains. We interpret that water from the West-Central zone may discharge out of fractured bedrock along major faults that extend north toward the southern Jemez Mountains, such as the San Ysidro and Zia faults (Fig. 11). The West-Central hydrochemical zone extends eastward under the adjoining zones to the east (see Plummer et al., 2004a, 2004c). The Northwestern zone has relatively low specific conductance and is likely recharged via low-elevation mountain-front recharge processes, with a component of infiltration from the Jemez River. In its northern part, there is relatively shallow groundwater trending subparallel to the Jemez River. The Northern Mountain Front hydrochemical zone has relatively dilute water (low specific conductance) and is recharged from the southern margin of the Jemez Mountains, with some infiltration occurring along the Rio Grande. The Central hydrochemical zone is centered on the Rio Grande. Chemical constituent and isotope (^{14}C, ^{2}H) data indicate that Rio Grande infiltration provides the primary source of recharge for the Central zone.

The presence of a long-term groundwater "trough" coinciding with the southern Montoyas graben was noted by Bexfield and Anderholm (2000) and Plummer et al. (2004a, 2004c). This trough is marked by the potentiometric surface being relatively low, about 100 ft (30 m) lower than near the Rio Grande (in terms of elevation). Plummer et al. (2004a) viewed this trough as a transient feature, perhaps reflecting lower rates of recharge from the Rio Grande during the drier middle–late Holocene. Prior to that time, the water-table surface may have been about the same elevation (in a west-east direction). The transitory nature is inferred from the reasoning that a long-term trough would result in the groundwater there (corresponding largely to the West-Central zone) having much more chemical affinity with the Rio Grande (Central zone), since a long-term water-table gradient would presumably drive Rio Grande flow toward that trough.

We emphasize that the groundwater trough coincides with geologic structures, particularly its alignment with the southern Montoyas graben, and that faults alongside and within the graben may be acting as groundwater barriers. Such a barrier effect is manifested by the geometry of the cones of depression associated with two areas: RRU-9 and the closely spaced NMU-1 and W-4 wells (Fig. 11). In particular, these cones of depression appear to be elongated north-south, parallel to nearby major faults (e.g., San Ysidro, Zia, and Doval faults, in addition to an inferred north-trending fault near Universe Boulevard; Figs. 11 and 35). The relatively high water-table gradients orthogonal to the northern Coronado-Alameda fault and the east-west faults near RRU-22 are consistent with those faults acting as groundwater barriers. We also note that the water-table geometry in southeast Rio Rancho very likely indicates a major component of westward recharge from the Rio Grande, accounting for the young ^{14}C ages in that area (e.g., wells RRU-2, NMU-2, HRP, and near Intel; Table 6, Fig. 35). However, westward flow farther west may be hampered by north-south structures, like the inferred fault along Universe Boulevard, or perhaps subsurface basaltic dikes.

This retarded flow may result in the recharge rate of relatively young groundwater (from the Rio Grande) being comparable to, or perhaps less than, the deep recharge replenishing the West-Central zone. The result would be a blended water that still retains much of the chemical character of the West-Central zone. Further modeling work could be used to test this alternative hypothesis regarding structural control of groundwater flow and groundwater chemistry near the southern end of the groundwater trough in our study area.

We suggest a spatial conceptualization of the hydrogeology as "regimes" by synthesizing groundwater flow, hydrochemical zones, and geologic structures (Fig. 35). These hydrogeologic regimes generally follow the hydrochemical zones of Plummer et al. (2004a, 2004c), but we add the Ziana regime, corresponding to most of the Ziana horst. We infer that the eastern boundary of the West-Central zone is strongly controlled by various north-south faults that act as fault barriers to some degree. These faults likely include the northern Zia fault, the middle Doval fault, and the inferred north-south fault near Universe Boulevard (Fig. 35). The relatively old groundwater in the trough (West-Central regime) may be a result of subsurface, bedrock discharge along the San Ysidro and perhaps Zia faults. These faults are inferred to transfer groundwater (probably in fractured bedrock) southward to the study area from the Jemez Mountains. The inferred fault along Universe Boulevard appears to act as a groundwater barrier (perhaps leaky to some extent), inhibiting inflow of younger groundwater sourced from the Rio Grande (Fig. 35). Compared to the Northwestern regime to the west and the Northern Mountain Front regime to the east, the Ziana regime is heavily influenced by salty (high TDS) water discharging from elevated, fractured, and faulted bedrock. This bedrock-derived groundwater may be mixing with shallower groundwater (Santa Fe Group) flowing southward between the faults bounding the Ziana horst block (Fig. 35). In the southeast corner of the study area, the western boundary of the Central hydrogeologic regime is extended westward (compared to that in Plummer et al., 2004c) based on groundwater elevation contours. This groundwater is interpreted to be largely derived from the Rio Grande (Plummer et al., 2004a, 2004c), consistent with low TDS values and low radiocarbon ages (Figs. 34 and 35). A leaky barrier at the inferred fault along Universe Boulevard may possibly allow minor groundwater flow from the Central zone westward to the West-Central regime, as reflected in the 18.8 ka groundwater age at NMU-1, but this flow is insufficient to notably alter the geochemical signature of the West-Central regime.

INTERPRETATIONS RELEVANT TO GROUNDWATER MANAGEMENT

1. The Upper Rio Rancho HSU is the most favorable of the HSUs.

Although there is some overlap in hydraulic conductivity data between the Upper and Middle Rio Rancho HSUs, the upper range of hydraulic conductivity data in the Upper Rio Rancho HSU includes considerably higher values, and its median value is three times greater than the median value of the Middle Rio Rancho HSU (Figs. 29 and 30, Table 6). The Upper Rio Rancho HSU also exhibits groundwater with the lowest TDS values (Fig. 34), excluding the anomalous data at well RRU-11, and is the shallowest of the HSUs. Therefore, the Upper Rio Rancho HSU can be considered the most favorable HSU for groundwater extraction potential.

The extent and thickness variations of the saturated portion of the Upper Rio Rancho HSU are shown in Figures 15 and 18. Most of the Upper Rio Rancho HSU is unsaturated, with its saturated area located in the southeast corner of the study area and along the eastern boundary. The saturated Upper Rio Rancho HSU thickens to the southeast, toward the intersection of Coors Boulevard and Paseo del Norte (partly due to the increase in the elevation of the potentiometric surface in that direction), and thins to the north. It may possibly thin abruptly—by perhaps around 1,000 ft (~300 m)—westward across the inferred east-down fault near Universe Boulevard, but more data are needed to ascertain the magnitude and rate of this thinning. Near the western extent of Paseo del Norte, extending north to Southern Boulevard, the saturated Upper Rio Rancho HSU is less than 500 ft (<150 m) thick, thinning in this zone to the west and north. It does not extend west of the Zia fault. The northern edge of the saturated Upper Rio Rancho HSU lies between Southern and Northern Boulevards, and it thins abruptly northeast of the Coronado-Alameda fault. East of the Tamaya fault in the northeastern study area, the saturated

Upper Rio Rancho HSU is inferred to be several hundred feet thick, thickening even more east of the Santa Ana section of the San Felipe fault.

2. The eastern and southeastern parts of the study area have favorable hydrogeology.

The area where the saturated Upper Rio Rancho HSU is thickest mainly corresponds with the Central and Northern Mountain Front hydrogeologic regimes. TDS values are low in these areas, except locally near faults (e.g., well RRU-12). Young (<15 ka) radiocarbon ages and groundwater flow directed away from rivers suggest a component of recharge from relatively young surface waters (Fig. 35). In terms of hydrogeologic properties, this area may be viewed as favorable for groundwater extraction potential.

3. The saturated Middle Rio Rancho HSU is important because of its large extent and thickness.

The extent and thickness variations of the saturated portion of the Middle Rio Rancho HSU are shown in Figure 19. Note that it extends notably farther northwest compared to the Upper Rio Rancho HSU, reaching to the San Ysidro fault. West of the Zia fault and north of Southern Boulevard, its saturated thickness is generally 1,000–1,500 ft (300–460 m), increasing southward to 2,000–2,500 ft (610–760 m) within 2 mi (3.2 km) west of the west end of Paseo del Norte. A 1,200- to 3,000-ft-thick (365–910 m) prong of saturated Middle Rio Rancho HSU extends northward into the Montoyas graben, inferred as being thickest between the Zia and Doval faults and thinning eastward from the Doval fault. The saturated part of the Middle Rio Rancho HSU covers much more of the Ziana horst than the saturated Upper Rio Rancho HSU, pinching out about 0.6 mi (~1 km) north of RRU-23. The saturated Middle Rio Rancho HSU is generally more than 1,500 ft (>460 m) thick east of the Tamaya fault and is possibly more than 2,000 ft (>600 m) thick east of the Santa Ana section of the San Felipe fault. In the southeast corner of the study area, the saturated Middle Rio Rancho HSU is interpreted to be 2,800–4,400 ft (850–1,340 m; Fig. 19) thick, but this thickness is poorly constrained.

Our sand versus clay permeability proxies, obtained from well data, suggest that the Middle Rio Rancho HSU has generally lower permeabilities at a given site compared to the Lower and Upper Rio Rancho HSUs (Figs. 26 and 28). Compilation of hydraulic conductivity and specific capacity data from pumping tests indicates that, in general, the Upper Rio Rancho HSU is likely to somewhat more likely to be more permeable compared to the Middle Rio Rancho HSU (Figs. 29 and 30), although these also show overlap in the data (especially for specific capacity). However, the relatively high thickness of the Middle Rio Rancho HSU would result in relatively high transmissivities (T = hydraulic conductivity multiplied by the thickness of saturated sediment), and the TDS values compiled for this unit were less than 500 ppm west and southwest of the Ziana horst. Therefore, the Middle Rio Rancho HSU can be considered an important component in groundwater management for the northwestern Albuquerque Basin.

Except for possibly two areas, we do not find any notable lateral permeability trends over most of the study area for the Middle Rio Rancho HSU (Figs. 27–29). The first of the two exceptions is located in the northwest corner of Rio Rancho's municipal boundary. Based on slightly higher sand body proportions in the Phoenix monitoring, Tamara No. 1-Y, and RRU-15 wells compared to wells to the south (Figs. 23, 26, and 27), there may be a slight northward coarsening of the Middle Rio Rancho HSU, and a corresponding increase in permeability, at distances more than 4 mi (6 km) north of Northern Boulevard.

The second area of exception lies in the southwest corner of the current boundary of the Rio Rancho municipality. There, pumping test data indicate hydraulic conductivities of 5–12 ft/day (Fig. 29, Table 6), which is more than the values of 2–5 ft/day plotted closer to the main, urbanized part of Rio Rancho (Fig. 29). The increased hydraulic conductivities there may be due to tongues of the relatively coarse-grained Benavidez unit (Koning et al., 2021), which are observed in exposures west of Ceja del Rio Puerco and whose tongues may extend into the Arroyo Ojito Formation (Middle Rio Rancho HSU) in the Black Ranch test well (depths of 840–1,010, 2,490–2,540, 2,710–2,740, and 2,890–2,900 ft [256–308, 759–774, 826–835, and 881–884 m]; Appendix 3).

4. There are inferred groundwater extraction limitations in the Middle and Upper Rio Rancho HSUs to the west.

West of the longitude corresponding to Universe Boulevard (106°43′0″), there are several issues that may limit groundwater extraction. First, the Upper Rio Rancho HSU, which we interpret as having a relatively high permeability, is thin west of Universe Boulevard and south of Southern Boulevard; there, it is less than 600 ft [180 m] thick and continues to thin to the northwest. Second, the groundwater potentiometric surface is particularly low in this area, corresponding to a temporally persistent trough (Bexfield and Anderholm, 2000). Third, groundwater recharge probably occurs at relatively slow rates, based on the low potentiometric surface and old groundwater radiocarbon ages (29–15 ka). This area corresponds to the West-Central hydrochemical zone of Plummer et al. (2004a, 2004c), where recharge is inferred to be ultimately derived from higher elevations in the Jemez Mountains (and/or during past periods of cooler temperatures) and probably discharged from faulted bedrock at the base of the Santa Fe Group. The fact that the upper bedrock consists of upper Paleozoic–Mesozoic strata (Connell, 2008b; Koning and Jochems, 2014; Koning and Rawling, 2017) is difficult to reconcile with the low observed TDS values of the groundwater (deep aquifers drilled in these strata typically return waters with high TDS; e.g., Intera Inc., 2008), which lends credence to the hypothesis of local recharge during an ice age. Although groundwater quality is relatively favorable, notable drawdown in two areas (well RRU-9 and the closely spaced wells NMU-1 and NMU-4) suggests that, at least locally, permeability can be low and groundwater flow rates limited. Other data suggesting low permeabilities are the slightly lower lithologic proportion of sand in this area (Figs. 23, 26, and 27) and low hydraulic conductivity values from pumping test data in the Middle Rio Rancho HSU (Fig. 29). An apparent exception is in the southwestern part of the study area, where two pumping tests show relatively higher hydraulic conductivities (Soil Amendment Facility well and Black Ranch test well). North of Southern Boulevard and west of the city's municipal boundary, a conservative approach in groundwater extraction would be prudent based on available data.

5. The Ziana horst—a problem and possibly an opportunity.

The middle and northern part of the Ziana horst, particularly north of Northern Boulevard, is spatially associated with high TDS and poorer-quality groundwater (Figs. 34 and 35). These issues are exemplified by the groundwater quality problems documented in Riesterer and Drakos (2008) and the lack of current pumping at well RRU-23. The Ziana horst corresponds to our informal Ziana hydrogeologic regime, where groundwater flow is southward and TDS values are relatively high (Fig. 35). The salty water is probably a result of upwelling of deep water from the relatively high (structurally elevated) and faulted (and presumably fractured at depth) horst block. The flow of deep water may also be directed southward in the lower Zia HSU between north-striking faults from the Jemez Mountains. Future water-well drilling in this zone probably has the best chances for success to the south, since the Upper and Middle Rio Rancho HSUs thicken southward (Figs. 18 and 19), and TDS values also lessen in that direction (Fig. 35).

A potential opportunity for groundwater management is the documentation of a relatively thick (up to 1,300 ft [400 m]) sandy zone in the lower–middle Zia HSU (Fig. 36). Based on outcrop correlatives of this zone near La Ceja and Ceja del Rio Puerco, corresponding to the Piedra Parada Member of the Zia Formation, there is localized cementation of this unit, where moderate to strong degrees of cementation are typically less than 15–20% of the member's volume (approximate visual estimate). If this low amount of cementation extends to the Ziana horst, then the lower–middle Zia HSU may be relatively permeable and a target aquifer. However, water from such an aquifer would need to be desalinated or blended to meet water quality standards. Whether such treatment or blending is practical or economically feasible warrants further study.

6. The Lower Rio Rancho HSU—probably high permeability but poor water quality.

Sand body thicknesses and the proportion of sand (net-to-gross ratios) indicate that the Lower Rio Rancho HSU should have relatively high permeabilities (Figs. 25 and 26). This inference is

bolstered by the single pumping test of this unit (well RRU-23), which returned a notably high value of 21 ft/day (Fig. 30). Since it is observed in well RRU-13R as well as on the Ziana horst, we interpret that this higher-permeability unit extends across the northern two-thirds of the study area. However, the apparent absence of this unit in the Black Ranch test well, at least in the depth interval of the well, suggests a possible facies change to a finer-grained unit south of Southern Boulevard (Plate 3, Fig. 14). Furthermore, there may be higher TDS values seen in wells sampled in this unit, particularly on the Ziana horst, compared to wells sampled in the Middle Rio Rancho and Upper Rio Rancho HSUs.

STRATIGRAPHIC AND TECTONIC FINDINGS

The work involved in correlating stratigraphic units in the subsurface across the study area, aided by Kingdom software analysis, resulted in the following observations pertaining to Santa Fe Group stratigraphy and Rio Grande rift tectonics.

- In a southward direction, it is increasingly difficult to differentiate the Loma Barbon Member from the Navajo Draw Member, both of the Arroyo Ojito Formation. This differentiation becomes particularly difficult south of Northern Boulevard. This is probably due to the southward converging of the two paleodrainage systems and the back-and-forth, east-west shifting of the common boundary.
- The Lower Rio Rancho HSU is extensive in an east-west direction and does not appear to thin across the Ziana horst block (Fig. 20, Plate 7); rather, eastward thickening may occur in that direction, consistent with northeast-thickening of the Cerro Conejo Formation in the cross sections in Riesterer et al. (2008). But this coarse-grained unit may grade southward into a finer-grained facies in the southern part of the study area, particularly south of Southern Boulevard. Deposited around 13–10 Ma, the Lower Rio Rancho HSU appears to reflect a wide, south-southeast-flowing distributary fan complex with relatively high stream power that carried copious sand eroded from the southeastern Colorado Plateau. Sand that was ablated from this fluvial system likely formed the Ojo Caliente sand dune field to the northeast, based on the similar 13–10 Ma age of that dune field compared to the Lower Rio Rancho HSU (upper Cerro Conejo Formation; cf. Connell, 2008a; Koning et al., 2011), the downwind position of that dune field (based on paleowind measurements of the Ojo Caliente sandstone; e.g., Koning, 2004; Koning et al., 2004, 2005), and broadly similar sand composition based on hand lens inspection.
- Two observations indicate that the Ziana horst was notably tectonically active after about 11 Ma. First, the Lower Rio Rancho HSU either thickens eastward or maintains about the same thickness across the Ziana horst, but the overlying Middle and Upper Rio Rancho HSUs thin across this structure (Plates 5–7, Figs. 18 and 19). Second, 11.3–11.2 Ma Trapper Creek B ashes are seen on the ground surface on the footwall of the Arroyo Venada fault, one of the major eastern-bounding faults of the horst, but lie at 2,070–2,080 ft (~630 m) depth on the hanging wall of the fault (in well RRU-18). Based on our structural contour map (Plate 3), there is around 500–1,000 ft (150–300 m) of post-10 Ma east-down vertical offset on that fault of the circa 10 Ma upper contact of the Lower Rio Rancho HSU (Appendix 8; age data from Connell et al., 1999; Connell, 2008a). Elsewhere, there is 1,400 ft (430 m) of throw of this contact by the Zia fault in the northern study area, and facies changes are observed in the Navajo Draw Member immediately adjacent to the Zia fault (on its hanging wall; see Koning and Personius, 2002). The top of the Middle Rio Rancho HSU, corresponding to about 6 Ma (Fig. 6; Connell, 2008a), is offset about 200 ft (~60 m) on the northern Zia fault. Therefore, significant fault activity occurred in this part of the study area from the late Miocene through the Pliocene, with the highest rates of throw occurring between 10 and 6 Ma. However, the Ziana horst and adjoining fault may also have been active in the late Oligocene to early Miocene, based on lithostratigraphic analyses of oil test holes drilled in the study area (Connell et al., 2007).

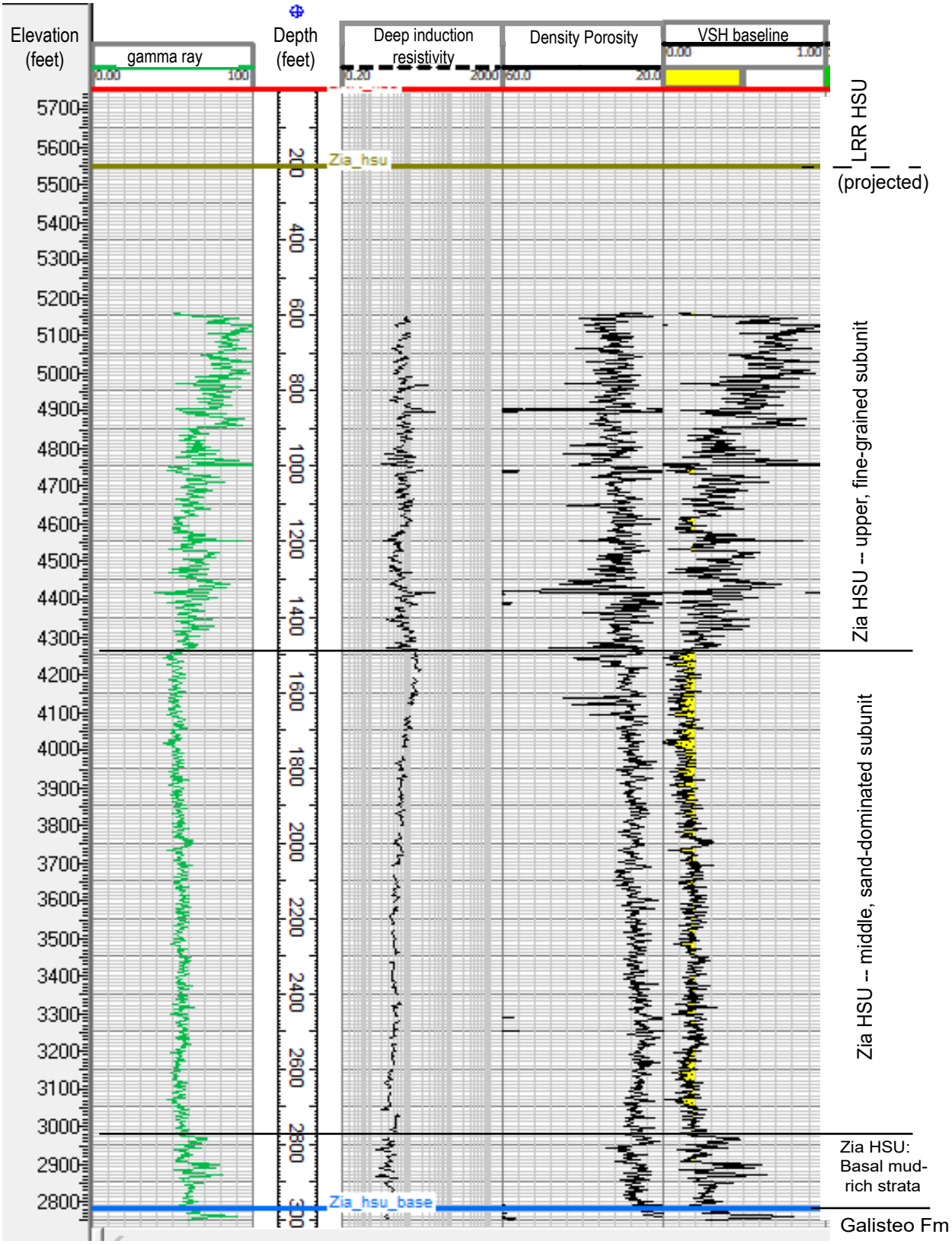

Figure 36. Gamma-ray, deep-induction, density-porosity, and Vshale wireline curves for the Santa Fe Pacific No. 1 well, located on the northern Ziana horst (labeled SFP1 in map figures). Within the Zia HSU, these indicate an upper finer-grained subunit and a middle sandier subunit (the latter occupying about half of the Zia HSU), as well as basal mud-rich strata. Interpretive annotations are provided along the right margin of the figure. The upper and middle subunits are also seen in wells T1Y and SFP3.

CONCLUSIONS

Our study differentiated four hydrostratigraphic units (HSUs) in the northwestern Albuquerque Basin, mapped them in the subsurface, and assessed permeability differences between and within them. We constructed a 3D geologic model showing the elevations of the bounding surfaces of these HSUs, and this model explicitly includes major faults that offset them. This model will be essential for potential future studies that calculate groundwater volumes and create groundwater flow models of the area. Although there is overlap in the data, the Upper Rio Rancho HSU generally exhibits higher hydraulic conductivity values (compiled from pumping tests) compared to the Middle Rio Rancho HSU, consistent with its higher sand-to-clay ratio inferred from well data and its higher density-porosity values. Furthermore, the TDS values of the Upper Rio Rancho HSU are quite acceptable, typically ranging from 200 to 400 ppm. However, the thick saturated portions of the Upper Rio Rancho HSU are only found east of the Tamaya fault and in the southeastern part of the study area, south of Southern Boulevard and south of the Coronado-Alameda fault. The saturated Middle Rio Rancho HSU is over 1,000 ft (300 m) thick across most of the study area, including a prong extending northward in the Montoyas graben between the Ziana horst and the Zia fault. Several wells indicate a coarsening-upward trend in this HSU (e.g., Fig. 12), so areas where its upper part is saturated are more favorable than where just its lower part is saturated. There are no strong lateral permeability trends across the saturated portion of the Middle Rio Rancho HSU over most of the study area, but hydraulic conductivities compiled from pumping tests do indicate higher permeability values in the southwestern part of the study area, within 5 mi (8 km) northwest of the western end of Paseo del Norte. A northward increase in sand proportions also occurs north of the approximate latitude of well RRU-9 (35°20′0″), suggesting a possible increase in permeability that remains to be confirmed by pumping test data. The Lower Rio Rancho HSU commonly exhibits relatively high TDS values, but various well-based permeability proxies and a single pumping test, in agreement with field observations of a high sand content, indicate it has relatively high permeability. The Lower Rio Rancho HSU extends across the northern two-thirds of the study area but may possibly undergo a southward facies change to a finer-grained unit south of Southern Boulevard. The lower–middle Zia HSU is notably sandy, based on outcrop observations and wildcat oil well data. Its relatively higher elevation on the Ziana horst may possibly provide an accessible deep-water aquifer in that area, provided that economically feasible methods can be found to either treat the high salinity or blend its groundwater to meet acceptable standards. An ancillary result of our study is a refinement of interpretations of past rift activity. Comparison of the amount of displacement of HSU surfaces of various ages across certain faults, in addition to stratigraphic positions of unconformities, indicates that notable tectonic activity associated with the Ziana horst and bounding faults occurred in the late Miocene and continued into the Pliocene.

REFERENCES

Aigner, T., Asprion, U., Hornung, J., Junghans, W.-D., and Kostrewa, R., 1996, Integrated outcrop analogue studies for Triassic alluvial reservoirs—Examples from southern Germany: Journal of Petroleum Geology, v. 19, no. 4, p. 393–406. https://doi.org/10.1111/j.1747-5457.1996.tb00446.x

Al-Ajmi, H., Hinderer, M., Keller, M., Rausch, R., Blum, P., and Bohnsack, D., 2011, The role of outcrop analogue studies for the characterization of aquifer properties: International Journal of Water Resources and Arid Environments, v. 1, no. 1, p. 48–54.

Allen, B.D., Connell, S.D., Hawley, J.W., and Stone, B.D., 1998, Core drilling provides information about Santa Fe Group aquifer system beneath Albuquerque's West Mesa: New Mexico Geology, v. 20, no. 1, p. 8–13. https://doi.org/10.58799/nmg-v20n1.8

Bartolino, J.R., and Cole, J.C., 2002, Ground-water resources of the Middle Rio Grande basin, New Mexico: U.S. Geological Survey Circular 1222, 132 p. https://doi.org/10.3133/cir1222

Becker, I., Busch, B., Koehrer, B., Adelmann, D., and Hilgers, C., 2019, Reservoir quality evolution of upper Carboniferous (Westphalian) tight gas sandstones, lower Saxony basin, NW Germany: Journal of Petroleum Geology, v. 42, no. 4, p. 371–392. https://doi.org/10.1111/jpg.12742

Berg, R.R., 1975, Capillary pressures in stratigraphic traps: AAPG Bulletin, v. 59, no. 6, p. 939–956.

Bexfield, L.M., and Anderholm, S.K., 2000, Predevelopment water-level map of the Santa Fe Group aquifer system in the Middle Rio Grande Basin between Cochiti Lake and San Acacia, New Mexico: U.S. Geological Survey Water-Resources Investigations Report 2000-4249, 1 sheet. https://doi.org/10.3133/wri004249

Bexfield, L.M., and Anderholm, S.K., 2002, Estimated water-level declines in the Santa Fe Group aquifer system in the Albuquerque area, central New Mexico, predevelopment to 2002: U.S. Geological Survey Water-Resources Investigations Report 2002-4233, 1 sheet. https://doi.org/10.3133/wri024233

Bexfield, L.M., and Plummer, L.N., 2003, Occurrence of arsenic in ground water of the Middle Rio Grande Basin, central New Mexico, *in* Welch, A.H., and Stollenwerk, K.G., eds., Arsenic in Ground Water: Boston, Massachusetts, Springer, p. 295–327. https://doi.org/10.1007/0-306-47956-7_11

Bexfield, L.M., Lindberg, W.E., and Anderholm, S.K., 1999, Summary of water-quality data for City of Albuquerque drinking-water supply wells, 1988–97: U.S. Geological Survey Open-File Report 99-195, 138 p., 1 plate. https://doi.org/10.3133/ofr99195

Bexfield, L.M., Danskin, W.R., and McAda, D.P., 2004, Simulation-optimization approach to management of ground-water resources in the Albuquerque area, New Mexico, 2006 through 2040: U.S. Geological Survey Scientific Investigations Report 2004-5140, 82 p. https://doi.org/10.3133/sir20045140

Biteman, S.E., Hyndman, D.W., Phanikumar, M.S., and Weissmann, G.S., 2004, Integration of sedimentologic properties for improved transport simulations, *in* Bridge, J.S., and Hyndman, D.W., eds., Aquifer Characterization: SEPM Special Publication No. 80, p. 3–13. https://doi.org/10.2110/pec.04.80.0003

Black, B.A., and Hiss, W.L., 1974, Structure and stratigraphy in the vicinity of the Shell Oil Co. Santa Fe Pacific No. 1 Test Well, southern Sandoval County, New Mexico, *in* Siemers, C.T., Woodward, L.A., and Callender, J.F., eds., Ghost Ranch: New Mexico Geological Society Fall Field Conference Guidebook 25, p. 365–370. https://doi.org/10.56577/ffc-25.365

Brandes, N.N., 2002, Lithostratigraphy and petrography of upper Santa Fe Group deposits in the northern Albuquerque Basin, New Mexico [MS thesis]: Socorro, New Mexico Institute of Mining and Technology, 208 p.

Bryan, K., and McCann, F.T., 1937, The Ceja del Rio Puerco—A border feature of the Basin and Range province in New Mexico. I. Stratigraphy and Structure: Journal of Geology, v. 45, no. 8, p. 801–828. https://doi.org/10.1086/624608

Bryan, K., and McCann, F.T., 1938, The Ceja del Rio Puerco—A border feature of the Basin and Range province in New Mexico. II. Geomorphology: Journal of Geology, v. 46, no. 1, p. 1–16. https://doi.org/10.1086/624618

Busch, B., Spitzner, A.-D., Adelmann, D., and Hilgers, C., 2022, The significance of outcrop analog data for reservoir quality assessment—A comparative case study of Lower Triassic Buntsandstein sandstones in the Upper Rhine Graben: Marine and Petroleum Geology, v. 141, 105701. https://doi.org/10.1016/j.marpetgeo.2022.105701

Caine, J.S., and Minor, S.A., 2009, Structural and geochemical characteristics of faulted sediments and inferences on the role of water in deformation, Rio Grande Rift, New Mexico: GSA Bulletin, v. 121, no. 9–10, p. 1325–1340. https://doi.org/10.1130/b26164.1

Carman, P.C., 1937, Fluid flow through granular beds: Transactions, Institution of Chemical Engineers, v. 15, p. 150–166. https://doi.org/10.1016/s0263-8762(97)80003-2

Carman, P.C., 1939, Permeability of saturated sands, soils, and clays: The Journal of Agricultural Science, v. 29, no. 2, p. 262–273. https://doi.org/10.1017/s0021859600051789

Cather, S.M., Connell, S.D., Heynekamp, M.R., and Goodwin, L.B., 1997, Geology of the Arroyo de las Calabacillas (Sky Village SE) 7.5-minute quadrangle, Sandoval County, New Mexico: New Mexico Bureau of Mines and Mineral Resources Open-File Geologic Map 9, scale 1:24,000. https://doi.org/10.58799/of-gm-9

Chapin, C.E., and Cather, S.M., 1994, Tectonic setting of the axial basins of the northern and central Rio Grande rift, *in* Keller, G.R., and Cather, S.M., eds., Basins of the Rio Grande Rift—Structure, stratigraphy, and tectonic setting: Geological Society of America Special Paper 291, p. 5–25. https://doi.org/10.1130/spe291-p5

Cikoski, C.T., Koning, D.J., and Connell, S.D., 2012, Geologic map of the La Mesita Negra 7.5-minute quadrangle, Bernalillo County, New Mexico: New Mexico Bureau of Geology and Mineral Resources Open-File Geologic Map 223, scale 1:24,000. https://doi.org/10.58799/of-gm-223

Connell, S.D., 1997 (revised Feb. 2000), Geology of the Alameda quadrangle, Bernalillo and Sandoval Counties, New Mexico: New Mexico Bureau of Mines and Mineral Resources Open-File Geologic Map 10, scale 1:24,000. https://doi.org/10.58799/of-gm-10

Connell, S.D., 2004, Geology of the Albuquerque Basin and tectonic development of the Rio Grande rift in north-central New Mexico, *in* Mack, G.H., and Giles, K.A., eds., The Geology of New Mexico—A geologic history: New Mexico Geological Society Special Publication 11, p. 359–388. https://doi.org/10.56577/SP-11

Connell, S.D., 2008a, Refinements to the stratigraphic nomenclature of the Santa Fe Group, northwestern Albuquerque Basin, New Mexico: New Mexico Geology, v. 30, no. 1, p. 14–35. https://doi.org/10.58799/nmg-v30n1.14

Connell, S.D., 2008b, Geologic map of the Albuquerque-Rio Rancho metropolitan area and vicinity, Bernalillo and Sandoval Counties, New Mexico: New Mexico Bureau of Geology and Mineral Resources Geologic Map 78, scale 1:50,000, 2 sheets. https://doi.org/10.58799/gm-78

Connell, S.D., Allen, B.D., and Hawley, J.W., 1998, Subsurface stratigraphy of the Santa Fe Group from borehole geophysical logs, Albuquerque area, New Mexico: New Mexico Geology, v. 20, no. 1, p. 2–7. https://doi.org/10.58799/nmg-v20n1.2

Connell, S.D., Koning, D.J., and Cather, S.M., 1999, Revisions to the stratigraphic nomenclature of the Santa Fe Group, northwestern Albuquerque Basin, New Mexico, *in* Pazzaglia, F.J., and Lucas, S.G., eds., Albuquerque Geology: New Mexico Geological Society Fall Field Conference Guidebook 50, p. 337–353. https://doi.org/10.56577/ffc-50.337

Connell, S.D., Koning, D.J., and Derrick, N.N., 2001, Preliminary interpretation of Cenozoic strata in the Tamara No. 1-Y well, Sandoval County, north-central New Mexico, *in* Connell, S.D., Lucas, S.G., and Love, D.W., eds., Stratigraphy and Tectonic Development of the Albuquerque Basin, Central Rio Grande Rift: New Mexico Bureau of Mines and Mineral Resources Open-File Report 454B, p. K79–K88. https://doi.org/10.58799/OFR-454B

Connell, S.D., Koning, D.J., Kelley, S.A., and Brandes, N.N., 2007, Oligocene and early Miocene sedimentation in the southwestern Jemez Mountains and northwestern Albuquerque Basin, New Mexico, *in* Kues, B.S., Kelley, S.A., and Lueth, V.W., eds., Geology of the Jemez Region II: New Mexico Geological Society Fall Field Conference Guidebook 58, p. 195–208. https://doi.org/10.56577/ffc-58.195

Connell, S.D., Smith, G.A., Geissman, J.W., and McIntosh, W.C., 2013, Climatic controls on nonmarine depositional sequences in the Albuquerque Basin, Rio Grande rift, north-central New Mexico, *in* Hudson, M.R., and Grauch, V.J.S., eds., New Perspectives on Rio Grande Rift Basins—From tectonics to groundwater: Geological Society of America Special Paper 494, p. 383–425. https://doi.org/10.1130/2013.2494(15)

Davis, J.M., Lohmann, R.C., Phillips, F.M., Wilson, J.L., and Love, D.W., 1993, Architecture of the Sierra Ladrones Formation, central New Mexico—Depositional controls on the permeability correlation structure: Geological Society of America Bulletin, v. 105, no. 8, p. 998–1007. https://doi.org/10.1130/0016-7606(1993)105%3C0998:aotslf%3E2.3.co;2

Fetter, C.W., Jr., 1988, Applied Hydrogeology (second edition): Long Grove, Illinois, Waveland Press, 592 p.

Galanter, A.E., and Curry, L.T.S., 2019, Estimated 2016 groundwater level and drawdown from predevelopment to 2016 in the Santa Fe Group aquifer system in the Albuquerque area, central New Mexico: U.S. Geological Survey Scientific Investigations Map 3433, 1 sheet, 13 p. https://doi.org/10.3133/sim3433

Galusha, T., 1966, The Zia Sand Formation, new early to medial Miocene beds in New Mexico: American Museum Novitates, no. 2271, p. 1–12.

Gaud, M.N., Smith, G.A., and McKenna, S.A., 2004, Relating small-scale permeability heterogeneity to lithofacies distribution, *in* Bridge, J.S., and Hyndman, D.W., eds., Aquifer Characterization: SEPM Special Publication 80, p. 56–66. https://doi.org/10.2110/pec.04.80.0055

Gawne, C.E., 1981, Sedimentology and stratigraphy of the Miocene Zia Sand of New Mexico—Summary: GSA Bulletin, v. 92, no. 12, p. 999–1007. https://doi.org/10.1130/0016-7606(1981)92%3C999:sasotm%3E2.0.co;2

Gillentine, J.M., 1994, Chapter 6—Petrology and diagenesis of the middle and lower Santa Fe Group in the northern Albuquerque Basin, New Mexico, *in* Haneberg, W.C., and Hawley, J.W., eds., Characterization of Hydrogeologic Units in the Northern Albuquerque Basin, New Mexico: New Mexico Bureau of Mines and Mineral Resources Open-File Report 402C, 97 p. https://doi.org/10.58799/OFR-402C

Grauch, V.J.S., 1999, Principal features of high-resolution aeromagnetic data collected near Albuquerque, New Mexico, *in* Pazzaglia, F.J., and Lucas, S.G., eds., Albuquerque Geology: New Mexico Geological Society Fall Field Conference Guidebook 50, p. 115–118. https://doi.org/10.56577/ffc-50.115

Grauch, V.J.S., and Connell, S.D., 2013, New perspectives on the geometry of the Albuquerque Basin, Rio Grande rift, New Mexico—Insights from geophysical models of rift-fill thickness, *in* Hudson, M.R., and Grauch, V.J.S., eds., New Perspectives on Rio Grande Rift Basins—From tectonics to groundwater: Geological Society of America Special Paper 494, p. 427–462. https://doi.org/10.1130/2013.2494(16)

Grauch, V.J.S., Keller, G.R., and Gillespie, C.L., 1999, Discussion of new gravity maps for the Albuquerque Basin area, *in* Pazzaglia, F.J., and Lucas, S.G., eds., Albuquerque Geology: New Mexico Geological Society Fall Field Conference Guidebook 50, p. 119–124. https://doi.org/10.56577/ffc-50.119

Grauch, V.J.S., Hudson, M.R., and Minor, S.A., 2001, Aeromagnetic expression of faults that offset basin fill, Albuquerque Basin, New Mexico: Geophysics, v. 66, no. 3, p. 707–720. https://doi.org/10.1190/1.1444961

Haneberg, W.C., 1996, Chapter 4—Compaction curves and virgin specific storage estimates for selected Albuquerque Basin water wells, *in* Haneberg, W.C., and Hawley, J.W., eds., Characterization of Hydrogeologic Units in the Northern Albuquerque Basin, New Mexico: New Mexico Bureau of Mines and Mineral Resources Open-File Report 402C, 33 p. https://doi.org/10.58799/OFR-402C

Hawley, J.W., 1996, Chapter 1—Hydrogeologic framework of potential recharge areas in the Albuquerque Basin, central Valencia County, New Mexico, *in* Hawley, J.W., and Whitworth, T.M., eds., Hydrogeology of Potential Recharge Areas for the Basin- and Valley-Fill Aquifer Systems, and Hydrogeochemical Modelling of Proposed Artificial Recharge of the Upper Santa Fe Aquifer, Northern Albuquerque Basin, New Mexico: New Mexico Bureau of Mines and Mineral Resources Open-File Report 402D, 68 p. https://doi.org/10.58799/OFR-402D

Hawley, J.W., and Haase, C.S., 1992, Hydrogeologic framework of the northern Albuquerque Basin: New Mexico Bureau of Mines and Mineral Resources Open-File Report 387, 176 p. https://doi.org/10.58799/OFR-387

Hawley, J.W., and Kernodle, J.M., 2000, Overview of the hydrogeology and geohydrology of the northern Rio Grande: Water Resources Research Institute Report No. 312, 1999 Conference Proceedings. https://nmwrri.nmsu.edu/publications/water-conference-proceedings/wcp-documents/w44/1999%20Conference%20Proceedings%20as%20one%20file.pdf?utm_source=chatgpt.com

Hawley, J.W., and Whitworth, T.M., 1996, Hydrogeology of potential recharge areas for the basin- and valley-fill aquifer systems, and hydrogeochemical modelling of proposed artificial recharge of the upper Santa Fe aquifer, northern Albuquerque Basin, New Mexico: New Mexico Bureau of Mines and Mineral Resources Open-File Report 402D, 611 p. https://doi.org/10.58799/OFR-402D

Hawley, J.W., Haase, C.S., and Lozinsky, R.P., 1995, An underground view of the Albuquerque Basin: The Water Future of Albuquerque and Middle Rio Grande Basin—Proceedings of the 39th annual New Mexico Water Conference, p. 37–55.

Hornung, J., and Aigner, T., 2006, Reservoir architecture in a terminal alluvial plain—An outcrop analogue study (Upper Triassic, southern Germany), Part 1—Sedimentology and petrophysics: Journal of Petroleum Geology, v. 25, no. 1, p. 3–30. https://doi.org/10.1111/j.1747-5457.2002.tb00097.x

Howell, J.A., Martinius, A.W., and Good, T.R., 2014, The application of outcrop analogues in geological modelling—A review, present status and future outlook, *in* Martinius, A.W., Howell, J.A., and Good, T.R., eds., Sediment-Body Geometry and Heterogeneity—Analogue studies for modelling the subsurface: Geological Society of London Special Publication 387, p. 1–25. https://doi.org/10.1144/sp387.12

Intera Inc., 2008, Sandoval County Rio Puerco Basin water development project, aquifer test and analysis report: Unpublished consultant report prepared for Sandoval County (Dec. 9, 2008), 46 p. and Appendices A–E.

Keller, M., Bohnsack, D., Koch, R., Hinderer, M., Hornung, J., Al-Ajmi, H., and Amarah, B.A., 2019, Chapter 10—Outcrop analog studies of the Wasia-Biyadh and Aruma aquifers of Saudi Arabia, *in* AlAnzi, H.R., Rahmani, R.A., Steel, R.J., and Soliman, O.M., eds., Siliciclastic Reservoirs of the Arabian Plate: The American Association of Petroleum Geologists Memoir 116. https://doi.org/10.1306/13642171M1183514

Kelley, V.C., 1977, Geology of the Albuquerque Basin, New Mexico: New Mexico Bureau of Mines and Mineral Resources Memoir 33, 60 p. https://doi.org/10.58799/M-33

Kernodle, J.M., 1998, Simulation of ground-water flow in the Albuquerque Basin, central New Mexico, 1901–95, with projections to 2020: U.S. Geological Survey Open-File Report 96-209, 54 p. https://doi.org/10.3133/ofr96209

Kernodle, J.M., and Scott, W.B., 1986, Three-dimensional model simulation of steady-state ground-water flow in the Albuquerque-Belen Basin, New Mexico: U.S. Geological Survey Water-Resources Investigations Report 84-4353, 58 p. https://doi.org/10.3133/wri844353

Kernodle, J.M., Miller, R.S., and Scott, W.B., 1987, Three-dimensional model simulation of transient ground-water flow in the Albuquerque-Belen Basin, New Mexico: U.S. Geological Survey Water-Resources Investigations Report 86-4194, 86 p. https://doi.org/10.3133/wri864194

Kernodle, J.M., McAda, D.P., and Thorn, C.R., 1995, Simulation of ground-water flow in the Albuquerque Basin, central New Mexico, 1901–1994, with projections to 2020: U.S. Geological Survey Water-Resources Investigations Report 94-4251, 114 p. https://doi.org/10.3133/wri944251

Klingbeil, R., Kleineidam, S., Asprion, U., Aigner, T., and Teutsch, G., 1999, Relating lithofacies to hydrofacies—Outcrop-based hydrogeological characterization of Quaternary gravel deposits: Sedimentary Geology, v. 129, no. 3–4, p. 299–310. https://doi.org/10.1016/s0037-0738(99)00067-6

Koning, D.J., 2004, Geologic map of the Lyden 7.5-minute quadrangle, Rio Arriba County, New Mexico: New Mexico Bureau of Geology and Mineral Resources Open-File Geologic Map 83, scale 1:24,000. https://doi.org/10.58799/OF-GM-83

Koning, D.J., and Jochems, A.P., 2014, Geologic map of the Benavidez Ranch 7.5-Minute quadrangle, Bernalillo and Sandoval Counties, New Mexico: New Mexico Bureau of Geology and Mineral Resources Open-File Geologic Map 234, scale 1:24,000. https://doi.org/10.58799/of-gm-234

Koning, D.J., and Personius, S.F., 2002, Geologic map of the Bernalillo NW quadrangle, Sandoval County, New Mexico: U.S. Geological Survey Miscellaneous Field Studies Map 2404, scale 1:24,000. https://doi.org/10.3133/mf2404

Koning, D.J., and Rawling, G.C., 2017, Geologic map of the San Felipe Mesa 7.5-minute quadrangle, Sandoval County, New Mexico: New Mexico Bureau of Geology and Mineral Resources Open-File Geologic Map 266, scale 1:24,000. https://doi.org/10.58799/of-gm-266

Koning, D.J., Pederson, J., Pazzaglia, F.J., and Cather, S.M., 1998, Geology of the Cerro Conejo (Sky Village NE) 7.5-minute quadrangle, Sandoval County, New Mexico: New Mexico Bureau of Mines and Mineral Resources Open-File Geologic Map 45, scale 1:24,000. https://doi.org/10.58799/of-gm-45

Koning, D.J., May, J., Aby, S., and Horning, R., 2004 (revised August 2020), Geologic map of the Medanales 7.5-minute quadrangle, Rio Arriba County, New Mexico: New Mexico Bureau of Geology and Mineral Resources Open-File Geologic Map 89, scale 1:24,000. https://doi.org/10.58799/OF-GM-89

Koning, D.J., Skotnicki, S., Kelley, S., and Moore, J., 2005, Geologic map of the Chili 7.5-minute quadrangle, Rio Arriba County, New Mexico: New Mexico Bureau of Geology and Mineral Resources Open-File Geologic Map 103, scale 1:24,000. https://doi.org/10.58799/OF-GM-103

Koning, D.J., McIntosh, W., and Dunbar, N., 2011, Geology of southern Black Mesa, Española Basin, New Mexico—New stratigraphic age control and interpretation of the southern Embudo fault system of the Rio Grande rift, *in* Koning, D.J., Karlstrom, K.E., Kelley, S.A., Lueth, V.W., and Aby, S.B., eds., Geology of the Tusas Mountains and Ojo Caliente Area: New Mexico Geological Society Field Conference Guidebook 62, p. 191–214.

Koning, D.J., Cikoski, C.T., Rinehart, A.J., and Jochems, A.P., 2019, Mapping suitability for managed aquifer recharge in the Albuquerque Basin: New Mexico Bureau of Geology and Mineral Resources Open-File Report 605, 83 p., 4 plates. https://doi.org/10.58799/OFR-605

Koning, D.J., Heizler, M., and Jochems, A., 2021, Clues from the Santa Fe Group for Oligocene–Miocene paleogeography of the southeastern Colorado Plateau near Grants, NM, *in* Frey, B.A., Kelley, S.A., Goff, F., Zeigler, K.E., McLemore, V.T., and Ulmer-Scholle, D.S., eds., Geology of the Mount Taylor Area: New Mexico Geological Society Fall Field Conference Guidebook 71, p. 267–280. https://doi.org/10.56577/FFC-71.267

Kozeny, J., 1927, Uber kapillare leitung des wassers im boden: Sitzungsberichte der Akademie der Wissenschaften in Wien, v. 136, p. 271. https://doi.org/10.1515/9783486753790

Lozinsky, R.P., 1988, Stratigraphy, sedimentology, and sand petrology of the Santa Fe Group and pre-Santa Fe Tertiary deposits in the Albuquerque Basin [PhD dissertation]: Socorro, New Mexico Institute of Mining and Technology, 298 p.

Lozinsky, R.P., 1994, Cenozoic stratigraphy, sandstone petrology, and depositional history of the Albuquerque Basin, central New Mexico, *in* Keller, G.R., and Cather, S.M., eds., Basins of the Rio Grande Rift—Structure, stratigraphy, and tectonic setting: Geological Society of America Special Paper 291, p. 73–82. https://doi.org/10.1130/spe291-p73

Machette, M.N., Personius, S.F., Kelson, K.I., Haller, K.M., and Dart, R.L., 1998, Map and data for Quaternary faults and folds in New Mexico: U.S. Geological Survey Open-File Report 98-521, 443 p., 1 plate. https://doi.org/10.3133/ofr98521

May, J.S., and Russell, L.R., 1994, Thickness of the syn-rift Santa Fe Group in the Albuquerque Basin and its relation to structural style, *in* Keller, G.R., and Cather, S.M., eds., Basins of the Rio Grande Rift—Structure, stratigraphy, and tectonic setting: Geological Society of America Special Paper 291, p. 113–123. https://doi.org/10.1130/spe291-p113

McAda, D.P., and Barroll, P., 2002, Simulation of ground-water flow in the Middle Rio Grande Basin between Cochiti and San Acacia, New Mexico: U.S. Geological Survey Water-Resources Investigations Report 2002-4200, 81 p. https://doi.org/10.3133/wri20024200

Minor, S.A., and Hudson, M.R., 2006, Regional survey of structural properties and cementation patterns of fault zones in the northern part of the Albuquerque Basin—Implications for ground-water flow: U.S. Geological Survey Professional Paper 1719, 28 p. https://doi.org/10.3133/pp1719

Nelson, P.H., 1994, Permeability-porosity relationships in sedimentary rocks: The Log Analyst, v. 35, no. 3, p. 38–62.

Personius, S.F., 2002, Geologic map of the Santa Ana Pueblo quadrangle, Sandoval County, New Mexico: U.S. Geological Survey Miscellaneous Field Studies Map 2405, scale 1:24,000. https://doi.org/10.3133/mf2405

Personius, S.F., Machette, M.N., and Stone, B.D., 2000, Preliminary geologic map of the Loma Machete quadrangle, Sandoval County, New Mexico: U.S. Geological Survey Miscellaneous Field Studies Map 2334, scale 1:24,000. https://doi.org/10.3133/mf2334

Plummer, L.N., Bexfield, L.M., Anderholm, S.K., Sanford, W.E., and Busenberg, E., 2001, Geochemical characterization of ground-water flow in the Santa Fe Group aquifer system, Middle Rio Grande Basin, New Mexico, *in* Cole, J.C., ed., U.S. Geological Survey Middle Rio Grande Basin Study—Proceedings of the Fourth Annual Workshop, Albuquerque, New Mexico, February 15–16, 2000: U.S. Geological Survey Open-File Report 00-488, p. 7–10. https://doi.org/10.3133/ofr00488

Plummer, L.N., Bexfield, L.M., Anderholm, S.K., Sanford, W.E., and Busenberg, E., 2004a, Hydrochemical tracers in the Middle Rio Grande Basin, USA—1. Conceptualization of groundwater flow: Hydrogeology Journal, v. 12, p. 359–388. https://doi.org/10.1007/s10040-004-0324-6

Plummer, L.N., Sanford, W.E., Bexfield, L.M., Anderholm, S.K., and Busenberg, E., 2004b, Using geochemical data and aquifer simulation to characterize recharge and groundwater flow in the Middle Rio Grande Basin, New Mexico, *in* Hogan, J.F., Phillips, F.M., and Scanlon, B.R., eds., Groundwater Recharge in a Desert Environment—The Southwestern United States Water Science and Applications Series, vol. 9: Washington, D.C., American Geophysical Union, p. 185–216.

Plummer, L.N., Bexfield, L.M., Anderholm, S.K., Sanford, W.E., and Busenberg, E., 2004c, Geochemical characterization of ground-water flow in the Santa Fe Group aquifer system, Middle Rio Grande Basin, New Mexico: U.S. Geological Survey Water-Resources Investigations Report 2003-4131, 395 p. https://doi.org/10.3133/wri034131

Rawling, G.C., and Goodwin, L.B., 2006, Structural record of the mechanical evolution of mixed zones in faulted poorly lithified sediments: Journal of Structural Geology, v. 28, no. 9, p. 1623–1639. https://doi.org/10.1016/j.jsg.2006.06.008

Rawling, G.C., Goodwin, L.B., and Wilson, J.L., 2001, Internal architecture, permeability structure, and hydrologic significance of contrasting fault-zone types: Geology, v. 29, no. 1, p. 43–46. https://doi.org/10.1130/0091-7613(2001)029%3C0043:iapsah%3E2.0.co;2

Reiter, M., 2001, Using precision temperature logs to estimate horizontal and vertical groundwater flow components: Water Resources Research, v. 37, no. 3, p. 663–674. https://doi.org/10.1029/2000wr900302

Reiter, M., 2003, Hydrogeothermal studies in the Albuquerque Basin—A geophysical investigation of ground water flow characteristics: New Mexico Bureau of Geology and Mineral Resources Circular 211, 74 p. https://doi.org/10.58799/c-211

Riesterer, J., and Drakos, P. (Glorieta Geoscience, Inc.), 2008 (revised 2009), Well drilling, completion, and testing report, City of Rio Rancho Well 23 (RG-6745-S-27): Unpublished consultant report prepared for City of Rio Rancho, August 2008, 45 p. plus an addendum (14 p.).

Riesterer, J., Hawley, J., Drakos, P., Lazarus, J., Lesh, M., and Chudnoff, M. (Glorieta Geoscience, Inc.), 2004, City of Rio Rancho ground water exploration program—Results of phase one study: Unpublished consultant report prepared for City of Rio Rancho, Feb. 25, 2004, 112 p.

Riesterer, J., Drakos, P., and Lazarus, J. (Glorieta Geoscience, Inc.), 2008, Evaluation of future production well locations, well replacement needs, and future water sources, City of Rio Rancho: Unpublished consultant report prepared for City of Rio Rancho, Nov. 2008, 18 p.

Russell, L.R., and Snelson, S., 1994, Structure and tectonics of the Albuquerque Basin segment of the Rio Grande rift—Insights from reflection seismic data, *in* Keller, G.R., and Cather, S.M., eds., Basins of the Rio Grande Rift—Structure, stratigraphy, and tectonic setting: Geological Society of America Special Paper 291, p. 83–112. https://doi.org/10.1130/spe291-p83

Sanford, W.E., Plummer, L.N., McAda, D.P., Bexfield, L.M., and Anderholm, S.K., 2004a, Hydrochemical tracers in the Middle Rio Grande Basin, USA—2. Calibration of a groundwater-flow model: Hydrogeology Journal, v. 12, p. 389–407. https://doi.org/10.1007/s10040-004-0326-4

Sanford, W.E., Plummer, L.N., McAda, D.P., Bexfield, L.M., and Anderholm, S.K., 2004b, Use of environmental tracers to estimate parameters for a predevelopment ground-water-flow model of the Middle Rio Grande Basin, New Mexico: U.S. Geological Survey Water-Resources Investigations Report 2003-4286, 102 p. https://doi.org/10.3133/wri034286

Smith, G.A., and Lavine, A., 1996, What is the Cochiti Formation?, *in* Goff, F., Kues, B.S., Rogers, M.A., McFadden, L.D., and Gardner, J.N., eds., Jemez Mountains Region: New Mexico Geological Society Fall Field Conference Guidebook 47, p. 219–224. https://doi.org/10.56577/ffc-47.219

Smyth, D.G., 2004, Sedimentology and permeability characteristics of the Arroyo Ojito Formation (upper Santa Fe Group) adjacent to the Sand Hill fault, Albuquerque Basin, New Mexico [MS thesis]: Socorro, New Mexico Institute of Mining and Technology, 96 p.

Spiegel, Z., 1961, Late Cenozoic sediments of the lower Jemez River region, *in* Northrop, S.A., ed., Albuquerque Country: New Mexico Geological Society Fall Field Conference Guidebook 12, p. 132–138. https://doi.org/10.56577/ffc-12.132

Spiegel, Z., and Baldwin, B., 1963, Geology and water resources of the Santa Fe area, New Mexico: U.S. Geological Survey Water Supply Paper 1525, 258 p. https://doi.org/10.3133/wsp1525

Tearpock, D.J., and Bischke, R.E., 2002, Applied Subsurface Geological Mapping, with Structural Methods (second edition): Upper Saddle River, New Jersey, Prentice-Hall PTR, 822 p.

Tedford, R.H., 1982, Neogene stratigraphy of the northwestern Albuquerque Basin, *in* Grambling, J.A., Wells, S.G., and Callender, J.F., eds., Albuquerque Country II: New Mexico Geological Society Fall Field Conference Guidebook 33, p. 273–278. https://doi.org/10.56577/ffc-33.273

Tedford, R.H., and Barghoorn, S.F., 1999, Santa Fe Group (Neogene), Ceja del Rio Puerco, northwestern Albuquerque Basin, Sandoval County, New Mexico, *in* Pazzaglia, F.J., and Lucas, S.G., eds., Albuquerque Geology: New Mexico Geological Society Fall Field Conference Guidebook 50, p. 327–335. https://doi.org/10.56577/ffc-50.327

Thompson, R.A., Shroba, R.R., Menges, C.M., Schmidt, D.L., Personius, S.F., and Brandt, T.R., 2009, Geologic map of the Volcanoes quadrangle, Bernalillo and Sandoval Counties, New Mexico: U.S. Geological Survey Scientific Investigations Map 3083, scale 1:24,000. https://doi.org/10.3133/sim3083

Thorn, C.R., McAda, D.P., and Kernodle, J.M., 1993, Geohydrologic framework and hydrologic conditions in the Albuquerque Basin, central New Mexico: U.S. Geological Survey Water-Resources Investigations Report 93-4149, 106 p. https://doi.org/10.3133/wri934149

Urumović, K., and Urumović, K., Sr., 2016, The referential grain size and effective porosity in the Kozeny-Carman model: Hydrology and Earth System Sciences, v. 20, no. 5, p. 1669–1680. https://doi.org/10.5194/hess-20-1669-2016

Williams, P.L., and Cole, J.C., 2007, Geologic map of the Albuquerque 30' x 60' quadrangle, north-central New Mexico: U.S. Geological Survey Scientific Investigations Map 2946, 31 p., scale 1:100,000. https://doi.org/10.3133/sim2946

Wright, H.E., Jr., 1946, Tertiary and Quaternary geology of the lower Rio Puerco area, New Mexico: GSA Bulletin, v. 57, no. 5, p. 383–456. https://doi.org/10.1130/0016-7606(1946)57[383:taqgot]2.0.co;2

Disclaimer:
The data, views, and conclusions included in this report are those of the authors and should not be interpreted as necessarily representing the official policies, either expressed or implied, of the New Mexico Bureau of Geology and Mineral Resources or the State of New Mexico. All data are for informational purposes only, and the user bears all responsibility in determining whether these data are fit for the intended use.

New Mexico Bureau of Geology and Mineral Resources
A research and service division of New Mexico Tech
geoinfo.nmt.edu
801 Leroy Place
Socorro, NM 87801-4796
(575) 835-5490